

Appendix

Implementation of the models

Introduction

This appendix is organized in three parts to describe computational implementations.

Part I: implementation of geometric models to create tissue shapes and fibre structure;

Part II: description of the programs originally written in C by Clayton [1] that were used to create transmembrane voltages in tissues using two models, plus an introduction to the high performance computer for compiling and running the programs;

Part III: description of the programs written in MATLAB that were used to extract the selected transmembrane voltages, detect the indices of AP upstroke and AP downstroke of the 6th normal S1 beats and premature S2 beats to calculate desired data.

Part I: Geometrical models

To simulate 3D heterogeneous ventricular tissue, two geometrical models were used:

(1) input-geometry file

This file is created by a shell script file generate-input-geometry and defines the shape of tissue.

(2) fibre-geometry file

This file defines the fibre orientation of each grid points. This file is created by a shell script file called generate-fibre-geometry to (1) calculate the fibre rotation angle θ as a function of distance in 3D cubes of tissue with $40 \times 40 \times 60$ grid points, and (2) calculate three components of the fibre orientation in three directions using $x = \sin(\theta(Z))$, $y = -\cos(\theta(Z))$, and $Z=0$. Therefore, each fibre-geometry file was created with three columns for Z, Y, and X components of fibre orientation in radian for total number of $40 \times 40 \times 60 = 96000$ cells in tissue.

For clarity, examples of the input-geometry files created for 2D and 3D tissues as well as the left ventricular wedge model are provided.

- 2D input-geometry

Figure 1 shows the scheme of 2D slim input-geometry that was filled with 1s as excited cells within tissue with 200 columns and 4 rows.

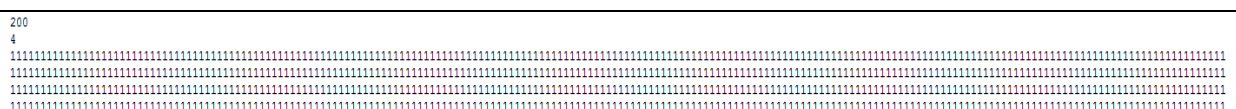


Figure 1: The scheme of 2D slim geometry with 200x4 grid points

- 2D H-geometry

Figure 2 shows an example of the 2D input-geometry with H-shape in which 1s represented excited cells within H-shape and 0s as unexcited cells outside the H-shape.

Figure 2: An example of 2D H-geometry with dimensions of 200x200 grid points

- An example of an input-geometry for 3D cube of tissue is shown in Figure 3. The first and last layers of the input-geometry were filled with 0s as boundaries. The layers between them were filled with 1s as excited cells within tissue and surrounded with 0s as boundaries. Layers were pointing to the Z direction. The tissue for the 3D simulation was therefore made up from a set of points in the space. Each point had a co-ordinate (X, Y, and Z) that defined its position. Each co-ordinate also had three fibre components in three directions which were specified in the fibre geometry.

Figure 3: The scheme of the 3D input-geometry with 40 rows, 40 columns, and 60 layers showing layers 1 and 60 made up from 0s as boundaries and layers from 2 to 59 contained 1s as excited cells within tissue surrounded by 0s as boundaries

- 284

Initially, a number of fibrosis input-geometry was created by progressively decreasing the probability from 0.90 to 0.30 (that a grid point was fibrosis). For consistency, several simulations were run for homogenous and heterogeneous fibrosis tissue to obtain the equivalent population of the excitable and inexcitable cells in all tissues. Not surprisingly, the number of inexcitable cells in heterogeneous fibrosed tissues was smaller than those in homogenous fibrosis tissues possibly due to an increase in heterogeneity and structural discontinuities.

```

40
41
42
43
44
45
46
47
48
49
50
51
52
53
54
55
56
57
58
59
60
61
62
63
64
65
66
67
68
69
70
71
72
73
74
75
76
77
78
79
80
81
82
83
84
85
86
87
88
89
90
91
92
93
94
95
96
97
98
99
100
101
102
103
104
105
106
107
108
109
110
111
112
113
114
115
116
117
118
119
120
121
122
123
124
125
126
127
128
129
130
131
132
133
134
135
136
137
138
139
140
141
142
143
144
145
146
147
148
149
150
151
152
153
154
155
156
157
158
159
160
161
162
163
164
165
166
167
168
169
170
171
172
173
174
175
176
177
178
179
180
181
182
183
184
185
186
187
188
189
190
191
192
193
194
195
196
197
198
199
200
201
202
203
204
205
206
207
208
209
210
211
212
213
214
215
216
217
218
219
220
221
222
223
224
225
226
227
228
229
230
231
232
233
234
235
236
237
238
239
240
241
242
243
244
245
246
247
248
249
250
251
252
253
254
255
256
257
258
259
260
261
262
263
264
265
266
267
268
269
270
271
272
273
274
275
276
277
278
279
280
281
282
283
284
285
286
287
288
289
290
291
292
293
294
295
296
297
298
299
300
301
302
303
304
305
306
307
308
309
310
311
312
313
314
315
316
317
318
319
320
321
322
323
324
325
326
327
328
329
330
331
332
333
334
335
336
337
338
339
340
341
342
343
344
345
346
347
348
349
350
351
352
353
354
355
356
357
358
359
360
361
362
363
364
365
366
367
368
369
370
371
372
373
374
375
376
377
378
379
380
381
382
383
384
385
386
387
388
389
390
391
392
393
394
395
396
397
398
399
400
401
402
403
404
405
406
407
408
409
410
411
412
413
414
415
416
417
418
419
420
421
422
423
424
425
426
427
428
429
430
431
432
433
434
435
436
437
438
439
440
441
442
443
444
445
446
447
448
449
450
451
452
453
454
455
456
457
458
459
460
461
462
463
464
465
466
467
468
469
470
471
472
473
474
475
476
477
478
479
480
481
482
483
484
485
486
487
488
489
490
491
492
493
494
495
496
497
498
499
500
501
502
503
504
505
506
507
508
509
510
511
512
513
514
515
516
517
518
519
520
521
522
523
524
525
526
527
528
529
530
531
532
533
534
535
536
537
538
539
540
541
542
543
544
545
546
547
548
549
550
551
552
553
554
555
556
557
558
559
560
561
562
563
564
565
566
567
568
569
570
571
572
573
574
575
576
577
578
579
580
581
582
583
584
585
586
587
588
589
590
591
592
593
594
595
596
597
598
599
600
601
602
603
604
605
606
607
608
609
610
611
612
613
614
615
616
617
618
619
620
621
622
623
624
625
626
627
628
629
630
631
632
633
634
635
636
637
638
639
640
641
642
643
644
645
646
647
648
649
650
651
652
653
654
655
656
657
658
659
660
661
662
663
664
665
666
667
668
669
670
671
672
673
674
675
676
677
678
679
680
681
682
683
684
685
686
687
688
689
690
691
692
693
694
695
696
697
698
699
700
701
702
703
704
705
706
707
708
709
710
711
712
713
714
715
716
717
718
719
720
721
722
723
724
725
726
727
728
729
730
731
732
733
734
735
736
737
738
739
740
741
742
743
744
745
746
747
748
749
750
751
752
753
754
755
756
757
758
759
760
761
762
763
764
765
766
767
768
769
770
771
772
773
774
775
776
777
778
779
780
781
782
783
784
785
786
787
788
789
790
791
792
793
794
795
796
797
798
799
800
801
802
803
804
805
806
807
808
809
810
811
812
813
814
815
816
817
818
819
820
821
822
823
824
825
826
827
828
829
830
831
832
833
834
835
836
837
838
839
840
841
842
843
844
845
846
847
848
849
850
851
852
853
854
855
856
857
858
859
860
861
862
863
864
865
866
867
868
869
870
871
872
873
874
875
876
877
878
879
880
881
882
883
884
885
886
887
888
889
890
891
892
893
894
895
896
897
898
899
900
901
902
903
904
905
906
907
908
909
910
911
912
913
914
915
916
917
918
919
920
921
922
923
924
925
926
927
928
929
930
931
932
933
934
935
936
937
938
939
940
941
942
943
944
945
946
947
948
949
950
951
952
953
954
955
956
957
958
959
960
961
962
963
964
965
966
967
968
969
970
971
972
973
974
975
976
977
978
979
980
981
982
983
984
985
986
987
988
989
990
991
992
993
994
995
996
997
998
999
1000
1001
1002
1003
1004
1005
1006
1007
1008
1009
1010
1011
1012
1013
1014
1015
1016
1017
1018
1019
1020
1021
1022
1023
1024
1025
1026
1027
1028
1029
1030
1031
1032
1033
1034
1035
1036
1037
1038
1039
1040
1041
1042
1043
1044
1045
1046
1047
1048
1049
1050
1051
1052
1053
1054
1055
1056
1057
1058
1059
1060
1061
106
```

Figure 4: A scheme of 3D fibrosis input-geometry with 40 rows, 40 columns, and 60 layers showing layers 1 and 60 as boundaries and fibrosis layers 2 and 59 filled randomly with 0s and 1s as unexcited and excited cells surrounded with 0s as boundaries

- The left ventricular wedge model

The wedge model had two input-geometries.

- (I) The input-geometry with 175 rows, 550 columns, and 300 layers contained a left ventricular geometry, with 1s and 0s as grid points within and outside tissue. This geometry was used to simulate homogenous tissues by allocating 1s to be epicardial cell, mid-myocardial cells, or endocardial cells.
- (II) The second input-geometry has the same size, but in this script file the distance from the middle of the left ventricle was measured and used to allocate the ventricular cell type. Thus, 1s correspond to epicardial cells with 2931822 grid points (42%), 2s to mid-myocardial cells with 1957384 grid points (28%), and 3s to endocardial cells with 2097274 grid points (30%). This geometry was used to study heterogeneous.

285

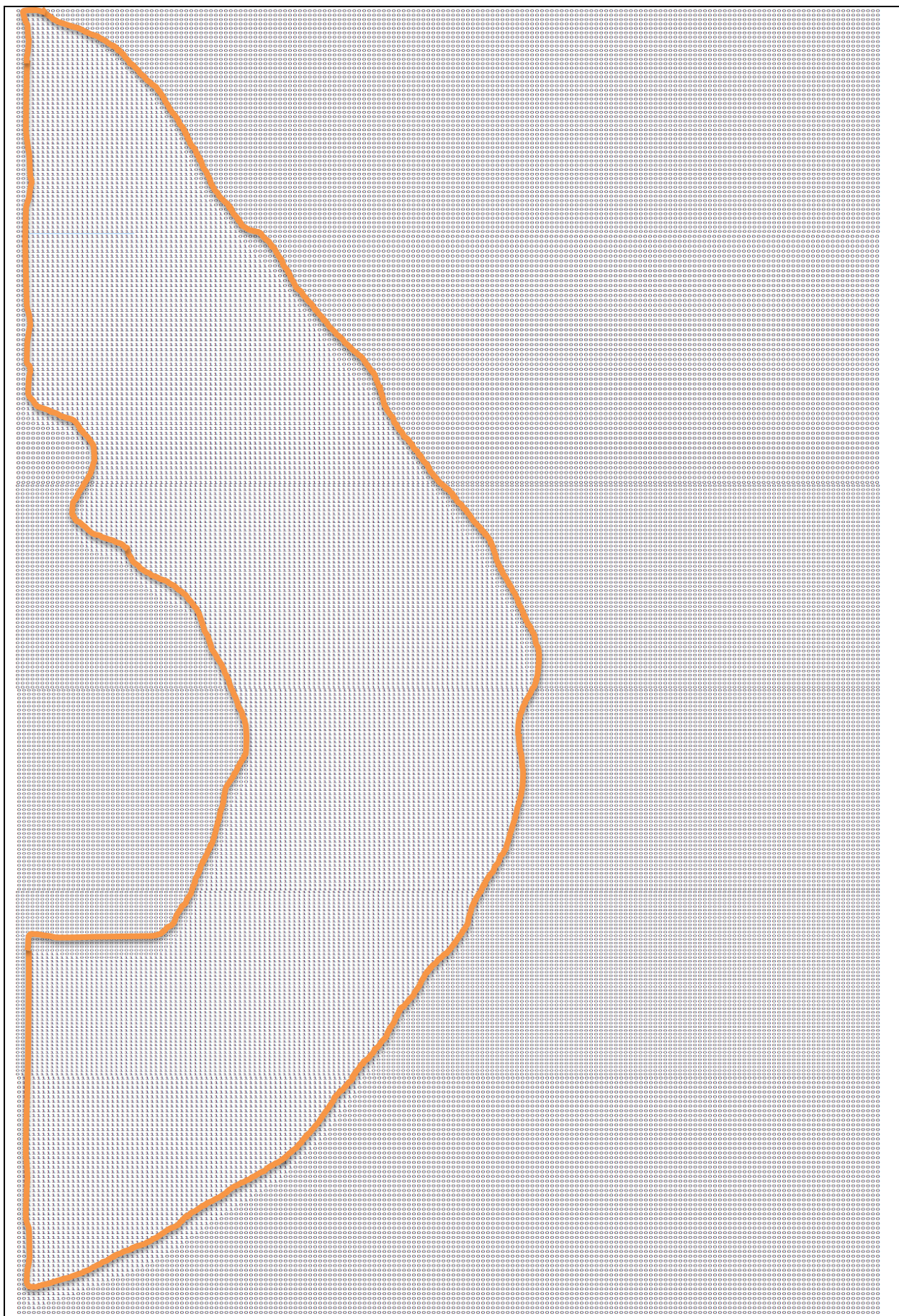


Figure 5: A scheme of one slice of the human left ventricular geometry un the wedge model made up from 1s and 0s as cells within (in orange) and outside tissue

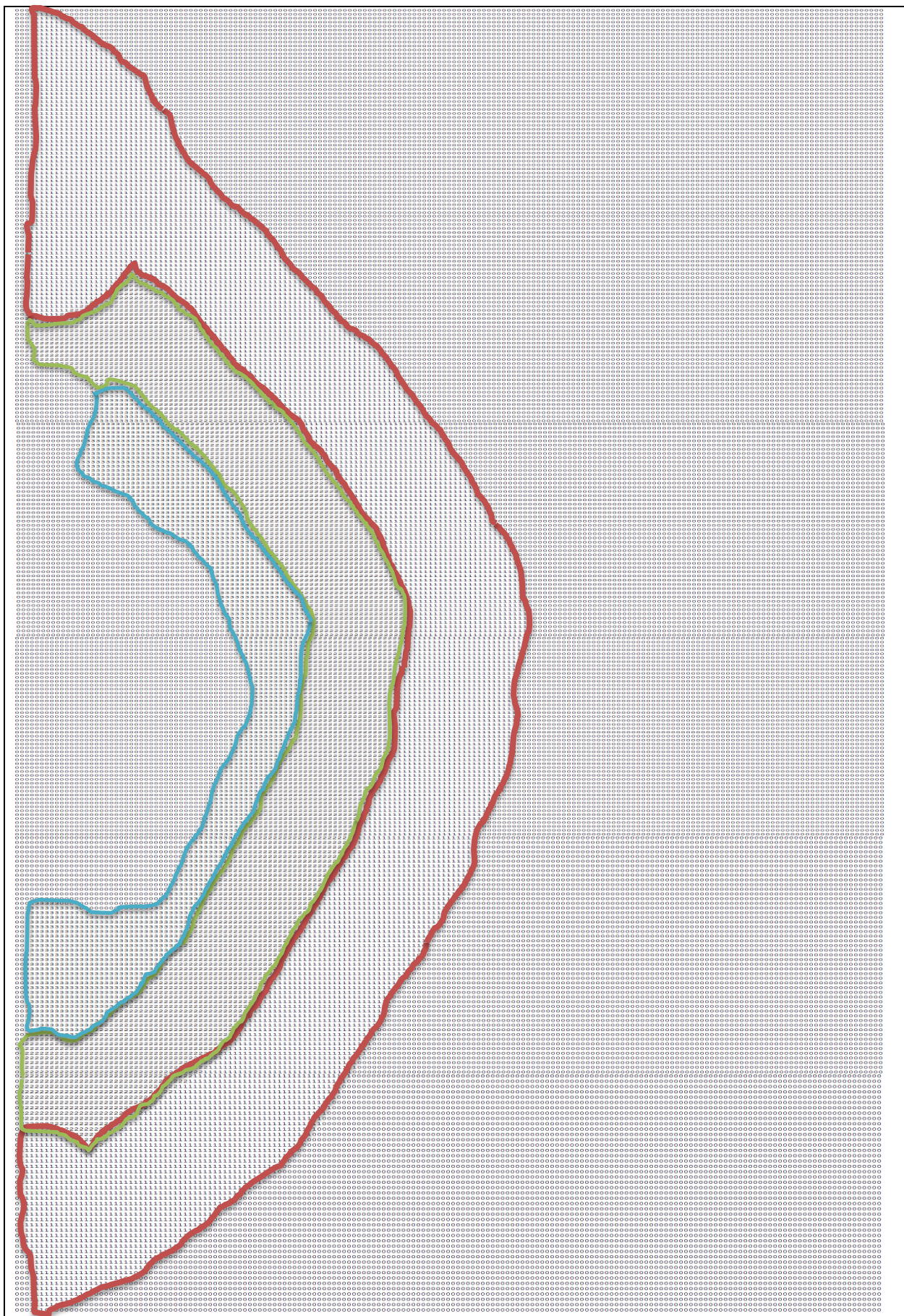


Figure 6: A scheme of 5th layer of the human left ventricular geometry in the wedge model filled with 0s, 1s, 2s, and 3s as outside tissue, epicardial (in red), mid-myocardial (in green), and endocardial (in blue) cells respectively

Part II: Programs written in C

This thesis used programs written in C that was able to be modified to (1) use geometric models that defined tissue shapes and fibre structure; (2) stimulate normal and premature beats at any pacing rate; (3) simulate tissues with different heterogeneity; and (4) use tissue models based on the FK4V [2] model and the TP06 model [3]. The programs that implemented the FK4V model [2] and the TP06 model [3] are referred to as FK4V program and TP06 program that are described as follows.

The programs were composed of 13 to 15 files that are explained in the following sections.

1 Header file

The header file with .h extension contains parameters, partial differential equation solvers and numerical recipe routines. The parameters in this file were changed for each simulation that is explained in the relative sections.

- **Isotropic and anisotropic diffusion coefficients**

In this thesis, the values of diffusion coefficients were obtained from experimental measurements that are explained here. The intracellular conductivity tensors in longitudinal and transverse direction are often determined by the passive properties of the cardiac tissue including the surface to volume ratio of the ventricular cell and the cytoplasm resistivity. In isotropic condition, these properties change similarly in both longitudinal and transverse directions. Figure 7 shows a typical ventricular cell estimated as a cylinder shape in 2D tissue with experimental measurements.

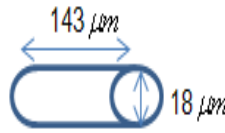


Figure 7: A ventricular cell described as a cylindrical shape with an average length of $143.3 \pm 8.8 \mu m$ [4] and an average diameter $18.5 \pm 1.2 \mu m$ [4]

S_v : The surface to volume ratio of the human ventricular cell 1/cm was given by [5]

$$S_v = \frac{Surface}{Volume} = \frac{2\pi \times radius \times length + 2\pi \times radius^2}{\pi \times radius^2 \times length} = 2\left(\frac{1}{radius} + \frac{1}{length}\right)$$

$$S_v = \frac{2}{18.5/2\mu m} + \frac{2}{143.3\mu m} = 2301.7295cm^{-1}$$

For isotropic condition, the diffusion coefficient along and across tissue was given by [5]:

$$D_i = \frac{1}{S_v \cdot R \cdot (C_m / A)} = \frac{1}{2301.7295cm^{-1} \times 180\Omega cm \times 179 \frac{PF}{cm^2}} = 0.001 \frac{cm^2}{ms}$$

R: the cytoplasm (intracellular) resistivity with value of $180 \pm 34 \Omega cm$ [6]

C_m : The specific capacitance of the membrane with value of $179 \pm 10 pF$ [4]

Dimensional analysis of the intercellular diffusion tensor:

The unit of diffusion tensor is obtained after substituting the given units in the formula:

$$D_i = \frac{1}{S_v C_m R_i} = \frac{1}{(cm^{-1}) \cdot (\frac{\mu F}{cm^2}) \cdot (\Omega cm)} = \frac{1}{\Omega \cdot (\frac{\mu F}{cm^2})} = \frac{1}{\frac{Volts}{Amps} \times \frac{\mu Amps \times Seconds}{Volts} \times \frac{1}{cm^{-2}}} = \frac{cm^2}{\mu s}$$

$$\Omega = \frac{Volts}{Amps} \text{ (Ohms' law } R = \frac{V}{I} \text{)}$$

$$\mu F = \frac{\mu Coulombs}{Volts} \text{ (} C = \frac{Q}{V} \text{ ; where Q is charge)}$$

$$\mu Coulombs = \mu Amps \times Seconds \text{ (} Q = I \times t \text{)}$$

• Specify tissue heterogeneity

To specify heterogeneity in 3D cubes of tissue, two variables Endo-M and M-Epi were defined in the header files. These variables behaved as the boundary to separate ventricular cell types along tissues. Table 1 shows the numerical values that were used to specify the configuration of ventricular cells close to the experimental studies (described in Chapter 3).

For example, in 3D simulated tissue composed of 15%Endo-55%M-30%Epi cells: layers 1 to 9 allocate cells to be endocardial cells if Endo-M<9, then layers 10 to 42 allocate cells to be mid-myocardial cells if 9<M-Epi<42, and finally layers 43 to 60 allocate cells to be epicardial cells for any other values.

Setting populations of ventricular cell types in 3D cubes of tissue in the FK4V & TP06 models			
1 cell type	100% Epi	Endo-M=0	M-Epi=0
1 cell type	100% Endo	Endo-M=60	M-Epi=60
1 cell type	100% M	Endo-M=1	M-Epi=59
50% Epi-50% Endo	50/100×6/6=30/60	Endo-M=30	M-Epi=30
60%Endo-30%M-10%Epi	60/100×6/6=36/60 30/100×6/6=18/60 10/100×6/6=6/60	Endo-M=36	M-Epi=36+18=54
10%Endo-30%M-60%Epi	10/100×6/6=6/60 30/100×6/6=18/60 60/100×6/6=36/60	Endo-M=6	M-Epi=6+18=24
15%Endo-55%M-30%Epi	15/100×6/6=9/60 55/100×6/6=33/60 30/100×6/6=18/60	Endo-M=9	M-Epi=33+9=42

Table 1: Numerical values used to specify epicardial, Mid-myocardial, and endocardial region in tissue

• Specify file name

The header file also defines the name of the output files to distinguish data base on the name of cell models. For example, "fk2d", "fk3d", "TP2d", and "TP3d" represent output data in 2D and 3D simulations with the FK4V [2] and the TP06 [3] models respectively.

2 Get dimensions file

This file reads and stores the first entries of the input-geometry file that correspond to dimensions of tissue in 2D or 3D geometries.

3 Read geometry file

This file read input-geometry and stores information about boundary points (0 or less) and tissue points (1 or more) in the geometry array.

4 Read fibre file

Here, the components of fibres in three axes were read and saved.

5 Allocate cell type file

This file initially reads the input-geometry and stores information about cell types in the layer array. Then the file allocates values in this array to indicate endocardial cells as 0s, mid-myocardial cells as 1s, and epicardial cells as 2s. The boundaries between these layers were given by ENDO_M and M_EPI, which were defined in the header file.

Regarding the second input-geometry for the left ventricular wedge model, the distance from the middle of the left ventricle was used to allocate cell types. So, in this input-geometry 1, 2, and 3 correspond to epicardial, mid-myocardial, and endocardial cells respectively. To allocate cell types array avoiding boundary points, the allocate-cell-type file was modified using ASCII code (i.e. 48, 49, 50, and 51 in ASCII as symbol of 0, 1, 2, and 3).

6 Find boundary file

To impose no-flux boundary conditions, the gradient of membrane voltage normal to the tissue edge was set to zero at boundary points. The method for finding the boundary of the medium in the 3D cube of tissue and the left ventricular wedge model was based on the study by Panfilov and Keener [7].

7 Find neighbours file

On average, a single ventricular cell is connected to about 11 to 12 neighbours via gap junctions based on experimental studies by Saffitz et al [8] and Luke et al. [9]. Accordingly, this file finds and set up the 8 and 26 nearest neighbours for each grid point in 2D and 3D geometries respectively.

8 Diffusion file

The continuous monodomain reaction-diffusion equations [5] were defined in the main file but the diffusion term and the reaction term were computed in the diffusion file and the cell model file. The main difference between diffusive term in 2D and 3D simulations were:

First, in 2D simulations, the diffusion of neighbouring cells, D , was approximated as constant, while in 3D simulations, diffusion tensor was a 3×3 diffusion matrix composed of elements d_{ij} ; Second, each grid point in 2D geometries had eight nearest neighbours while in 3D geometries, the number of the nearest neighbours were 26 based on the experimental study [8].

- **Diffusive term in 2D isotropic monodomain equation**

In 2D monodomain equation [5], diffusion of ionic currents through gap junctions between neighbouring cells was described by the diffusive term for each grid point X with 8 nearest neighbours [8]. Figure 8 shows how the rates of change of transmembrane potential were numerically approximated by central difference across and along fibre axis for a typical ventricular cell X in 2D tissue from [5].

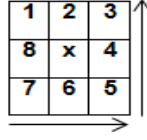


Figure 8: The scheme of one ventricular cell X with 8 nearest neighbours in a 2D geometry

$\frac{\partial^2 u}{\partial x^2} = \frac{u_6 - u_2 - 2u_{62}}{\Delta x^2}$: The rate of change of transmembrane potential across tissue in which u_6 , u_2 , and u_{62} corresponded to the transmembrane voltage of neighbour 6, 2 and the gradient transmembrane voltage of cells 6 and 2.

$\frac{\partial^2 u}{\partial y^2} = \frac{u_4 - u_8 - 2u_{84}}{\Delta y^2}$: The rate of change of transmembrane potential along tissue in which u_4 , u_8 , and u_{48} corresponded to the transmembrane voltage of neighbour 4, 8 and the gradient transmembrane voltage of cells 4 and 8.

• Diffusive term in 3D anisotropic monodomain equation

In programs, the diffusion terms were computed in two files. First, the initialise-diffusion-aniso.c file initialized pre-computed arrays to save time for calculating the diffusion.

1. Computation in the initialise-diffusion-aniso.c file

This file calculates the 9 elements of the diffusion matrix for each grid point in tissue. These elements were the product of diffusion along and across fibre axes and the fibre components. In addition, this file derived the components of the fibre vector that are used in diffusion-aniso.c file.

$D_{3 \times 3}$: The 3x3 diffusion matrix [7] given by:

$$\begin{bmatrix} D2 + D1a_1a_1 & (D1 - D2)a_1a_2 & (D1 - D2)a_1a_3 \\ (D1 - D2)a_2a_1 & D2 + D1a_2a_2 & (D1 - D2)a_2a_3 \\ (D1 - D2)a_3a_1 & (D1 - D2)a_3a_2 & D2 + D1a_3a_3 \end{bmatrix}$$

D1 or Diffusion1: Diffusion coefficient along fibre

D2 or Diffusion 2: Diffusion coefficient across fibre

The components of the fibre vector:

$$\begin{aligned} \frac{da_1}{\Delta x} &= \frac{a_{16} - a_{11}}{2\Delta x}, & \frac{da_2}{\partial x} &= \frac{a_{14} - a_{13}}{2\Delta x}, & \frac{da_3}{\partial x} &= \frac{a_{22} - a_5}{2\Delta x} \\ \frac{da_4}{\partial x} &= \frac{a_{16} - a_{11}}{2\Delta x}, & \frac{da_5}{\partial x} &= \frac{a_{14} - a_{13}}{2\Delta x}, & \frac{da_6}{\partial x} &= \frac{a_{22} - a_5}{2\Delta x} \\ \frac{da_7}{\Delta x} &= \frac{a_{16} - a_{11}}{2\Delta x}, & \frac{da_8}{\partial x} &= \frac{a_{14} - a_{13}}{2\Delta x}, & \frac{da_9}{\partial x} &= \frac{a_{22} - a_5}{2\Delta x} \end{aligned}$$

2. Computation of diffusive term in the diffusion-aniso.c file

The diffusion-aniso.c file computed the diffusive components for each cell in tissue in the X, Y, and Z based on [7]:

$$\nabla \cdot (D_{3 \times 3} \nabla u) = \sum_{i=1}^3 \sum_{j=1}^3 \frac{\partial}{\partial x_i} (d_{ij} \frac{\partial u}{\partial x_j}) = \sum_{i=1}^3 \sum_{j=1}^3 (\frac{\partial d_{ij}}{\partial x_i} \frac{\partial u}{\partial x_j} + d_{ij} \frac{\partial^2 u}{\partial x_i \partial x_j})$$

Here, X coordinate pointing to the rows, Y coordinate to the columns, and Y coordinate to the layers.

Table 2 provides examples of numerical solutions of the first element of the diffusive term.

$$\nabla \cdot (D \nabla V_m) = \frac{\partial}{\partial x} [d_{11} \frac{\partial V_m}{\partial x}] + \frac{\partial}{\partial x} [d_{12} \frac{\partial V_m}{\partial y}] + \frac{\partial}{\partial x} [d_{13} \frac{\partial V_m}{\partial z}] + \quad \text{1st row of diffusion matrix}$$

$$\frac{\partial}{\partial y} [d_{21} \frac{\partial V_m}{\partial x}] + \frac{\partial}{\partial y} [d_{22} \frac{\partial V_m}{\partial y}] + \frac{\partial}{\partial y} [d_{23} \frac{\partial V_m}{\partial z}] + \quad \text{2nd row of diffusion matrix}$$

$$\frac{\partial}{\partial z} [d_{31} \frac{\partial V_m}{\partial x}] + \frac{\partial}{\partial z} [d_{32} \frac{\partial V_m}{\partial y}] + \frac{\partial}{\partial z} [d_{33} \frac{\partial V_m}{\partial z}] \quad \text{3rd row of diffusion matrix}$$

	Derivation	Substituting into derivations
1st term of the 1st row of the diffusion matrix	$\frac{\partial}{\partial x} [d_{11} \frac{\partial u}{\partial x}] = d_{11} \frac{\partial^2 u}{\partial x^2} + \frac{\partial}{\partial x} d_{11} \frac{\partial u}{\partial x} = d_{11} \frac{\partial^2 u}{\partial x^2} + [2a_1 \frac{da_1}{dx} (D_1 - D_2)] \frac{\partial u}{\partial x} + d_{11} \frac{\partial^2 u}{\partial x^2}$	$d_{11} = D_2 + (D_1 - D_2)a_1^2$
		$\frac{\partial^2 u}{\partial x^2} = \frac{u_{16} - u_{11} - 2u}{\Delta x^2}$
		$\frac{\partial u}{\partial x} = \frac{u_{16} - u_{11}}{2\Delta x}$
		$\frac{da_1}{dx} = \frac{a_{16} - a_{11}}{2\Delta x}$
2nd term of the 1st row of the diffusion matrix	$\frac{\partial}{\partial x} [d_{12} \frac{\partial u}{\partial y}] = d_{12} \frac{\partial^2 u}{\partial x \partial y} + \frac{\partial}{\partial x} d_{12} \frac{\partial u}{\partial y} = d_{12} \frac{\partial^2 u}{\partial x \partial y} + \frac{\partial u}{\partial y} [a_2 \frac{da_1}{dx} + a_1 \frac{da_2}{dx}] \times (D_1 - D_2)$	$d_{12} = (D_1 - D_2) \cdot a_1 \cdot a_2$
		$\frac{\partial^2 u}{\partial x \partial y} = \frac{(u_{17} - u_{15}) - (u_{12} - u_{10})}{4\Delta x^2}$
		$\frac{\partial u}{\partial y} = \frac{u_{14} - u_{13}}{2\Delta x}$
		$\frac{\partial a_2}{\partial x} = \frac{a_{14} - a_{13}}{2\Delta x}$

Table 2: The first and second terms of the first row of the diffusion matrix for (i=j=1)

The rate of change of transmembrane potential in 3D tissue is numerically approximated by central difference for a typical cell XX surrounded with 26 nearest neighbours [8] as shown in Figure 9.

Layer n-1	layer n	layer n+1	
1 2 3	10 11 12	18 19 20	$\frac{\partial u}{\partial x} = \frac{u_{16} - u_{11}}{2\Delta x}$ Rate of change of membrane potential across tissue
4 5 6	13 XX 14	21 22 23	$\frac{\partial u}{\partial y} = \frac{u_{14} - u_{13}}{2\Delta x}$ Rate of change of membrane potential along tissue
7 8 9	15 16 17	24 25 26	$\frac{\partial u}{\partial z} = \frac{u_{22} - u_5}{2\Delta x}$ Rate of change of membrane potential across tissue

Figure 9: The scheme of the grid point XX with 26 nearest neighbours and examples of rate of change of membrane potential

9 Initialise variables file

This file contains variables that initialise variables to their starting values. For example, the number of variables in the FK4V model [2] and the TP06 model [3] were 4 and 21 respectively. In this file, model parameters set 0, 1, and 2 were equivalent to 'default' endocardial, mid-myocardial, and epicardial cells.

10 Cell models file

The cell model file computed the reaction term of the monodomain equations [5] based on the FK4V [2] and the TP06 [3] equations.

- Reaction term based on the FK4V model

The `fk4v.c` file estimated and the kinetic of two gates v and w variables, the state variable and three phenomenological currents [2] including a fast inward current, a slow outward current, and a slow inward current.

The model parameters [2] for simulating epicardial, mid-myocardial, and endocardial cells are provided in Table 3. For time parameters that were used in these equations as functions of the voltage variable u please refer to the original paper [2].

- Reaction term based on the TP06 model

In TP06 program, two files were used to compute the reaction term.

Initially, the `create-TNNPv2-lookup-OpSplit` file pre-calculated the gating variables for the time-dependent currents including sodium current, transient outward current, rapid delayed rectifier current, slow delayed rectifier current, and L-type calcium current.

Then, another file called `calculate_TNNPv2_current_OpSplit` calculated the reaction term based on 13 ionic currents equations [3] described by ordinary differential equations (described in Chapter 3). The model parameters are provided in Table 4.

Role of model parameters	Parameters	mnemonics	Epi	Endo	M
Controls resting membrane potential	Resting membrane potential	u_o	0	0	0
Controls AP amplitude	Upper voltage value	u_u	1.55	1.56	1.61
Controls Na^+ -like activation threshold	Threshold voltage for the fast activation gate (the step function)	θ_v	0.3	0.3	0.3
Controls threshold of opening /closing of the slow gate	Threshold voltage for the slow activation gate (the step function)	θ_w	0.13	0.13	0.13
Controls switch btw. opening time constants of fast gate	Threshold voltage for the fast inactivation gate (the step function)	θ_v^-	0.006	0.2	0.1
Controls decay to resting membrane potential	Threshold voltage for the slow gate variable (the step function)	θ_o	0.006	0.006	0.005
Controls minimum DI	Opening time constant for the fast gate variable	τ_{v1}^-	60	75	80
Controls minimum DI (the steepness of the curve)	Opening time constant for the fast gate variable	τ_{v2}^-	1150	10	1.4506
Controls closing of fast gate / maximum AP upstroke velocity	Closing time constant for the fast gate variable	τ_v^+	1.4506	1.4506	1.4506
Controls APD restitution curve	Opening time constant for the slow gate variable	τ_{w1}^-	60	6	70
Controls APD restitution curve	Opening time constant for the slow gate variable	τ_{w2}^-	15	140	8
Helps to control curvature of APD restitution curve	Rate of change of opening time constants for the slow gate variable	k_w^-	65	200	200
Controls switch btw. opening time constants of w gate	The potential for the opening slow gate variable	u_w^-	0.03	0.016	0.016
Control maximum & minimum APD	Closing time constant for the slow gate variable	τ_w^+	200	280	280
Controls maximum AP upstroke velocity	Depolarization time for the fast inward current (sodium)	τ_{fi}	0.11	0.1	0.078
Controls decay of AP to resting membrane potential	The time constant for the voltage dependent component of outward current	τ_{o1}	400	470	410
Controls decay of AP to resting membrane potential	The time constant for the voltage dependent component of outward current	τ_{o2}	6	6	7
Control maximum & minimum APD	The time constant for the slow outward current at low voltages	τ_{so1}	30.0181	40	91
Control maximum & minimum APD	The time constant for the slow outward current at high voltages	τ_{so2}	0.9957	1.2	0.8
Helps to control curvature of AP repolarization	Rate of change of opening time constants for the slow outward current	k_{so}	2.0458	2	2.1
Helps to control curvature of AP repolarization	The potential of the slow outward current	u_{so}	0.65	0.65	0.6
Controls shape of the AP	The time constant of activation for the shape gate variable	τ_{s1}	2.7342	2.7342	2.7342
Controls shape of the AP	The time constant of recovery for the shape gate variable	τ_{s2}	16	2	7
Controls dome of the AP	Rate of change of the shape gate variable	k_s	2.0994	2.0994	2.0994
Controls dome of the AP	The potential of the surface area of the human ventricular cell	u_s	0.9087	0.9087	0.9087
Controls stiffness of repolarization phase	Repolarization time for the slow inward current (calcium)	τ_{si}	1.8875	2.9013	3.3849
Helps to control slope of APD restitution at long DIs	Time constant for the steady-state value of the slow variable at long DIs	$\tau_{w\infty}$	0.07	0.0273	0.01
Helps to control slope of APD restitution at short DIs	Steady-state value of the slow variable at short DIs	w_{∞}^*	0.94	0.78	0.5

Table 3: Model parameters of the FK4V model [2]

Parameter	Definition	Value
R	Gas constant	$8.3143 \text{ J}\cdot\text{K}^{-1}\cdot\text{mol}^{-1}$
T	Temperature	310 K
F	Faraday constant	96.4867 C/mmol
C_m	Cell capacitance per unit surface area	$2.0 \text{ }\mu\text{F}/\text{cm}^2$
S	Surface to volume ratio	$0.2 \text{ }\mu\text{m}^{-1}$
ρ	Cellular resistivity	$162 \text{ }\Omega\cdot\text{cm}$
V_c	Cytoplasmic volume	$16.404 \text{ }\mu\text{m}^3$
V_{sr}	Sarcoplasmic reticulum volume	$1.094 \text{ }\mu\text{m}^3$
V_{ss}	Subspace volume	$0.05468 \text{ }\mu\text{m}^3$
K_o	Extracellular K^+ concentration	5.4 mM
Na_o	Extracellular Na^+ concentration	140 mM
Ca_o	Extracellular Ca^{2+} concentration	2 mM
G_{Na}	Maximal I_{Na} conductance	14.838 nS/pF
G_{K1}	Maximal I_{K1} conductance	5.405 nS/pF
$G_{\text{to}, \text{epi}, \text{M}}$	Epicardial I_{to} conductance	0.294 nS/pF
$G_{\text{to}, \text{endo}}$	Maximal endocardial I_{to} conductance	0.073 nS/pF
G_{Kr}	Maximal I_{Kr} conductance	0.153 nS/pF
$G_{\text{Ks}, \text{epi}, \text{endo}}$	Maximal epi-and endocardial I_{Ks} conductance	0.392 nS/pF
$G_{\text{Ks}, \text{M}}$	Maximal M cell I_{Ks} conductance	0.098 nS/pF
ρ_{KNa}	Relative I_{Ks} permeability to Na^+	0.03
G_{CaL}	Maximal I_{CaL} conductance	$3.980^{-5} \text{ cm}\cdot\text{ms}^{-1}\cdot\mu\text{F}^{-1}$
k_{NaCa}	Maximal I_{NaCa}	1,000 pA/pF
γ	Voltage dependence parameter of I_{NaCa}	0.35
K_{mCa}	Ca_i half-saturation constant for I_{NaCa}	1.38 mM
K_{mNa}	Na_i half-saturation constant for I_{NaCa}	87.5 mM
k_{sat}	Saturation factor for I_{NaCa}	0.1
α	Factor enhancing outward nature of I_{NaCa}	2.5
P_{NaK}	Maximal I_{NaK}	2.724 pA/pF
K_{mK}	K_o half-saturation constant of I_{NaK}	1 mM
K_{mNa}	Na_i half-saturation constant of I_{NaK}	40 mM
G_{pK}	Maximal I_{pK} conductance	0.0146 nS/pF
G_{pCa}	Maximal I_{pCa} conductance	0.1238 nS/pF
K_{pCa}	Half-saturation constant of I_{pCa}	0.0005 mM
G_{bNa}	Maximal I_{bNa} conductance	0.000290 nS/pF
G_{bCa}	Maximal I_{bCa} conductance	0.000592 nS/pF
V_{maxup}	Maximal I_{up} conductance	0.006375 mM/ms
K_{up}	Half-saturation constant of I_{up}	0.00025 mM
V_{rel}	Maximal I_{rel} conductance	40.8 mM/ms
k_1'	R to O and RI to I I_{rel} transition rate	$0.15 \text{ mM}^{-2}\cdot\text{ms}^{-1}$
k_2'	O to I and R to RI I_{rel} transition rate	$0.045 \text{ mM}^{-1}\cdot\text{ms}^{-1}$
k_3	O to R and I to RI I_{rel} transition rate	0.060 ms^{-1}
k_4	I to O and RI to I I_{rel} transition rate	0.000015 ms^{-1}
EC	Ca_{SR} half-saturation constant of k_{casr}	1.5 mM
max_{sr}	Maximum value of k_{casr}	2.5 (dimensionless)
min_{sr}	Minimum value of k_{casr}	1 (dimensionless)
V_{leak}	Maximal I_{leak} conductance	0.00036 mM/ms
V_{xfer}	Maximal I_{xfer} conductance	0.0038 mM/ms
Buf_c	Total cytoplasmic buffer concentration	0.2 mM
K_{bufc}	Ca_i half-saturation constant for cytoplasmic buffer	0.001 mM
Buf_{sr}	Total sarcoplasmic buffer concentration	10 mM
K_{bufsr}	Ca_{SR} half-saturation constant for sarcoplasmic buffer	0.3 mM
Buf_{ss}	Total subspace buffer concentration	0.4 mM
K_{bufss}	Ca_{SS} half-saturation constant for subspace buffer	0.00025 mM

Table 4: Model parameters for the TP06 model [3]

11 Main file

The main file evaluates equations by calling other files plus four major processes: (1) simulation protocol; (2) solving partial differential equations; (3) deliver stimuli to a small region in tissue; and (4) creating output files every 1 ms.

Furthermore, the main file creates an additional output file called eg.out that contained two columns: the first column corresponds to timing of premature S2 beats, and the second column corresponds to the voltage of premature S2 beats sampled from central region of the tissue. This file can be used to keep a track of timings of output text files.

12 Output text file

Finally, this file prints out the transmembrane voltage with three decimal places in the whole tissue using the stfout.c function. The format of the file name was modelxxxxxx.stf, where model corresponds to the name of the model, xxxxxx is the time defined by the variable stf count in the main file to keep track of timing. For example, FK3d002500.stf.gz shows an output data file (containing transmembrane voltages) in the form of the zip file created after 2500 ms with the FK4V model [2] in 3D cubes of tissue.

The other files allocate free memory for the variables.

How to run programs in C

The programs were run on the Linux based high performance computing cluster at University of Sheffield called iceberg [10]. High performance computing server iceberg is the Sheffield node of the 'White Rose Computing Grid'. Iceberg has hardware including two head-nodes for logging into iceberg, AMD-based cluster, and INTEL-based cluster. In the INTEL-based cluster, there are in total 3584 total GPU cores and 48 GB GPU memory [10]. Regarding file store, there are three file stores that users by default can store 5 GBytes of storage on /home area, 50GBytes in /data area, and no limits on the /fastdata [10].

To access iceberg, users should initially apply for an account, log into a head node, and then use one worker node to run their jobs on. The link in the web address (<http://www.shef.ac.uk/wrgrid/using/access>) provides a terminal access to the iceberg from the user browser. A job defined as a completely defined computational task. The 'Sun Grid Engine' software is responsible to manage the scheduling of the users' jobs on the worker nodes. Jobs can be run in two methods interactively (qsh) or submitted as batch jobs (qsub). To submit a batch job to the iceberg cluster, it is required to write a text script file containing a set of commands. Before running a job, it is important to note that

- the maximum running time is 8 wall_clock i.e. real-time hours [11];
- the default memory allocation is 6 Gigabytes [11] on all nodes.

So that if the job exceeds its allocated time or memory gets terminated without any warning. In addition a job can be submitted as serial or parallel method.

Accordingly, the shell script in this study for all serial jobs specified the maximum running time of 168 hours [11] and the total real memory of 6 Giga byte [11] plus the directory to define where the programs written in C were saved in the file store /data area. This script file should be saved as a shell script file with .sh extension. The shell is a command interpreter and a shell program, called a script, is an easy-to-use tool for building applications by putting together system calls, tools, utilities, and compiled binaries [12].

Part III: Programs written in MATLAB

Simulations in C produced output files in the form of a series of stf files containing transmembrane voltage for every other cell in tissues (in 2D for the whole tissue). An additional file was also created containing transmembrane voltage sampled from the central region of tissues. Subsequently, three procedures were performed in MATLAB in order to: (1) extract voltage from the selected region i.e. the central region of tissues; (2) calculate the desired time for the 6th normal S1 beats and premature S2 beats; and (3) visualize the data as images and movies. These procedures are explained here.

1 How to extract transmembrane voltage

In all simulations, the created output files produced by programs written in C were in the form of the zip text files with .stf.gz extension. To read and unzip these output files, two programmes ReadStf.m and PlotStf.m were used that were originally written by Clayton [1]. In addition, another program in MATLAB called APDtaskarray.m was written to extract voltage from the selected region in tissues.

1. ReadStf file

The function `StfData=ReadStf (dimension, filename)` reads and returns the transmembrane potential from the simple text files. For the 2D geometry with dimension of 2, the returned variable was a 2D matrix with the name of the file (filename), and for the 3D geometry with dimension of 3, the returned variables was a 3D matrix.

2. PlotStf file

The function `PlotStf (filename, iso)`, reads the transmembrane voltage using `DataToPlot=ReadStf (3, filename)` and saves the values of rows, columns, and layers. For plotting an iso-surface of 3D data from the simple text files, the value of iso-surface was set to 0.

3. APDtaskarray file

This file initially reads filename from the defined directory, puts together the simple text files based on the defined file numbers from the starts to the stops, reads and returns the transmembrane voltage from the relative text files by calling function `ReadStf`, extracts data from the desired region in 2D or 3D data and saves them in the files for each S1S2 interval.

4. Shell script file

In order to run these MATLAB files, a shell script called `APDTASK.sh` was written that calls `APDtaskarray.m`. It is important to note that this file with other MATLAB files should be in the same folder to be executable.

Furthermore, to visualize AP propagation the file `MakeMovie3Dmpg.m` was used that is described here.

5. MakeMovie3Dmpg.m

The file `MakeMovie3Dmpg.m` initially calls `ReadStf.m` and `PlotStf.m` to read and return the transmembrane potential from the simple text files. Then the function `MakeMovie3Dmpg (froot, start, stop, step, iso)` makes movies from 3D simple text files. Start corresponds to the indices of AP upstroke for the 6th normal S1 beats and stop corresponds to the indices of AP at rest for premature S2 beats. For example in simulated mid-myocardial tissue with the

FK4V model, images in the form of jpg were created from simple text files fk3d053331.stf to fk3d054785.stf for the last S1S2 interval of 455 ms. For the text file with the name of fk3d053331.stf, froot is set to 'fk3d', start is set to 53331 and stop is to 54785 that incremented by steps 1.

For clarity, an example of extracting voltage in 2D tissue is described here. The aim of this example is to describe how transmembrane voltages were extracted from the middle region of the 2D slim geometry with 200x4 grid points for epicardial tissue using the TP06 model [3]. In this tissue, the transmembrane voltage was created for 11 S1S2 intervals of 1000, 900, 800, 700, 600, 500, 450, 400, 350, 345, and 340 ms.

After running program in C with 11 S1S2 intervals, 17385 text files containing the transmembrane voltage were created with the following format: TP2d004002, TP2d004003,..., TP2d061397 in which TP corresponds to the TP06 model [3] and the numbers 4002 to 61397 act as a counter of text files and correspond to the timings of the S1S2 sequence. Table 5 shows how to find the start and stop time of each S1S2 sequence during decreasing S1S2 intervals from 1000 ms to 340 ms in this example.

S1S2 interval (ms)	Start of the 6 th S1S2 sequence (ms)	Stop of the 6 th S1S2 sequence (ms)	Names of text file	Number of text files	Dimension of matrices
1000	$1000 \times 4 + 1 + 1 = 4002$	$4002 + 1000 + 1000 - 1 = 6001$	TP2d004002 to TP2d006001	2000	2000x200
900	$4002 + 5000 + 1000 + 1 = 10003$	$10003 + 1000 + 900 - 1 = 11902$	TP2d010003 to TP2d011902	1900	1900x200
800	$10003 + 5000 + 900 + 1 = 15904$	$15904 + 1000 + 800 - 1 = 17703$	TP2d015904 to TP2d017703	1800	1800x200
700	$15904 + 5000 + 800 + 1 = 21705$	$21705 + 1000 - 700 - 1 = 23404$	TP2d021705 to TP2d023404	1700	1700x200
600	$21705 + 5000 + 700 + 1 = 27406$	$27406 + 1000 - 600 - 1 = 29005$	TP2d027406 to TP2d029005	1600	1600x200
500	$27406 + 5000 + 600 + 1 = 33007$	$33007 + 1000 - 500 - 1 = 34506$	TP2d033007 to TP2d034506	1500	1500x200
450	$33007 + 5000 + 500 + 1 = 38508$	$38508 + 1000 - 450 - 1 = 39957$	TP2d038508 to TP2d039957	1450	1450x200
400	$38508 + 5000 + 450 + 1 = 43959$	$43959 + 1000 - 400 - 1 = 45358$	TP2d043959 to TP2d045358	1400	1400x200
350	$43959 + 5000 + 400 + 1 = 49360$	$49360 + 1000 - 350 - 1 = 50709$	TP2d049360 to TP2d050709	1350	1350x200
345	$49360 + 5000 + 350 + 1 = 54711$	$54711 + 1000 - 345 - 1 = 56055$	TP2d054711 to TP2d056055	1345	1345x200
340	$54711 + 5000 + 345 + 1 = 60058$	$60058 + 1000 - 340 - 1 = 61397$	TP2d060058 to TP2d061397	1340	1340x200

Table 5: The start and stop time of the 6th S1S2 sequence for 11 S1S2 intervals in 2D slim geometry of 200 x 4 grid points for isotropic epicardial tissue with the TP06 model [3]

Note: The fixed cycle length in the S1S2 protocol was 1000 ms, so for S1S2 interval of 1000 ms, Start of the 6th S1S2 sequence (ms) = 1000 ms x 4 normal S1 beats + 1 + 1 (counter) = 4002, Stop of the 6th S1S2 sequence (ms) = Start of the 6th S1S2 sequence (ms) + 1000 (ms) + S1S2 interval (ms) - 1 (counter) = 4002 ms + 1000 ms + 1000 ms - 1 = 6001 ms

In the MATLAB APDtaskarray.m file, the columns 2 and 3 from Table 5 were defined by variables start1 and start 11 and stop1 to stop11 respectively. Then, for each S1S2 interval, (i.e. start 1=4002 and stop1=6002) the relative text files were saved and read by ReadStf.m

file. Finally, the transmembrane voltage was extracted from the central region of 2D tissue (row 2 and columns 1-200 highlighted in red as shown in Figure 10), and saved in a matrix.

```
NAME Vm
RANK 2
DIMENSIONS 200 4
BOUNDS 0 199 0 3 800
SCALAR
DATA
-85.380 -85.379 -85.375 -85.366 -85.360 -85.357 -85.354 -85.353 -85.352 -85.352 -85.352 -85.352 -85.341 -85.341 -85.341 -85.340 -85.339 -85.338 -85.336 -85.333 -85.329 -85.326
-85.380 -85.379 -85.375 -85.366 -85.360 -85.357 -85.354 -85.353 -85.352 -85.352 -85.352 -85.352 -85.341 -85.341 -85.341 -85.340 -85.339 -85.338 -85.336 -85.333 -85.329 -85.326
-85.380 -85.379 -85.375 -85.366 -85.360 -85.357 -85.354 -85.353 -85.352 -85.352 -85.352 -85.352 -85.341 -85.341 -85.341 -85.340 -85.339 -85.338 -85.336 -85.333 -85.329 -85.326
-85.380 -85.379 -85.375 -85.366 -85.360 -85.357 -85.354 -85.353 -85.352 -85.352 -85.352 -85.352 -85.341 -85.341 -85.341 -85.340 -85.339 -85.338 -85.336 -85.333 -85.329 -85.326
```

Figure 10: An example of a text file in 2D slim geometry showing transmembrane voltage

Consequently, 11 matrices were created containing transmembrane voltages for 11 S1S2 intervals. Figure 11 shows an example of the created matrix for S1S2 interval of 700 ms with dimensions of 1700×200 that represent 200 transmembrane voltages extracted every 1 ms over a period of 1700 ms.

These matrices were used to calculate the desired time for normal and premature beats.

V 700 <1700x200 double>																				
1	2	3	4	5	6	7	8	9	10	11	12	13	14	15	16	17	18	19	20	21 to 193
1	29.4940	25.6670	21.6770	13.7500	-38.5420	-72.3990	-81.8910	-84.3430	-85.0350	-85.2330	-85.2870	-85.3000	-85.3030	-85.3040	-85.3040	-85.3050	-85.3050	-85.3050	-85.3050	-85.3050
2	21.9340	21.7470	21.1580	20.0830	17.5910	8.2670	7.3730	-64.0680	-79.6220	-83.8340	-84.9220	-85.2030	-85.2780	-85.2970	-85.3030	-85.3040	-85.3050	-85.3050	-85.3050	-85.3050
3	20.3820	20.4030	20.6450	20.8810	20.6730	19.7260	16.9360	15.1790	15.3310	-47.6290	-75.7490	-82.8380	-84.6680	-85.1420	-85.2630	-85.2940	-85.3020	-85.3050	-85.3050	-85.3060
4	18.1320	18.1190	18.2970	18.8860	19.7440	20.5890	20.8250	20.1160	18.7180	17.4790	9.2900	-26.7880	-49.2100	-81.0950	-84.2390	-85.0320	-85.2360	-85.2880	-85.3010	-85.3050
5	15.8750	15.9220	16.0780	16.4840	17.1400	18.0330	19.1290	20.2750	20.7640	20.3700	19.3680	16.6190	9.7430	18.6470	-56.2780	-78.3390	-83.8440	-84.8420	-85.1880	-85.2760
6	14.6970	14.6920	14.7250	14.9220	15.3010	15.8650	16.6260	17.5650	18.6340	19.7390	20.5640	20.7000	19.8600	17.7190	16.8530	13.0300	-41.1560	-73.3320	-82.2960	-84.5280
7	14.1210	14.0700	14.0060	14.0380	14.1960	14.4900	14.9290	15.5170	16.2420	17.1110	18.1340	19.2960	20.4230	20.7790	20.1510	18.9510	17.0440	7.8520	-7.4550	-66.1090
8	13.9020	13.8250	13.7010	13.6250	13.6310	13.7330	13.9420	14.2640	14.6900	15.2340	15.9150	16.7610	17.7710	18.8960	19.9960	20.6290	20.5230	19.6880	16.8420	14.4880
9	13.9350	13.8410	13.6820	13.5370	13.4450	13.4180	13.4670	13.5980	13.8060	14.1010	14.4940	15.0070	15.6590	16.4280	17.3410	18.4010	19.5730	20.6050	20.8160	19.9790
10	14.1250	14.0230	13.8440	13.6580	13.5030	13.3940	13.3390	13.3430	13.3990	13.5120	13.6990	13.9610	14.3280	14.7980	15.3810	16.1010	16.9660	18.0350	19.1870	20.2610
11	14.4000	14.2990	14.1170	13.9110	13.7190	13.5580	13.4350	13.3540	13.3110	13.3040	13.3440	13.4420	13.6120	13.8550	14.1810	14.6040	15.1490	15.8250	16.6380	17.5870
12	14.7270	14.6270	14.4470	14.2390	14.0340	13.8430	13.6770	13.5410	13.4310	13.3470	13.2950	13.2830	13.3210	13.4070	13.5430	13.7480	14.0380	14.4270	14.9220	15.5330
13	15.0910	14.9920	14.8150	14.6060	14.3980	14.1980	14.0120	13.8420	13.6900	13.5540	13.4410	13.3560	13.3060	13.2880	13.3010	13.3590	13.4720	13.6580	13.9220	14.2710
14	15.4720	15.3790	15.2080	15.0030	14.7920	14.5870	14.3930	14.2120	14.0370	13.8700	13.7160	13.5830	13.4740	13.3860	13.3190	13.2820	13.2830	13.3340	13.4350	13.5880
15	15.8600	15.7700	15.6070	15.4100	15.2050	14.9990	14.8000	14.6100	14.4270	14.2480	14.0750	13.9110	13.7640	13.6300	13.5100	13.4100	13.3260	13.2970	13.2900	13.3160
16	16.2530	16.1680	16.0120	15.8210	15.6210	15.4200	15.2230	15.0300	14.8400	14.6530	14.4710	14.2960	14.1310	13.9700	13.8160	13.6740	13.5490	13.4500	13.3710	13.3130
17	16.6450	16.5650	16.4180	16.2360	16.0420	15.8430	15.6470	15.4560	15.2670	15.0770	14.8890	14.7050	14.5300	14.3590	14.1910	14.0290	13.8690	13.7290	13.6030	13.4900
18	17.0350	16.9590	16.8200	16.6460	16.4590	16.2670	16.0750	15.8840	15.6940	15.5060	15.3180	15.1330	14.9510	14.7710	14.5940	14.4200	14.2510	14.0900	13.9350	13.7850
19	17.4240	17.3530	17.2210	17.0550	16.8730	16.6860	16.4980	16.3120	16.1250	15.9350	15.7470	15.5610	15.3810	15.2000	15.0180	14.8360	14.6580	14.4870	14.3210	14.1550
20	17.8060	17.7400	17.6160	17.4590	17.2850	17.1030	16.9190	16.7340	16.5500	16.3650	16.1790	15.9930	15.8110	15.6290	15.4470	15.2650	15.0840	14.9060	14.7300	14.5550
21 to 193	194	195	196	197	198	199	200													
	-85.2870	-85.2870	-85.2860	-85.2860	-85.2850	-85.2840	-85.2830													
	-85.2870	-85.2870	-85.2870	-85.2860	-85.2850	-85.2840	-85.2830													
	-85.2880	-85.2870	-85.2870	-85.2870	-85.2860	-85.2850	-85.2830													
	-85.2880	-85.2880	-85.2880	-85.2870	-85.2860	-85.2850	-85.2840													
	-85.2890	-85.2880	-85.2880	-85.2870	-85.2870	-85.2850	-85.2840													
	-85.2890	-85.2890	-85.2880	-85.2880	-85.2880	-85.2870	-85.2850													
	-85.2900	-85.2900	-85.2900	-85.2890	-85.2880	-85.2870	-85.2860													
	-85.2910	-85.2900	-85.2900	-85.2900	-85.2890	-85.2880	-85.2860													
	-85.2910	-85.2910	-85.2910	-85.2900	-85.2890	-85.2880	-85.2870													
	-85.2920	-85.2920	-85.2910	-85.2910	-85.2910	-85.2900	-85.2880													
	-85.2920	-85.2920	-85.2920	-85.2910	-85.2900	-85.2890	-85.2880													
	-85.2930	-85.2930	-85.2920	-85.2920	-85.2910	-85.2900	-85.2880													
	-85.2930	-85.2930	-85.2930	-85.2920	-85.2920	-85.2910	-85.2890													
	-85.2930	-85.2930	-85.2930	-85.2920	-85.2920	-85.2910	-85.2890													
	-85.2940	-85.2940	-85.2930	-85.2930	-85.2920	-85.2910	-85.2890													
	-85.2940	-85.2940	-85.2940	-85.2930	-85.2920	-85.2910	-85.2890													
	-85.2950	-85.2940	-85.2940	-85.2940	-85.2930	-85.2920	-85.2900													

Figure 11: An example of the created matrix for S1S2 interval of 700 ms containing the extracted transmembrane voltage from the central region of the 2D slim geometry with 4 × 200 grid points

2 Calculation of the desired data

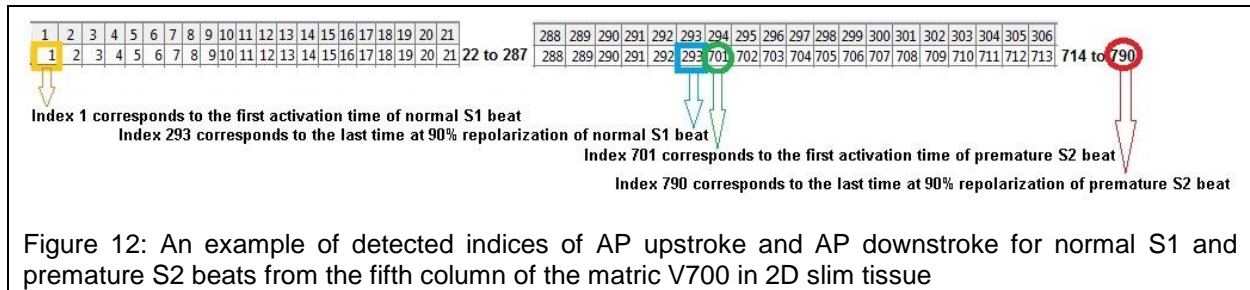
The second computational implementation in MATLAB was to calculate activation time, APD, diastolic interval, repolarization time of normal S1 and premature S2 beats based on the created matrices containing the extracted transmembrane voltages. To achieve this purpose, the MATLAB file called calculation.m was written to:

- load the created matrices;
- find the voltages above the threshold voltage which was 0.15 mV in 2D and 0.1 mV in 3D simulations with the FK4V model [2] and -65 mV with the TP06 model [3];
- detect and save the indices of these transmembrane voltages;
- detect and save the first index of AP upstroke for normal S1 beats that correspond to activation time for normal S1 beats;
- detect and save the last index of AP downstroke for normal S1 beat that correspond to repolarization time for normal S1 beats;
- detect and save the first index of AP upstroke for premature S2 beat that correspond to activation time for premature S2 beats;
- detect and save the last index of AP downstroke for premature S2 beats that corresponds to repolarization time for premature S2 beats;

- calculate diastolic interval as the difference between activation time of premature S2 beats and repolarization time of 6th normal S1 beats, and calculate APD as the difference between repolarization time and activation time for premature beats
- calculate the other desired data i.e. three measures of dispersion in activation time, repolarization time, and APD for normal and premature beats, and speed of depolarization conduction for premature beats

For clarity, an example is provided to describe how to detect indices of AP upstroke and AP downstroke based on the previous example. The calculation.m file in this example initially (1) loads the V700 matrix and selects the voltages of the 5th column of the matrix as highlighted in blue in Figure 11; (2) finds the transmembrane voltages above the voltage threshold -65 mV.

Figure 12, shows the detected indices of these transmembrane voltages in the form of two series of continuous number, distinguished by a number greater than 1 (i.e. 701>293+1). The calculation.m file uses this feature to separate the indices of the normal S1 beat from 1 to 293 and the indices of the premature S2 beats from 701 to 790.



References

1. Clayton RH, Influence of cardiac tissue anisotropy on re-entrant activation in computational models of ventricular fibrillation. *Physica D-Nonlinear Phenomena*, 2009. **238**.
2. Bueno-Orovio A and Cherry EM and Fenton FH, Minimal model for human ventricular action potentials in tissue *Journal of Theoretical Biology*, 2008. **235**(3): p. 544-560.
3. Ten Tusscher K.H and Panfilov A.V., Alternans and spiral breakup in a human ventricular tissue model. *Am J Physiol Heart Circ Physiol*, 2006. **291**: p. H1088–H1100.
4. Li GR and Yang B and Feng J and Bosch RF and Carrier M and Nattel S., Transmembrane ICa contributes to rate-dependent changes of action potentials in human ventricular myocytes. *Am J Physiol*, 1999. **276**: p. H98-H106.
5. Clayton RH and Bernus O and Cherry EM and Dierckx H and Fenton FH and Mirabella L and Panfilov AV and Sachse FB and Seemann G and Zhang H., Models of cardiac tissue electrophysiology: Progress, challenges and open questions. *Progress in Biophysics and Molecular Biology*, 2010. **104**: p. 22-48.
6. M Lieberman and T Sawanobori and JM Kootsey and EA Johnson., A synthetic strand of cardiac muscle: its passive electrical properties. *J Gen Physiol*, 1975. **65**: p. 527-550.
7. Panfilov AV and Keener JP, Re-entry in three-dimensional Fitzhugh-Nagumo medium with rotational anisotropy. *Physica D*, 1995. **84**: p. 545–552.
8. Saffitz JE and Kanter HL and Green KG and Tolley TK and Beyer EC, Tissue-specific determinants of anisotropic conduction velocity in canine atrial and ventricular myocardium. *Circulation Research*, 1994. **74**.
9. Luke RA and Saffitz JE, Remodeling of ventricular conduction pathways in healed canine infarct border zones. *J Clin Invest* 1991. **87**: p. 1594–1602.
10. The university of Sheffield. Iceberg high performance computing cluster. Available from: <http://www.shef.ac.uk/wrgrid/iceberg>.
11. The university of Sheffield. Submitting Jobs and the Sun Grid Engine. Available from: <http://www.shef.ac.uk/wrgrid/using/runapps>.
12. Cooper M. Advanced Bash-Scripting Guide. 27 Nov 2012; Available from: <http://tldp.org/LDP/abs/html/>.

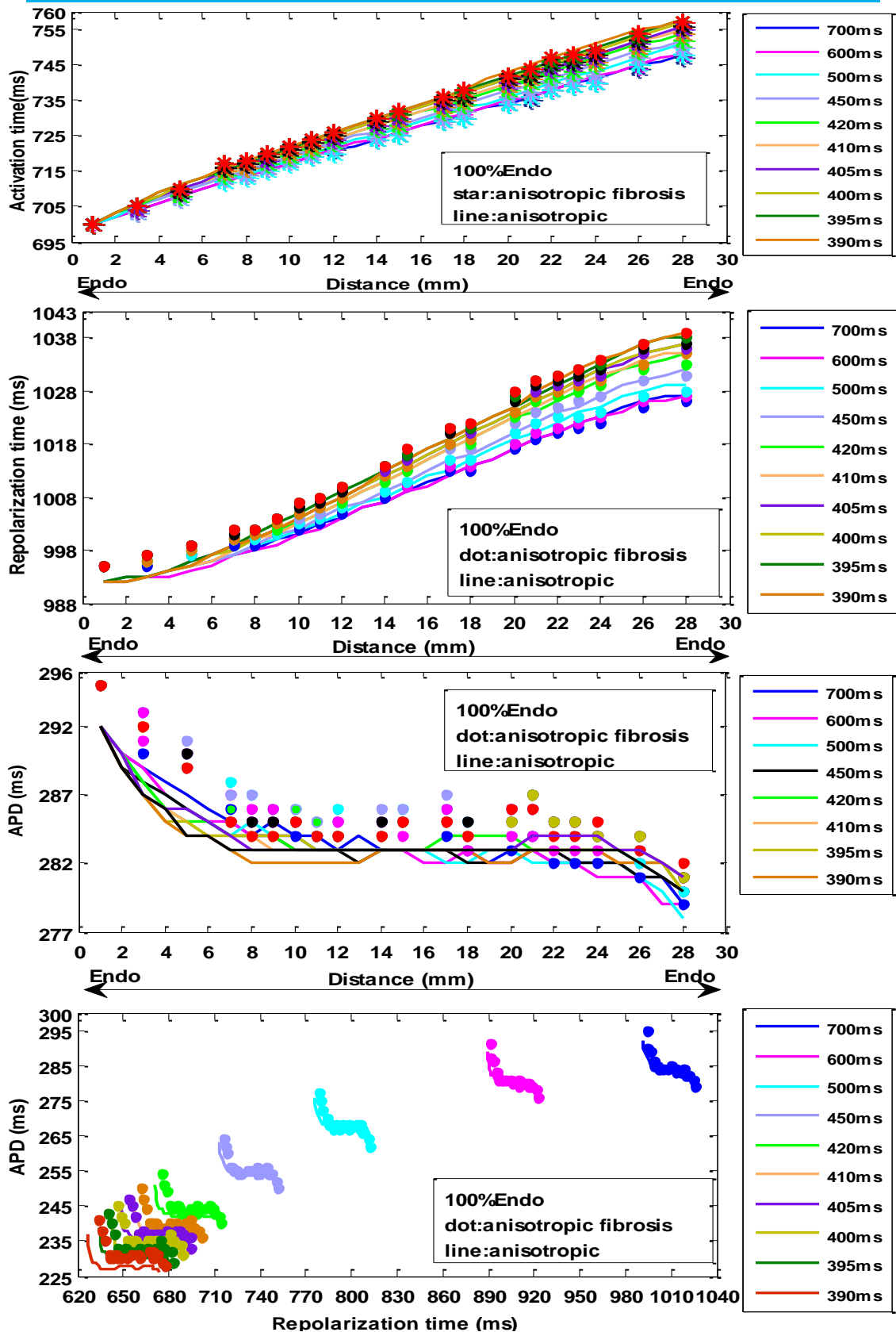
Appendix 1

Group P: Profiles of anisotropic & anisotropic fibrosis tissues

Figure P1 to P43 show spatial profiles of (1) activation time; (2) repolarization time; (3) APD; and (4) profiles of APD against repolarization time for anisotropic tissues with and without fibrosis with the TP06 model.

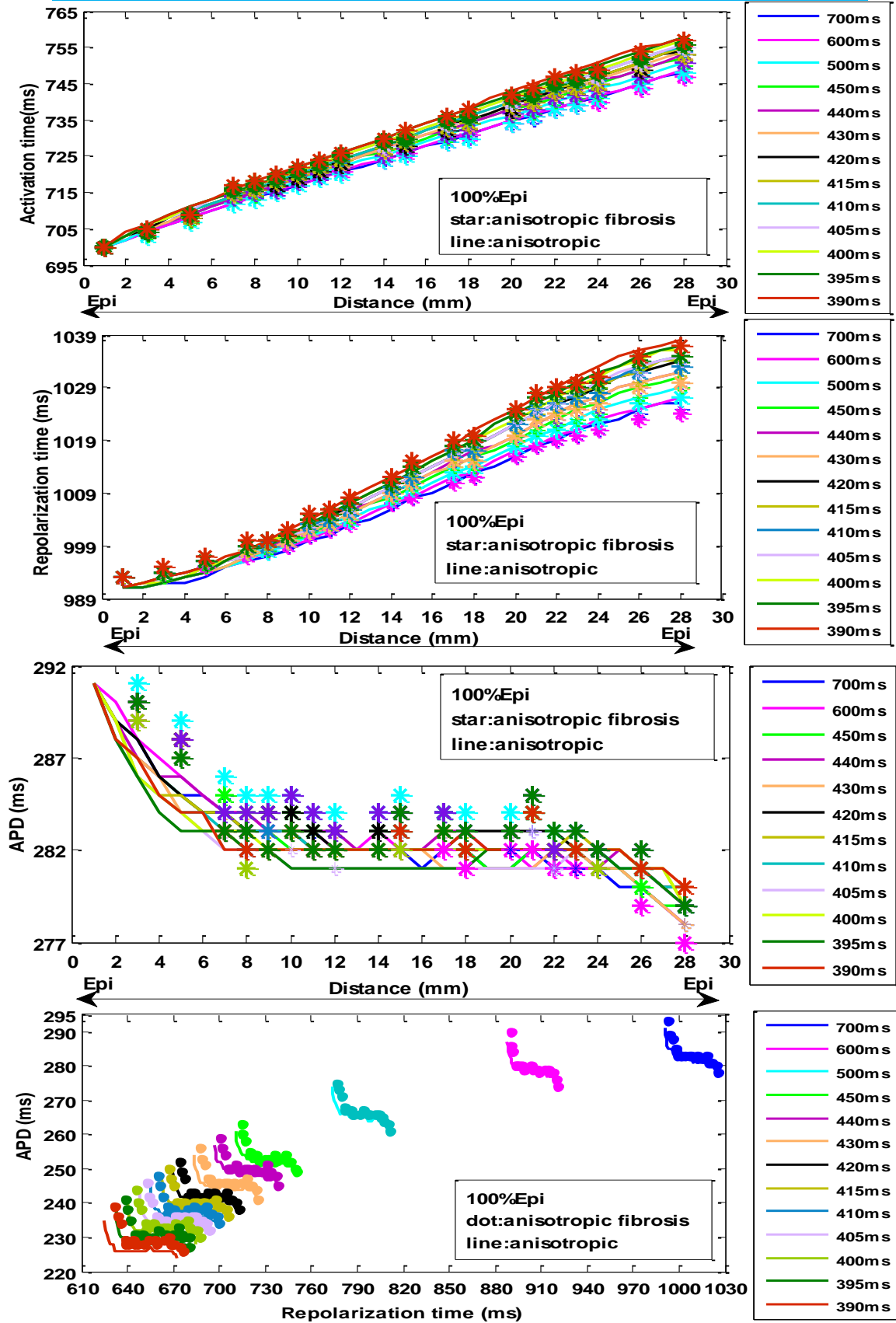
1 cell type

Group P: TP06 model of anisotropic & anisotropic fibrosis endocardial tissue



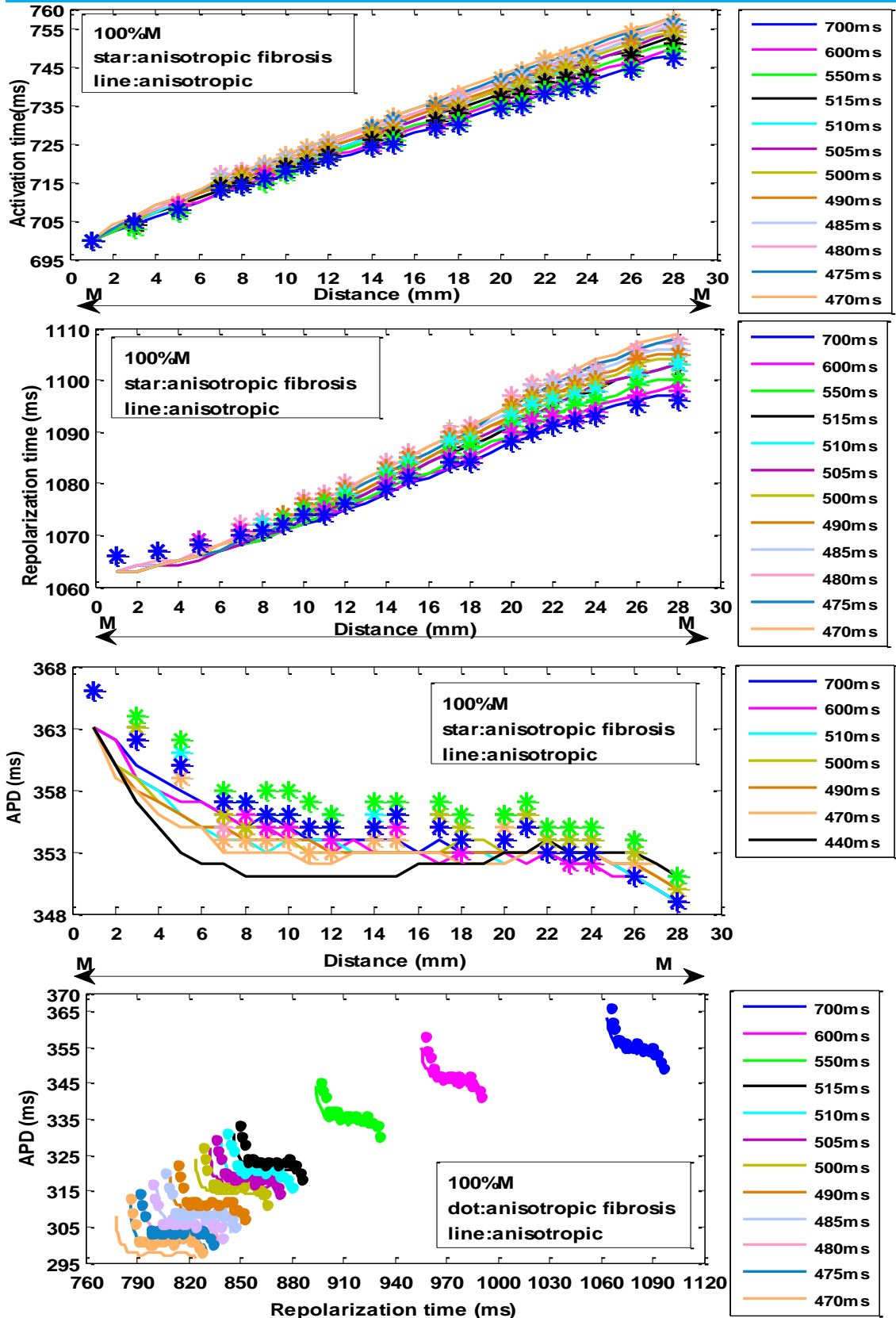
Figures P1-P4: Spatial profiles of activation time, repolarization time, and APD and profiles of APD against repolarization time in 3D anisotropic homogenous endocardial tissues with and without fibrosis paced from the bottom edge of tissue

Group P: TP06 model of anisotropic & anisotropic fibrosis epicardial tissue



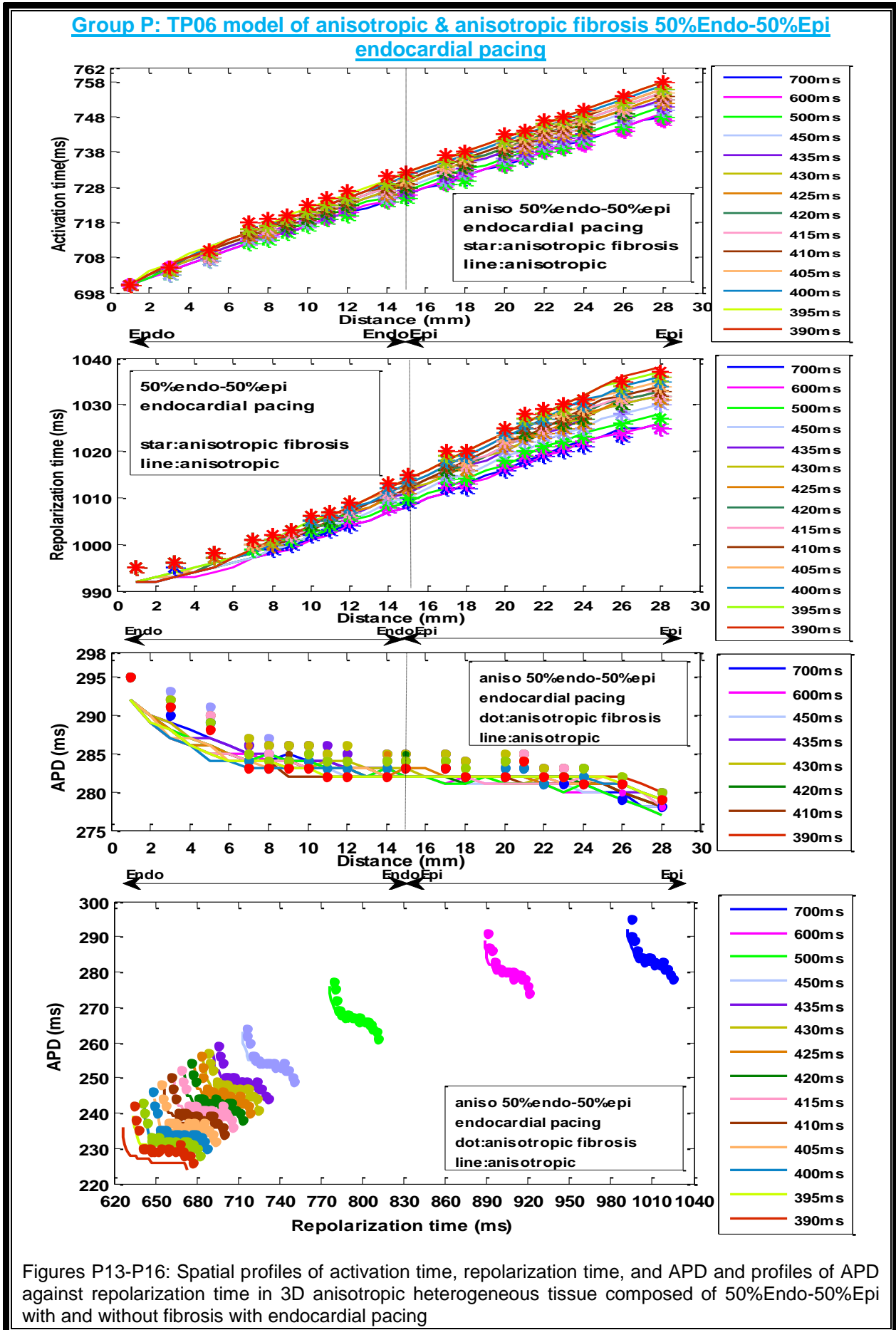
Figures P5-P8: Spatial profiles of activation time, repolarization time, and APD and profiles of APD against repolarization time in 3D anisotropic homogenous epicardial tissues with and without fibrosis paced from the bottom edge of tissue

Group P: TP06 model of anisotropic & anisotropic fibrosis mid-myocardial tissue

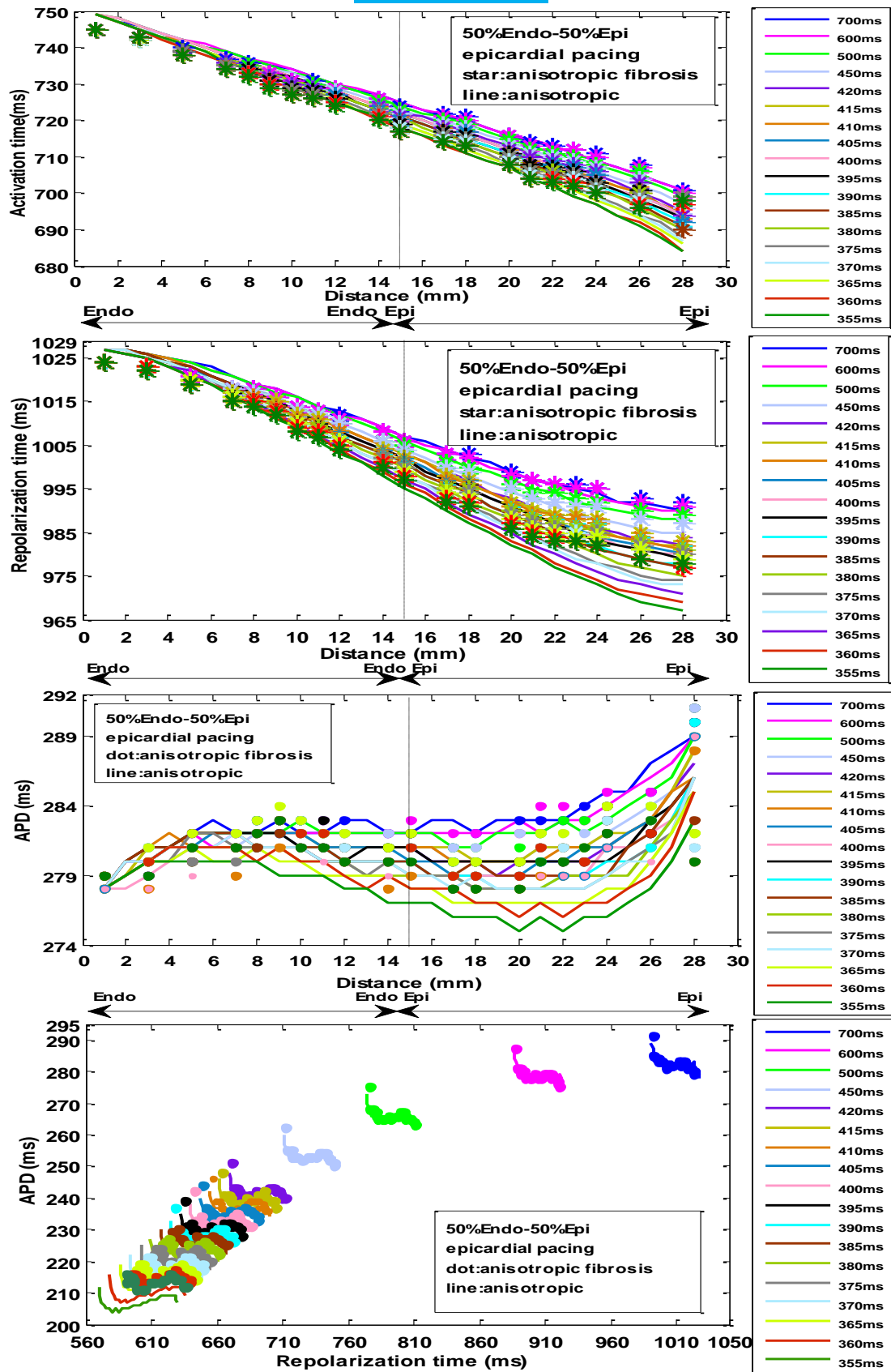


Figures P9-P12: Spatial profiles of activation time, repolarization time, and APD and profiles of APD against repolarization time in 3D anisotropic homogenous mid-myocardial tissues with and without fibrosis paced from the bottom edge of tissue

2 cell type



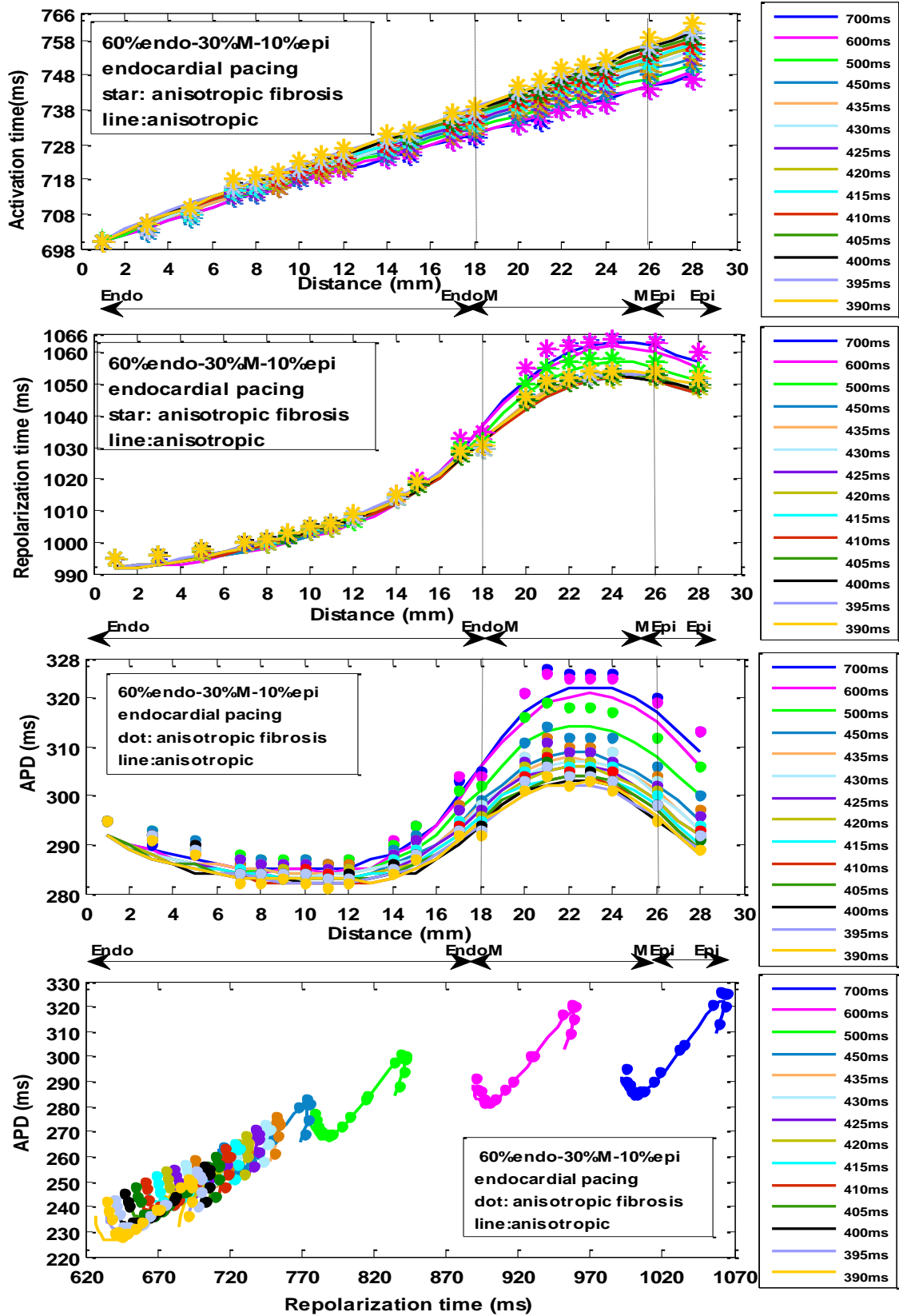
**Group P: TP06 model of anisotropic & anisotropic fibrosis 50%Endo-50%Epi
epicardial pacing**



Figures P16-P19: Spatial profiles of activation time, repolarization time, and APD and profiles of APD against repolarization time in 3D anisotropic heterogeneous tissue composed of 50%Endo-50%Epi with and without fibrosis with epicardial pacing

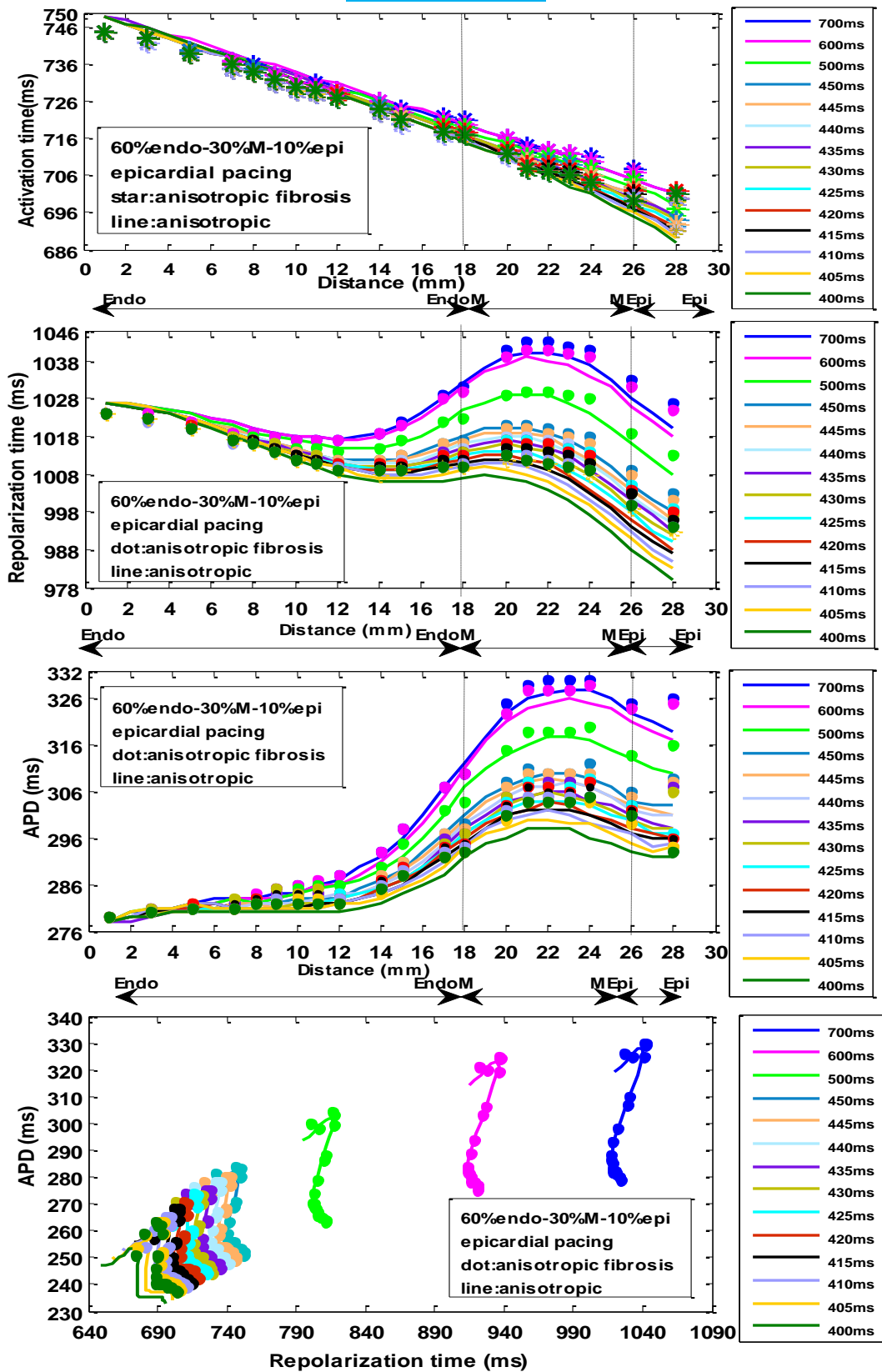
3 cell type (30%M-10%Epi)

Group P: TP06 model of anisotropic & anisotropic fibrosis 60%Endo-30%M-10%Epi endocardial pacing



Figures P20-P23: Spatial profiles of activation time, repolarization time, and APD and profiles of APD against repolarization time in 3D anisotropic heterogeneous tissue composed of 60%Endo-30%M-10%Epi with and without fibrosis with endocardial pacing

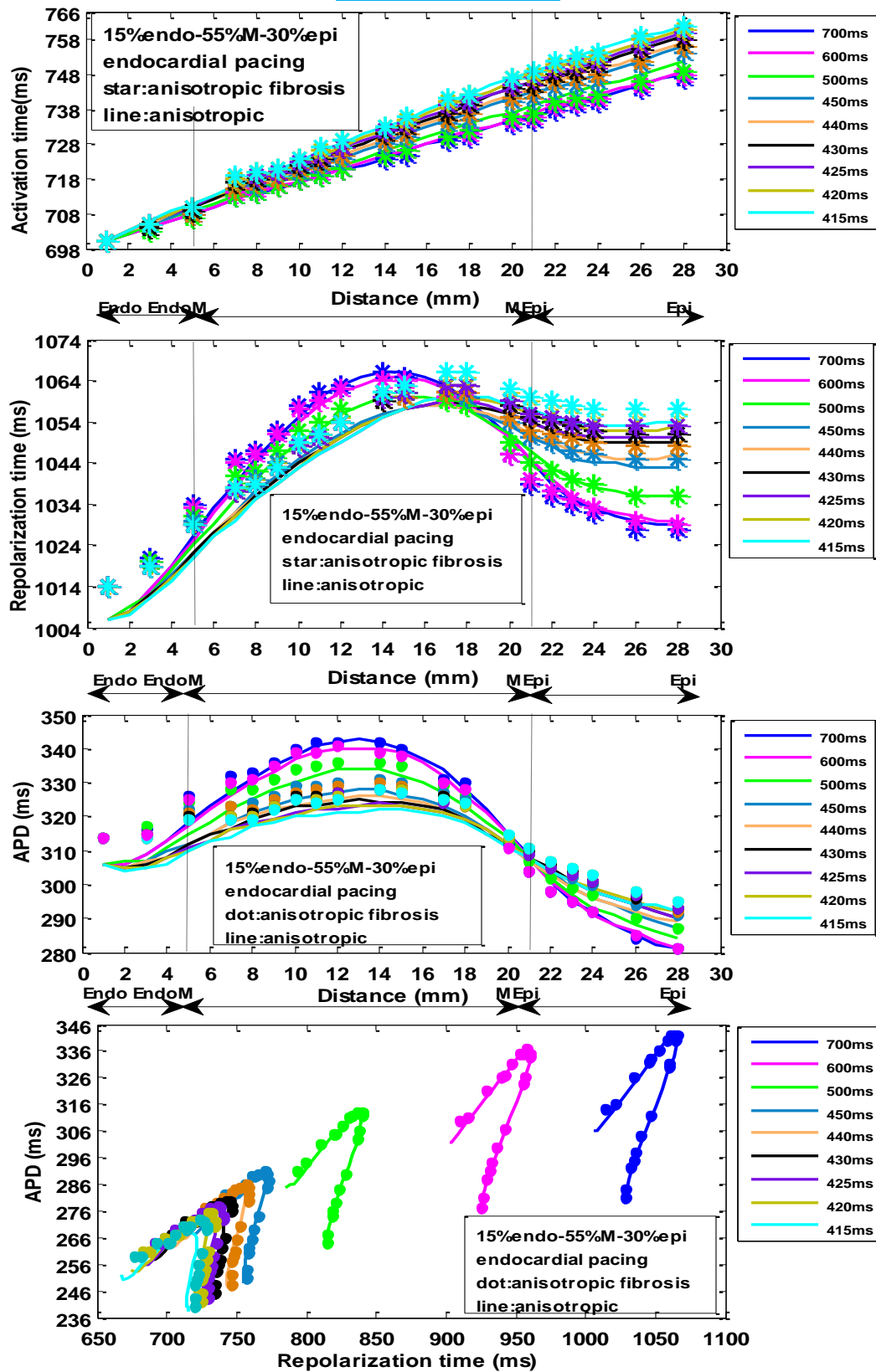
Group P: TP06 model of anisotropic & anisotropic fibrosis 60%Endo-30%M-10%Epi
epicardial pacing



Figures P24-P27: Spatial profiles of activation time, repolarization time, and APD and profiles of APD against repolarization time in 3D anisotropic heterogeneous tissue composed of 60%Endo-30%M-10%Epi with and without fibrosis with epicardial pacing

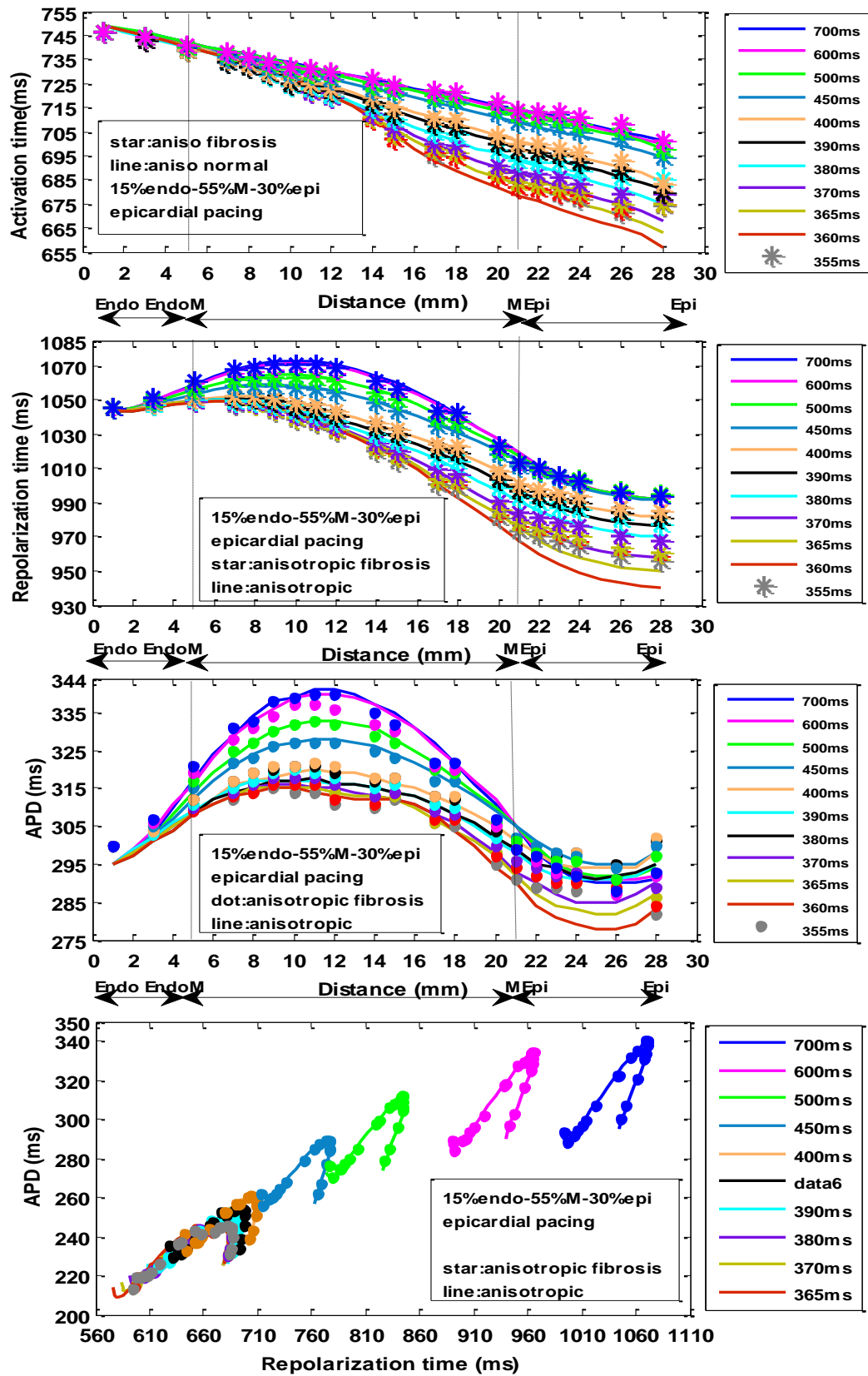
3 cell type (55%M)

Group P: TP06 model of anisotropic & anisotropic fibrosis 15%Endo-55%M-30%Epi endocardial pacing



Figures P28-P31: Spatial profiles of activation time, repolarization time, and APD and profiles of APD against repolarization time in 3D anisotropic heterogeneous tissue composed of 15%Endo-55%M-30%Epi with and without fibrosis with endocardial pacing

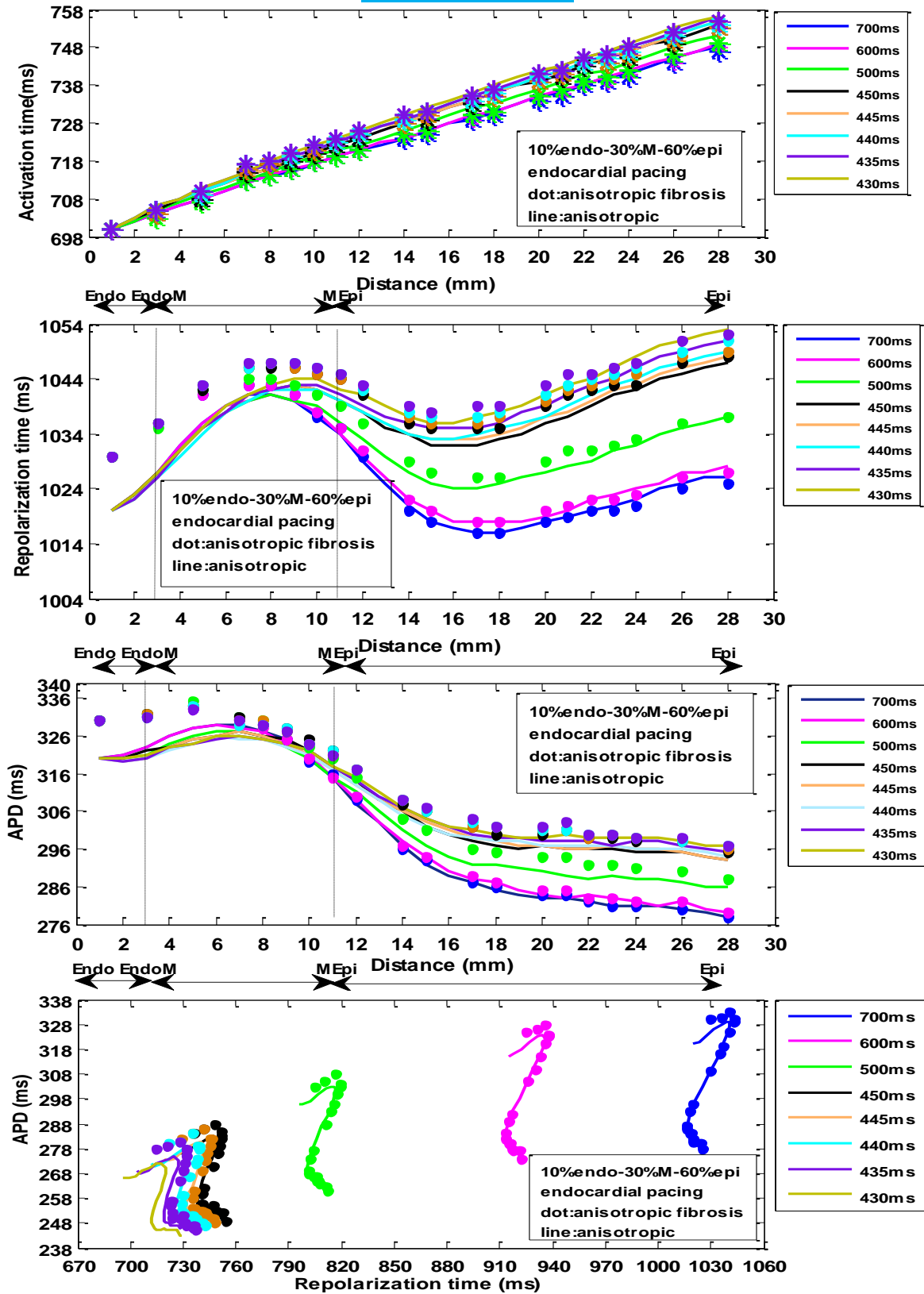
Group P: TP06 model of anisotropic & anisotropic fibrosis 15%Endo-55%M-30%Epi
epicardial pacing



Figures P32-P35: Spatial profiles of activation time, repolarization time, and APD and profiles of APD against repolarization time in 3D anisotropic heterogeneous tissue composed of 15%Endo-55%M-30%Epi with and without fibrosis with epicardial pacing

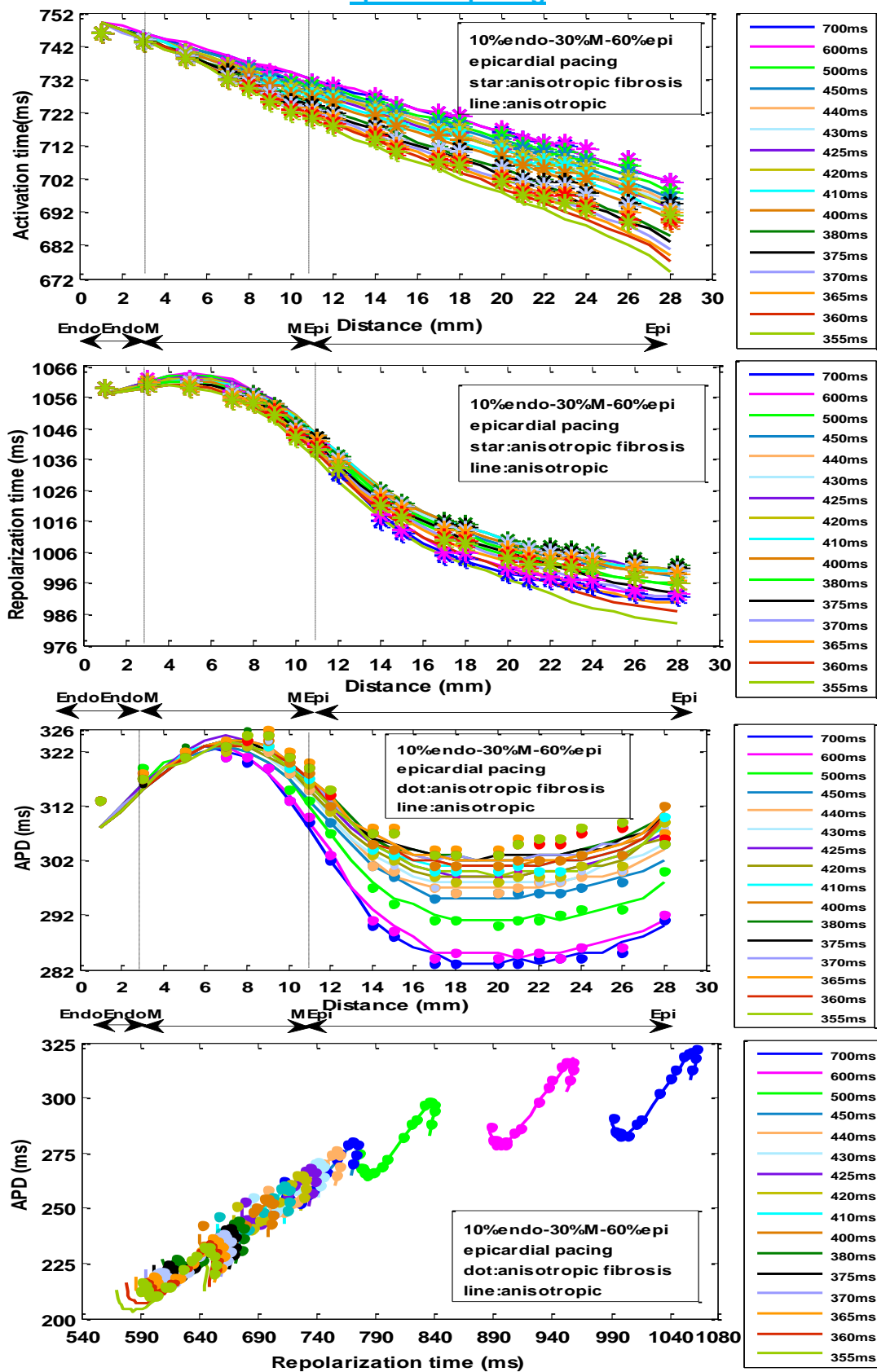
3 cell type (30%M-60%Epi)

Group P: TP06 model of anisotropic & anisotropic fibrosis 10%Endo-30%M-60%Epi endocardial pacing



Figures P36-P39: Spatial profiles of activation time, repolarization time, and APD and profiles of APD against repolarization time in 3D anisotropic heterogeneous tissue composed of 10%Endo-30%M-60%Epi with and without fibrosis with endocardial pacing

Group P: TP06 model of anisotropic & anisotropic fibrosis 10%Endo-30%M-60%Epi
epicardial pacing



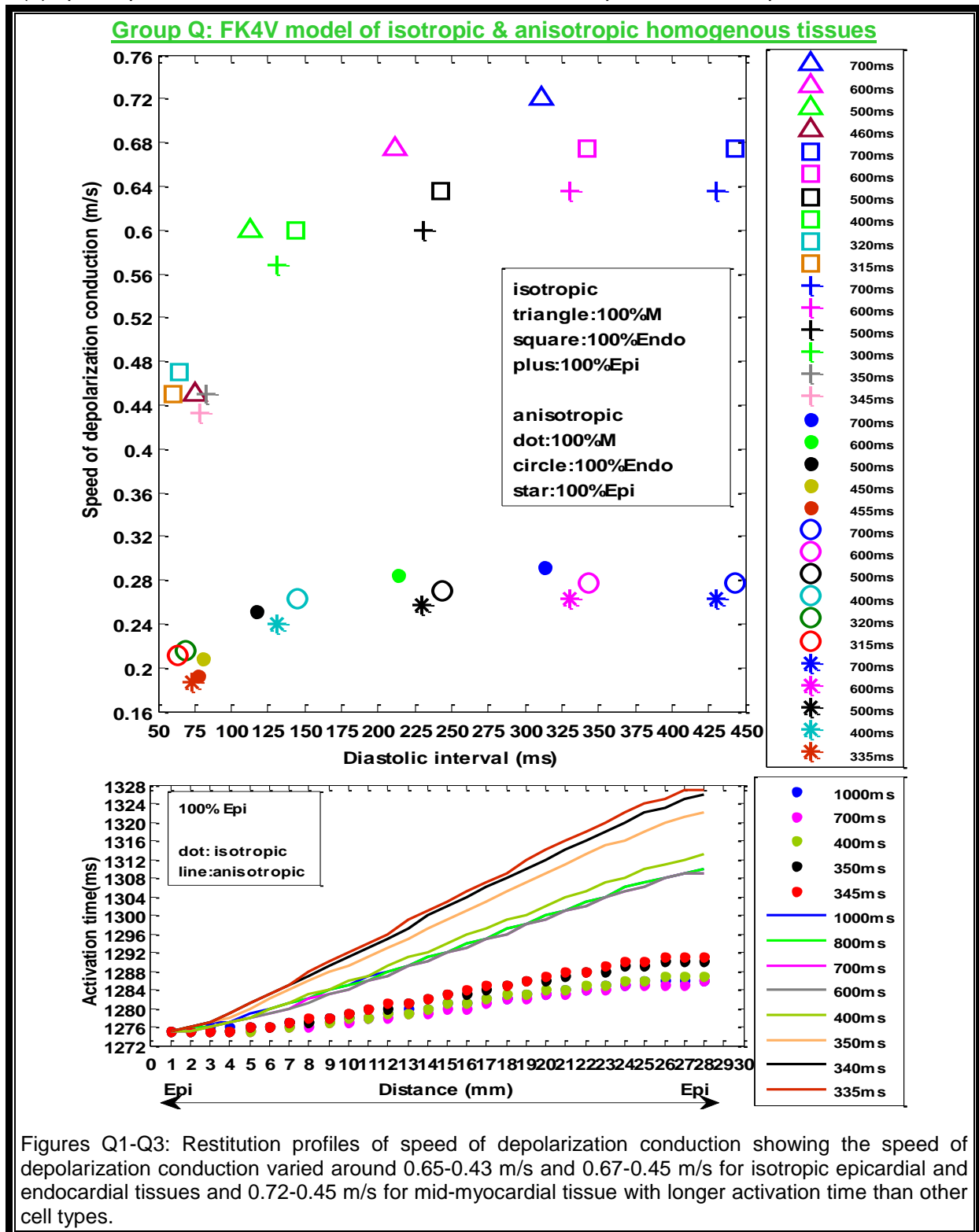
Figures P40-P43: Spatial profiles of activation time, repolarization time, and APD and profiles of APD against repolarization time in 3D anisotropic heterogeneous tissue composed of 10%Endo-30%M-60%Epi with and without fibrosis with epicardial pacing

Group Q: Profiles of speed of depolarization conduction1

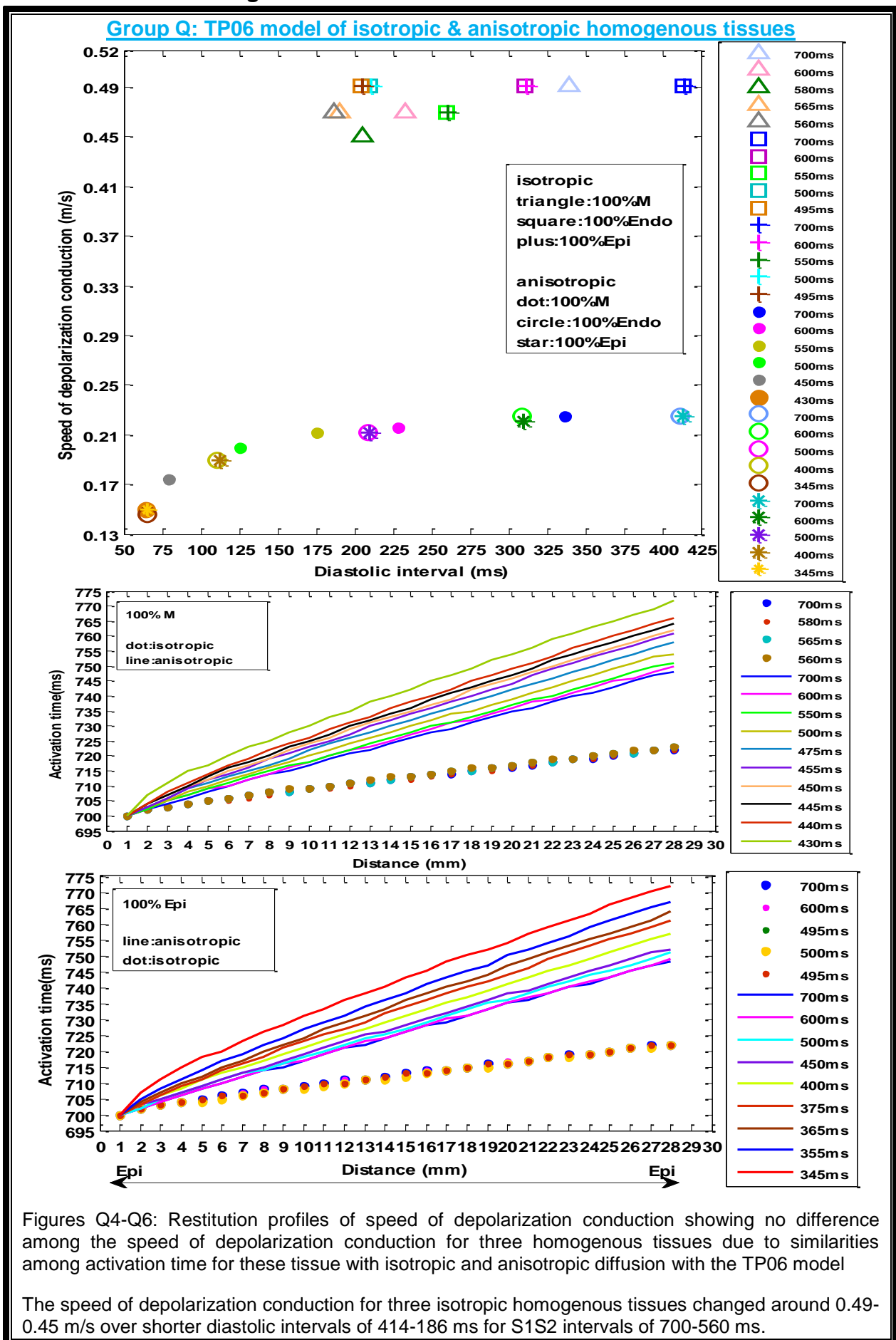
1 cell type

Fk4V model of homogenous tissues

Figure Q1 to Q38 show (1) restitution profiles of speed of depolarization conduction and (2) spatial profiles of activation time for tissues with isotropic and anisotropic diffusions.

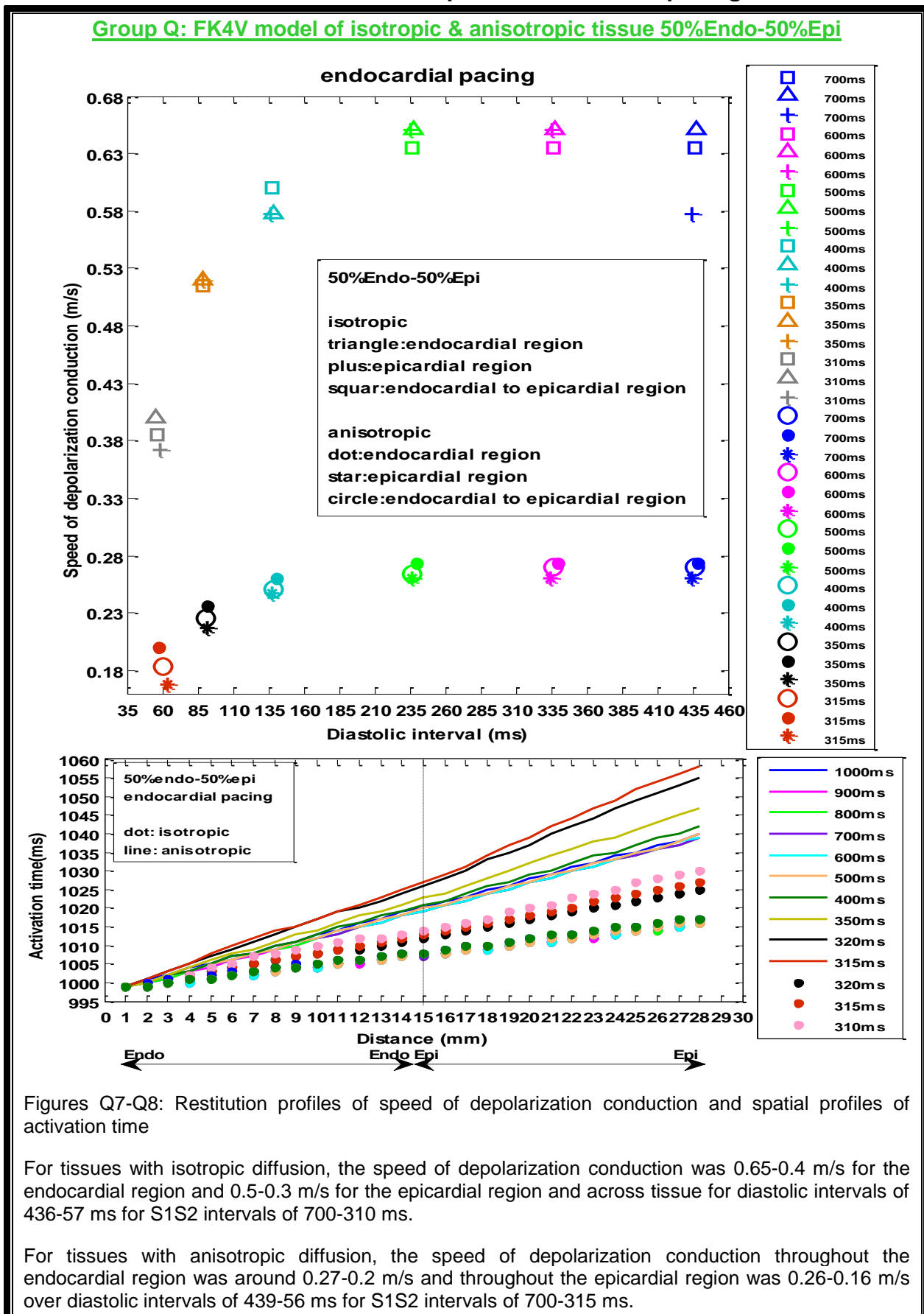


TP06 model of homogenous tissues



2 cell type

FK4V model of tissue 50%Endo-50%Epi with endocardial pacing



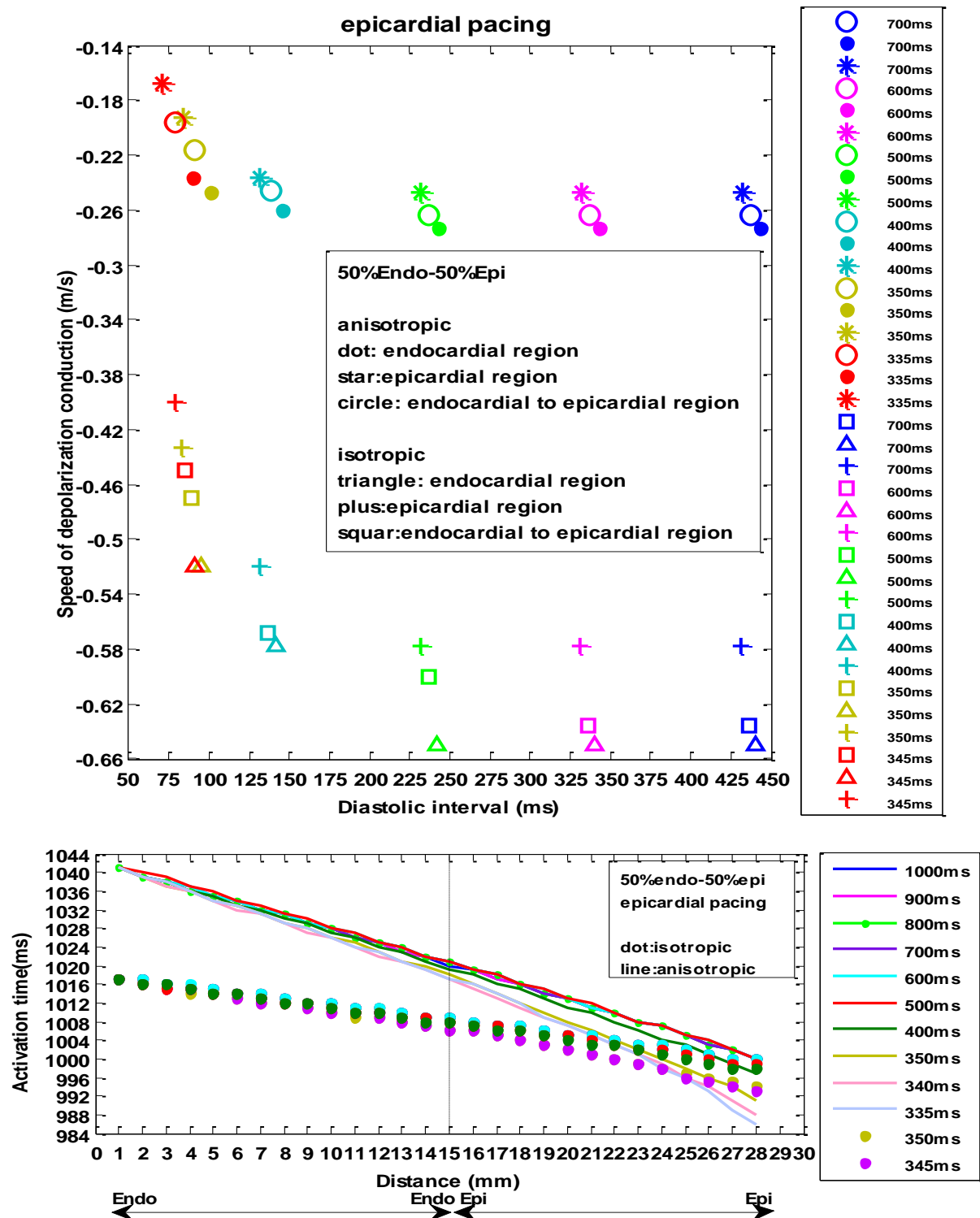
Figures Q7-Q8: Restitution profiles of speed of depolarization conduction and spatial profiles of activation time

For tissues with isotropic diffusion, the speed of depolarization conduction was 0.65-0.4 m/s for the endocardial region and 0.5-0.3 m/s for the epicardial region and across tissue for diastolic intervals of 436-57 ms for S1S2 intervals of 700-310 ms.

For tissues with anisotropic diffusion, the speed of depolarization conduction throughout the endocardial region was around 0.27-0.2 m/s and throughout the epicardial region was 0.26-0.16 m/s over diastolic intervals of 439-56 ms for S1S2 intervals of 700-315 ms.

FK4V model of 50%Endo-50%Epi with epicardial pacing

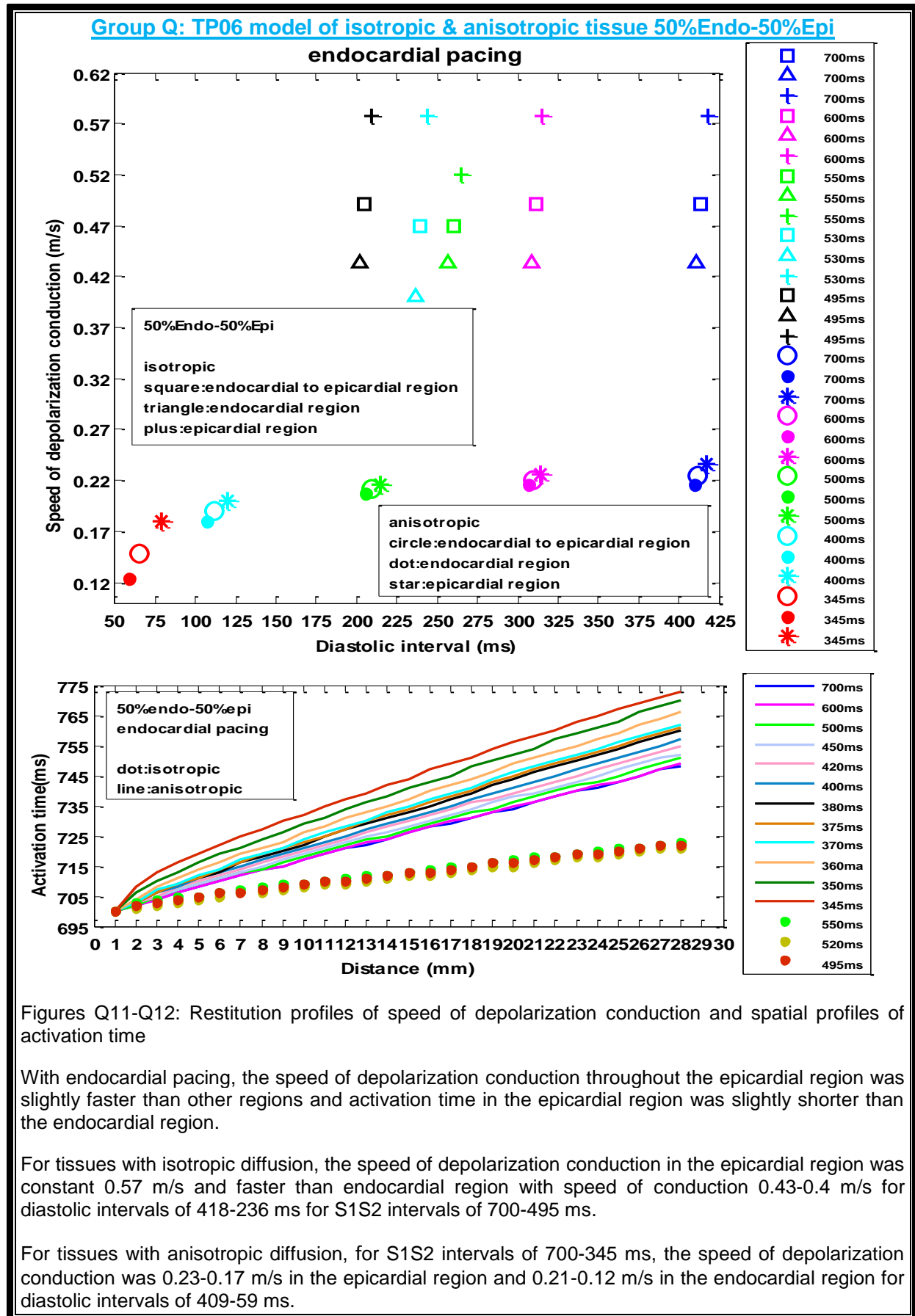
Group Q: FK4V model of isotropic & anisotropic tissue 50%Endo-50%Epi



Figures Q9-Q10: Restitution profiles of speed of depolarization conduction and spatial profiles of activation time

Endocardial region had shorter activation time and faster speed of depolarization conduction than the epicardial region of tissues with isotropic and anisotropic diffusion.

TP06 model of 50%Endo-50%Epi with endocardial pacing



Group Q: TP06 model of isotropic & anisotropic tissue 50%Endo-50%Epi

epicardial pacing

Speed of depolarization conduction (m/s)

Diastolic interval (ms)

50%Endo-50%Epi

anisotropic
square: endocardial to epicardial region
triangle: endocardial region
plus: epicardial region

isotropic
circle: endocardial to epicardial region
dot: endocardial region
star: epicardial region

700ms
700ms
700ms
600ms
600ms
600ms
500ms
500ms
500ms
400ms
400ms
400ms
345ms
345ms
345ms
700ms
700ms
700ms
600ms
600ms
600ms
550ms
550ms
550ms
510ms
510ms
510ms
495ms
495ms
495ms

750
745
740
735
730
725
720
715
710
705
700
695
690
685
680

0 1 2 3 4 5 6 7 8 9 10 11 12 13 14 15 16 17 18 19 20 21 22 23 24 25 26 27 28 29 30

Distance (mm)

50%endo-50%epi
epicardial pacing

dot: isotropic
line: anisotropic

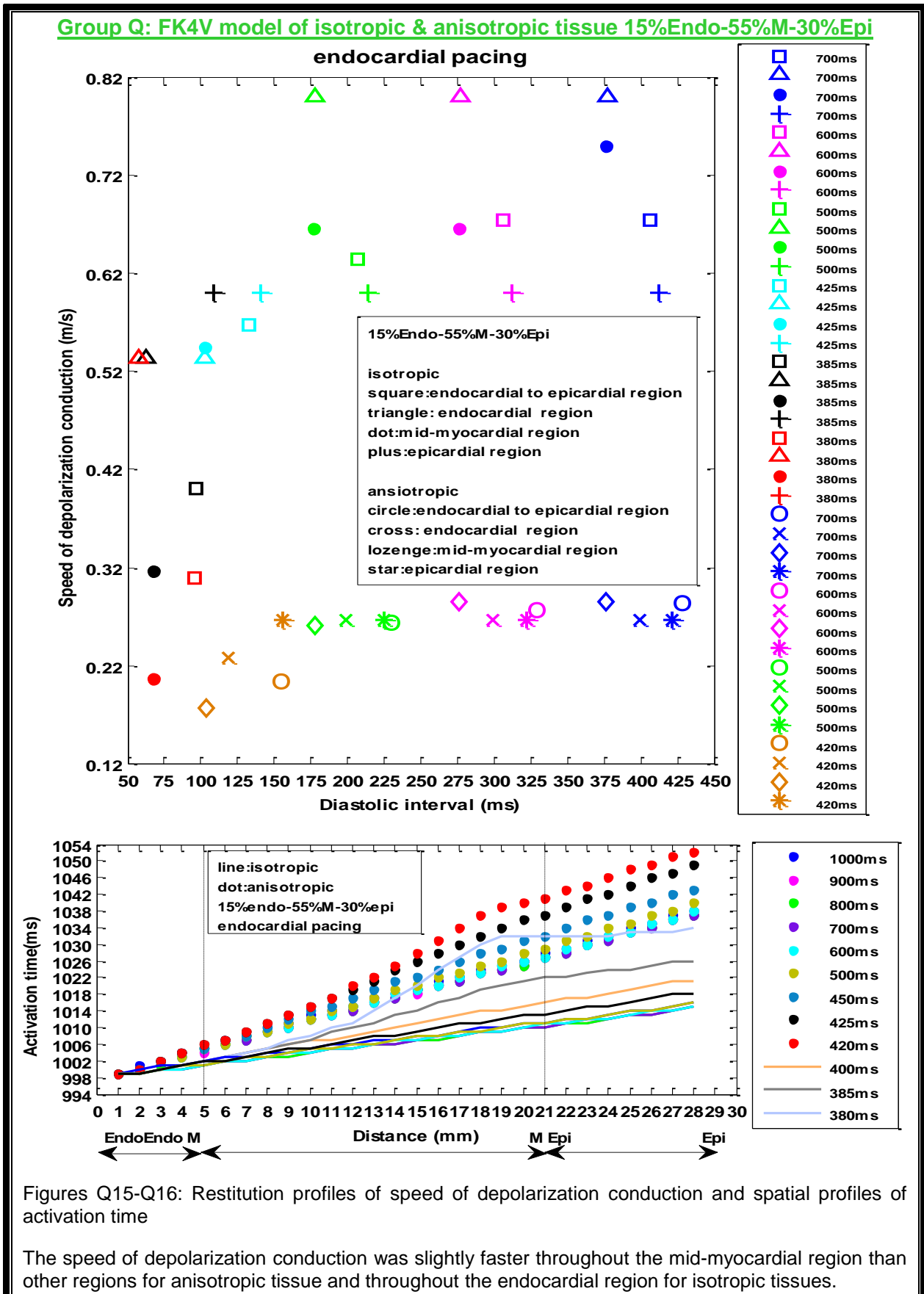
700ms
600ms
500ms
450ms
420ms
405ms
385ms
375ms
360ms
355ms
350ms
345ms
550ms
510ms
495ms

Figures Q13-Q14: Restitution profiles of speed of depolarization conduction and spatial profiles of activation time

With epicardial pacing, the speed of depolarization conduction was faster throughout the endocardial region due to shorter activation time in the endocardial region than the epicardial region.

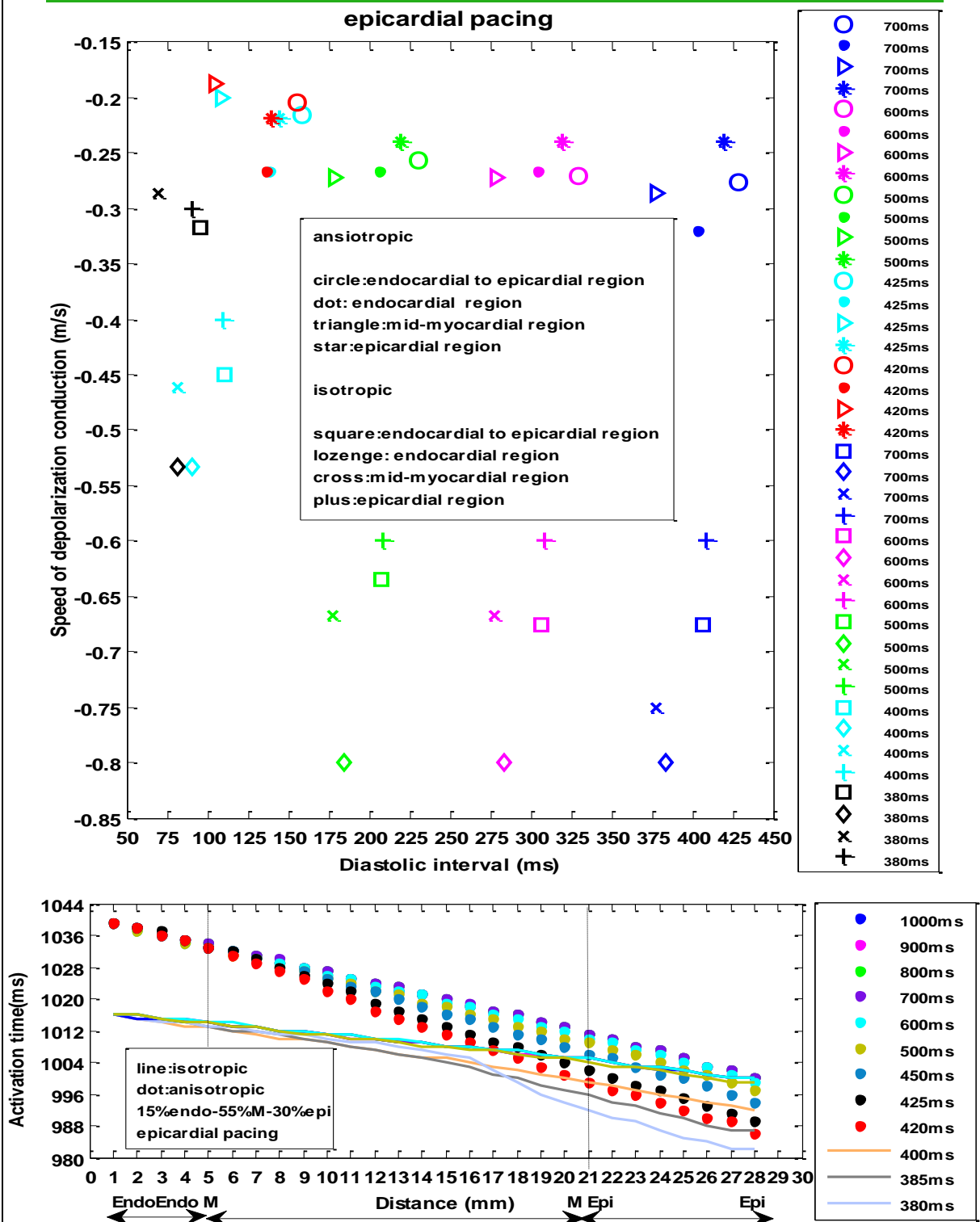
3 cell type (55%M)

FK4V model of 15%Endo-55%M-30%Epi with endocardial pacing



FK4V model of 15%Endo-55%M-30%Epi with epicardial pacing

Group Q: FK4V model of isotropic & anisotropic tissue 15%Endo-55%M-30%Epi



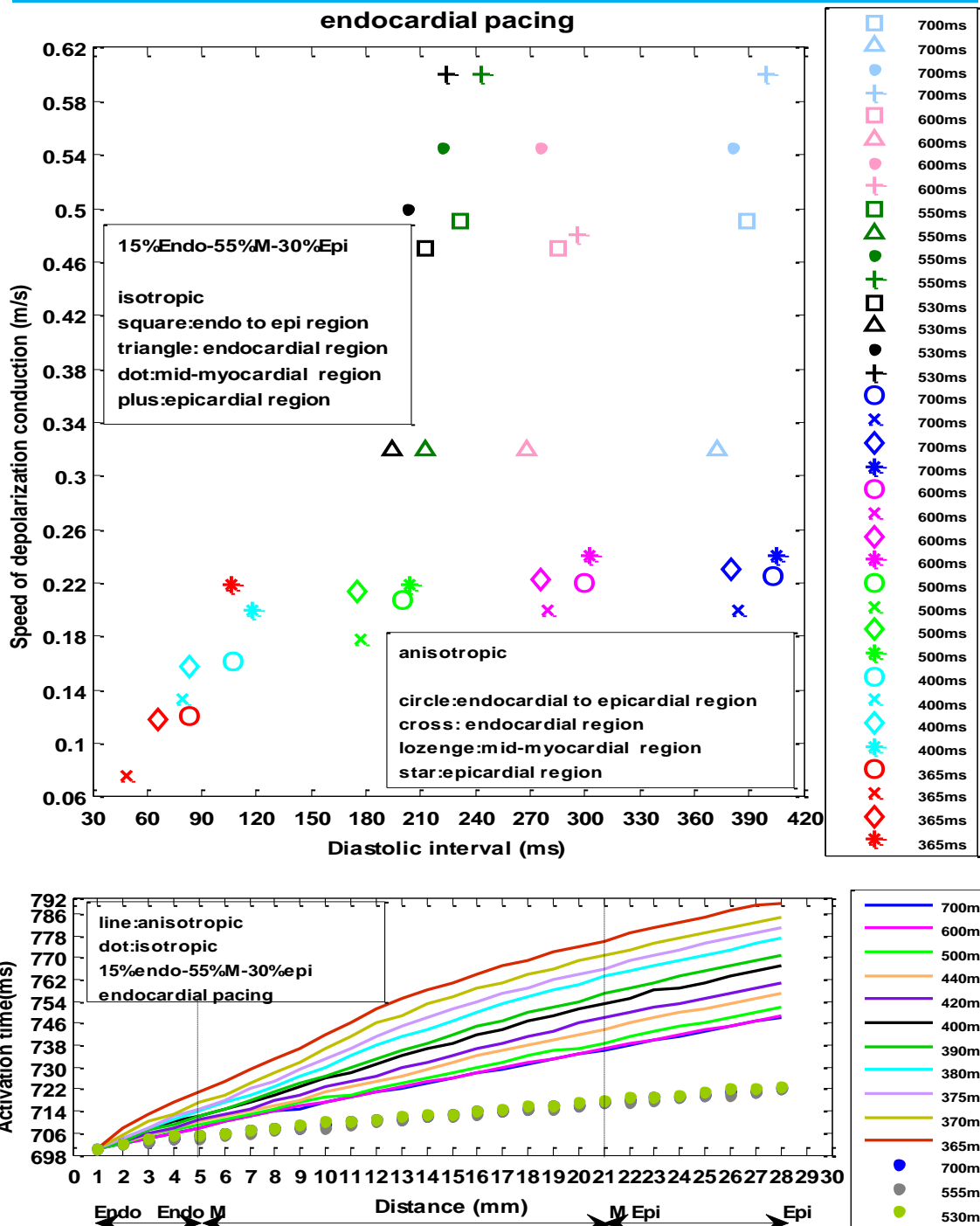
Figures Q17-Q18: Restitution profiles of speed of depolarization conduction and spatial profiles of activation time

In tissues with isotropic diffusion, the speed of depolarization conduction throughout the endocardial region was faster than other regions.

In anisotropic tissue, the speed of depolarization conduction throughout the mid-myocardial region was faster than other regions of tissue.

TP06 model of 15%Endo-55%M-30%Epi with endocardial pacing

Group Q: TP06 model of isotropic & anisotropic tissue 15%Endo-55%M-30%Epi



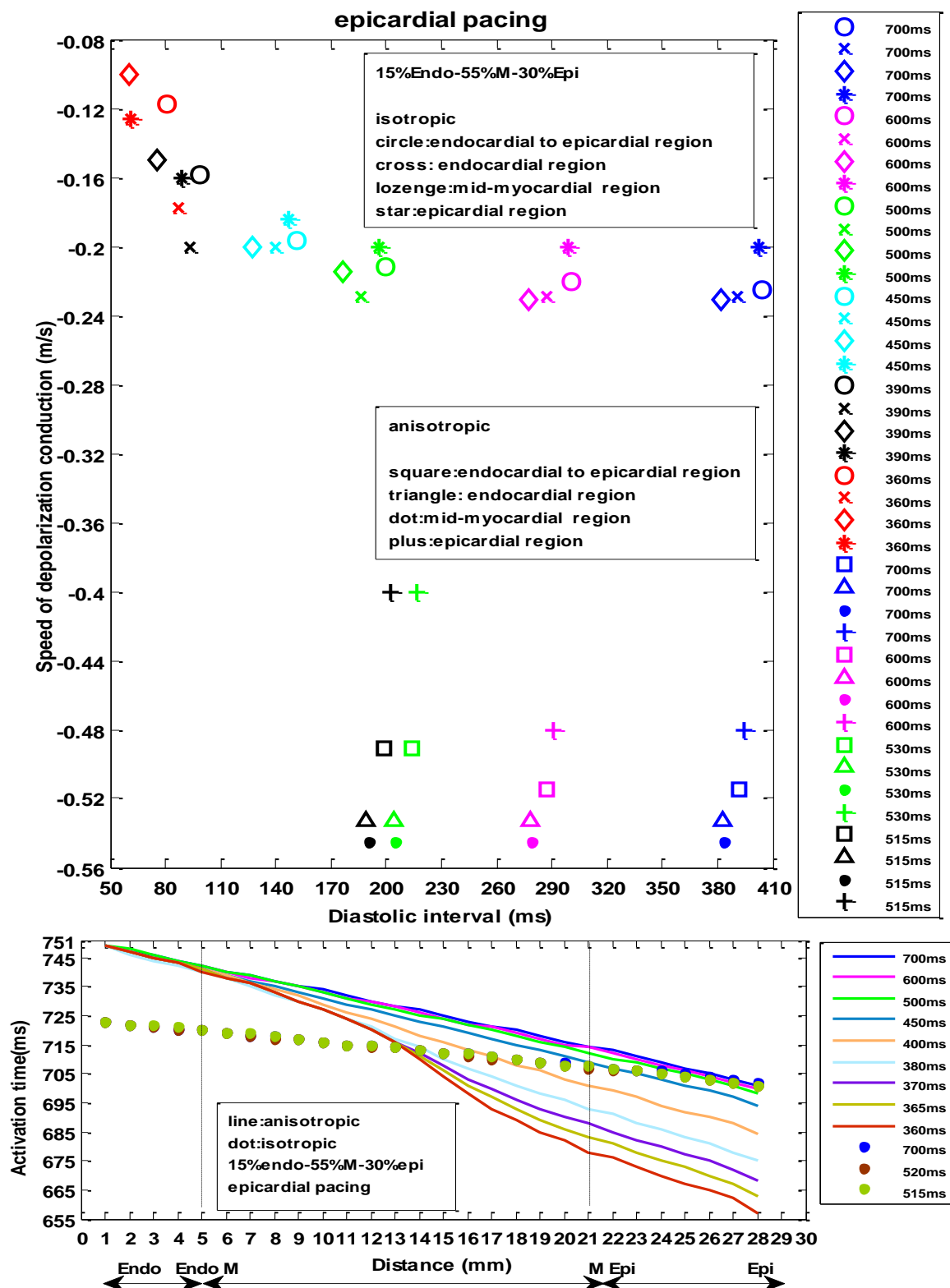
Figures Q19-Q20: Restitution profiles of speed of depolarization conduction and spatial profiles of activation time

For tissue with isotropic diffusion, the speed of depolarization conduction was faster in the epicardial region than other regions and was around 0.6 m/s while the speed of depolarization conduction was slower in the endocardial region than other regions and was around 0.32 m/s over short range of diastolic intervals of 399-194 ms.

For tissue with anisotropic diffusion, the epicardial region had the fastest speed of depolarization conduction around 0.24-0.2 m/s over diastolic intervals of 405-106 ms for S1S2 intervals of 700-365 ms and then the mid-myocardial region with speed of conduction 0.23-0.117 m/s over diastolic intervals of 380-65 ms.

TP06 model of 15%Endo-55%M-30%Epi with epicardial pacing

Group Q: TP06 model of isotropic & anisotropic tissue 15%Endo-55%M-30%Epi



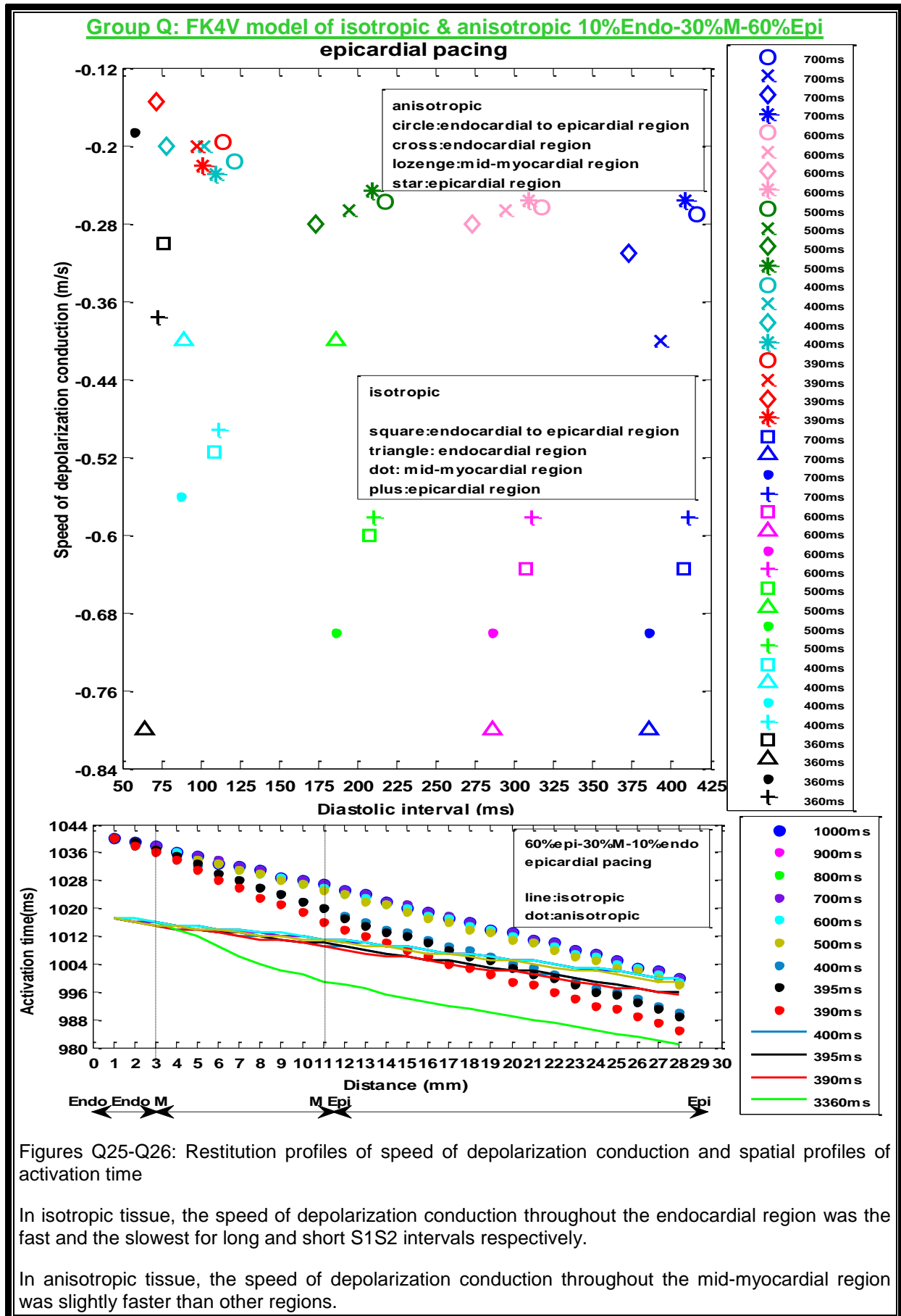
Figures Q20-Q21: Restitution profiles of speed of depolarization conduction and spatial profiles of activation time

In tissues with isotropic and anisotropic diffusions, the speed of depolarization conduction throughout the mid-myocardial region was faster than other regions.

FK4V model of 10%Endo-30%M-60%Epi with endocardial pacing



FK4V model of 10%Endo-30%M-60%Epi with epicardial pacing

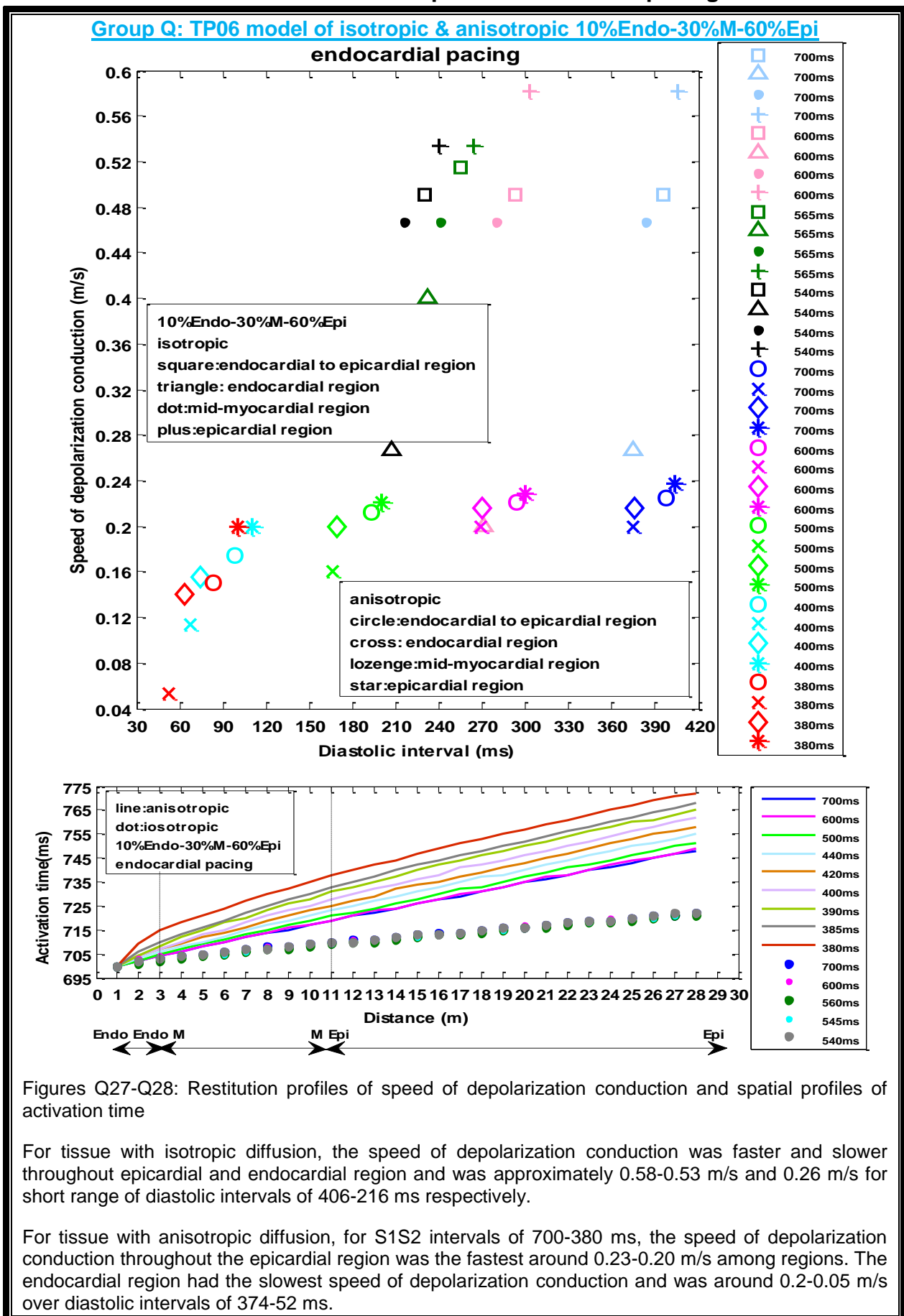


Figures Q25-Q26: Restitution profiles of speed of depolarization conduction and spatial profiles of activation time

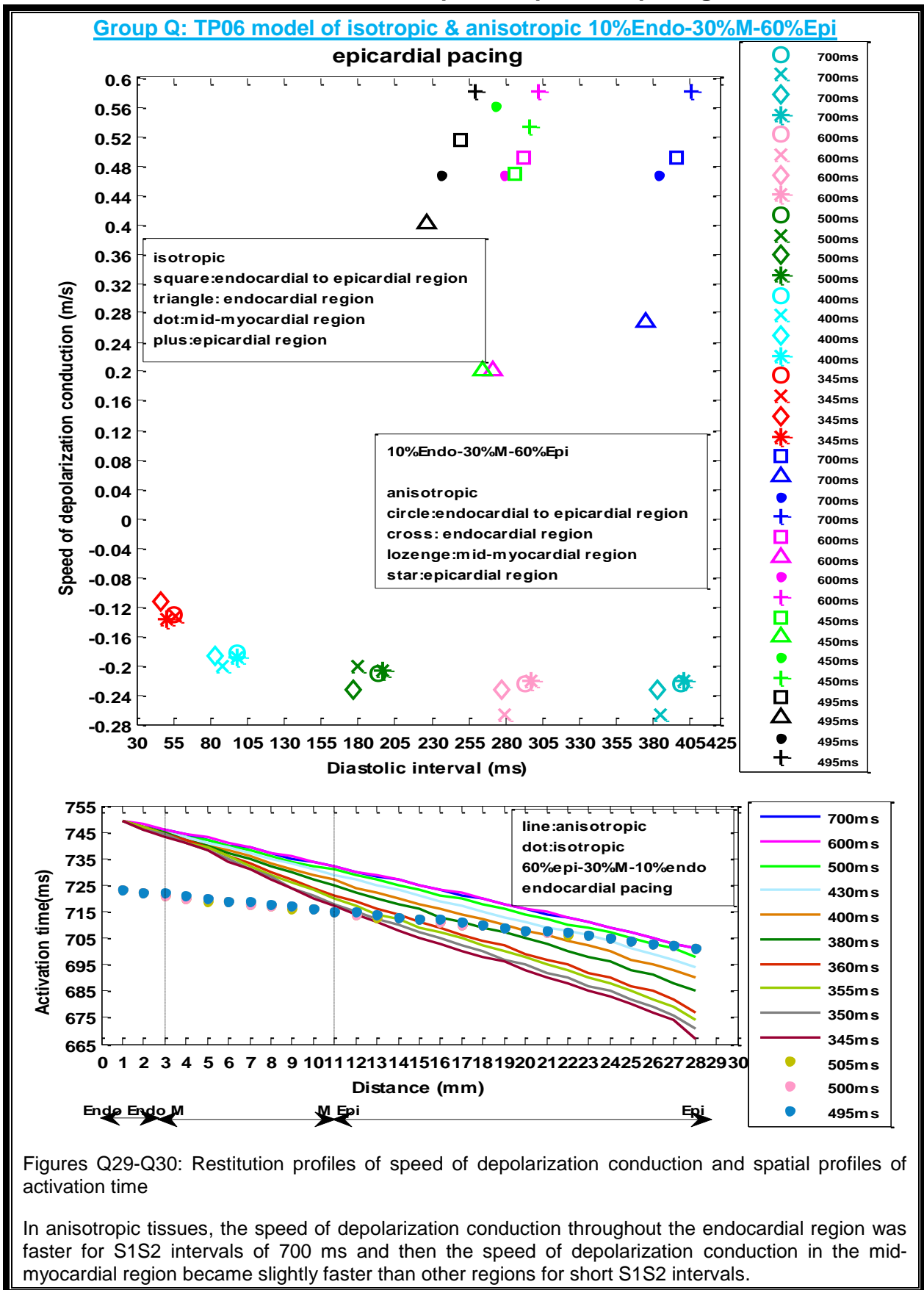
In isotropic tissue, the speed of depolarization conduction throughout the endocardial region was the fast and the slowest for long and short S1S2 intervals respectively.

In anisotropic tissue, the speed of depolarization conduction throughout the mid-myocardial region was slightly faster than other regions.

TP06 model of 10%Endo-30%M-60%Epi with endocardial pacing

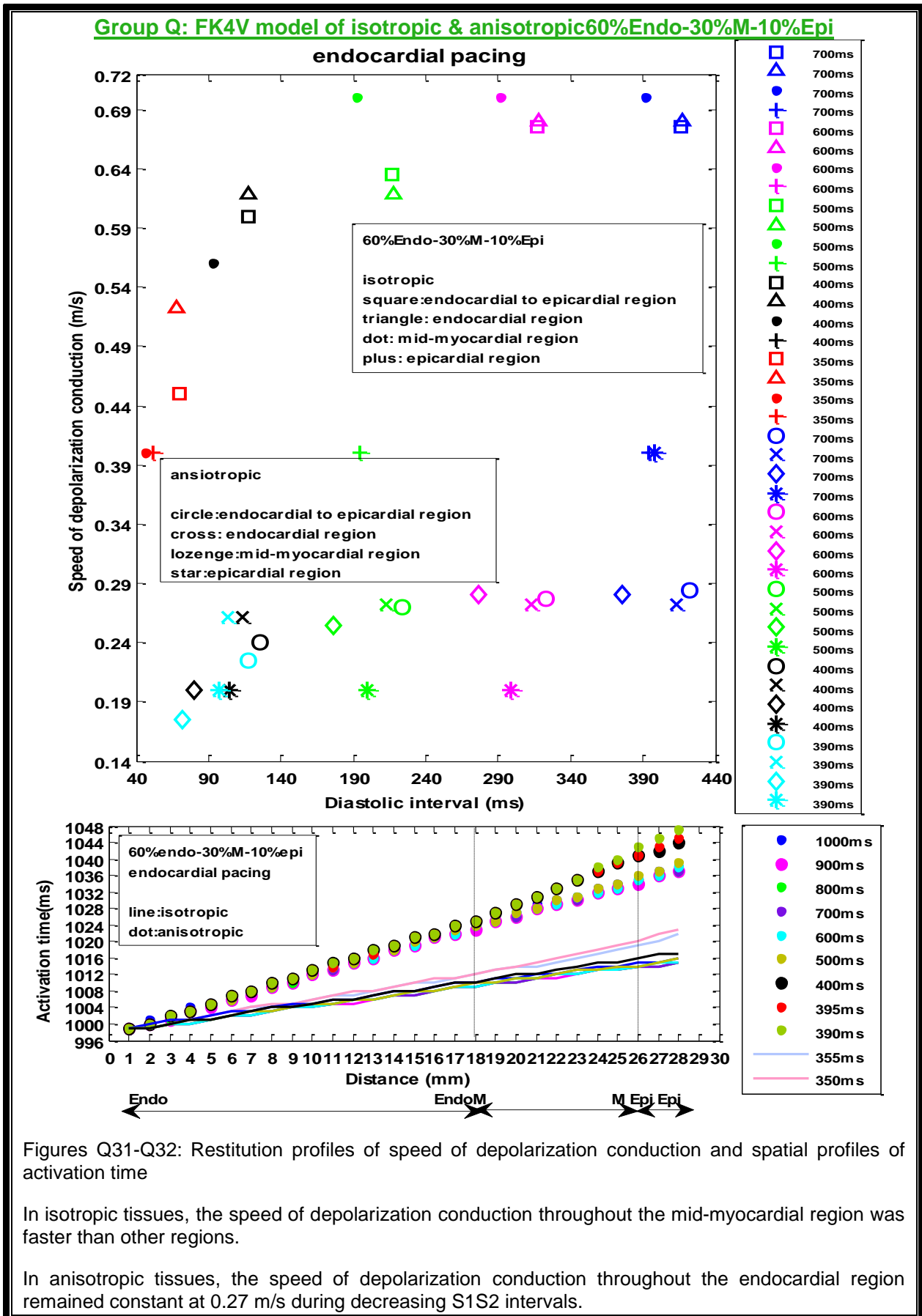


TP06 model of 10%Endo-30%M-60%Epi with epicardial pacing



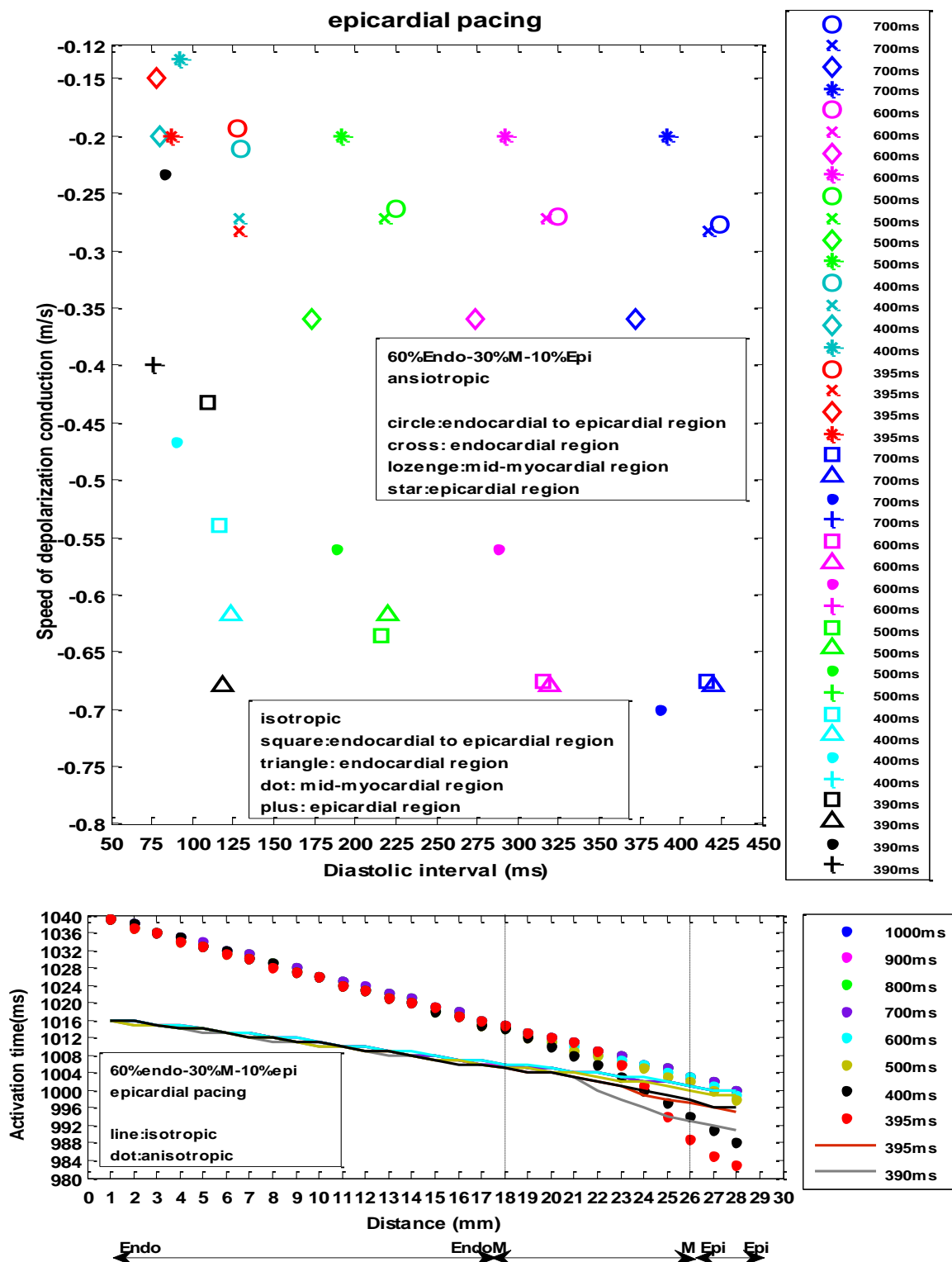
3 cell type (30%M-10%Epi)

FK4V model of 60%Endo-30%M-10%Epi with endocardial pacing



FK4V model of 60%Endo-30%M-10%Epi with epicardial pacing

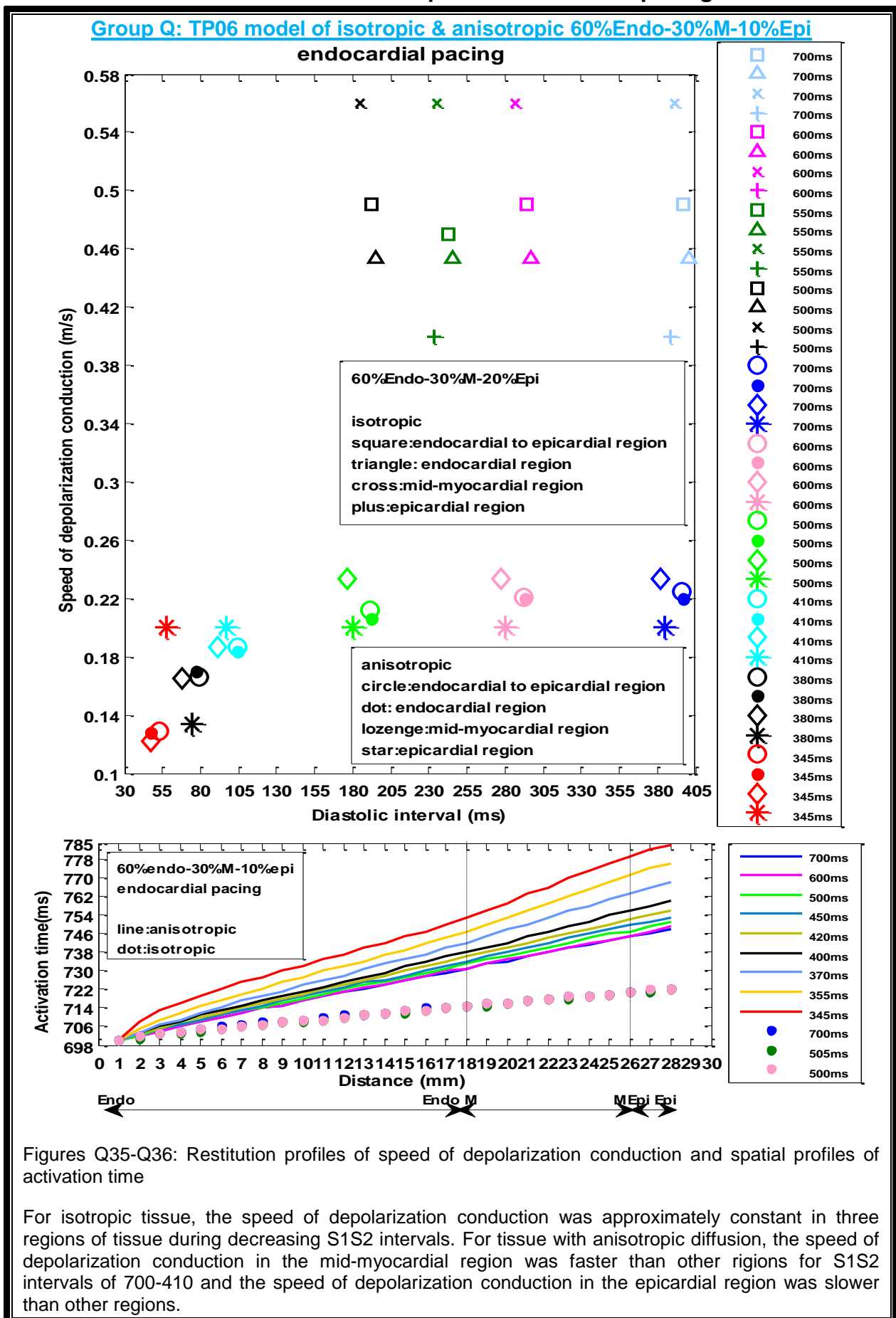
Group Q: FK4V model of isotropic & anisotropic 60%Endo-30%M-10%Epi



Figures Q33-Q34: Restitution profiles of speed of depolarization conduction and spatial profiles of activation time

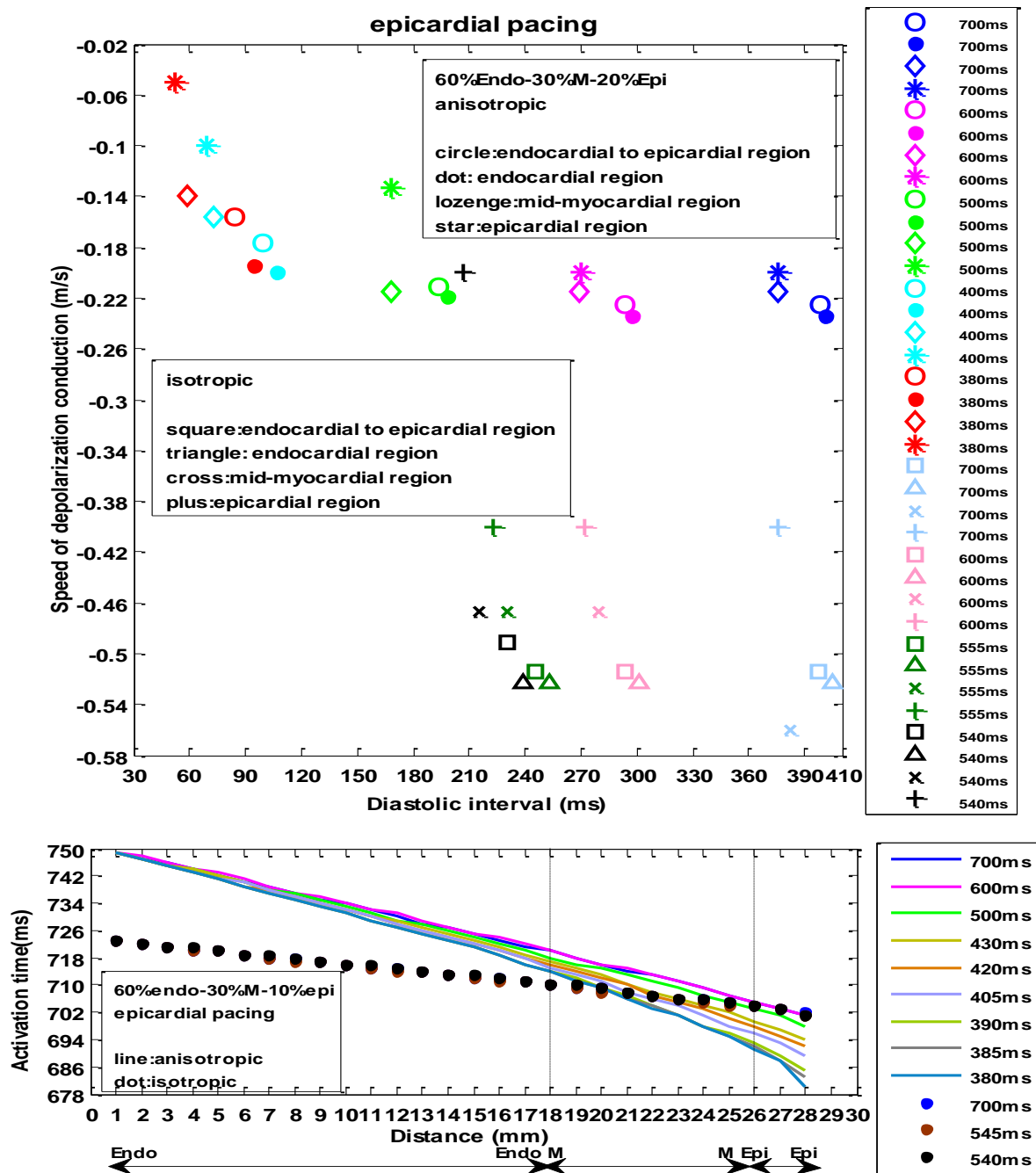
In tissues with anisotropic diffusion, the speed of depolarization conduction throughout the mid-myocardial region was faster than other regions.

TP06 model of 60%Endo-30%M-10%Epi with endocardial pacing



TP06 model of 60%Endo-30%M-10%Epi with epicardial pacing

Group Q: TP06 model of isotropic & anisotropic tissue 60%Endo-30%M-10%Epi



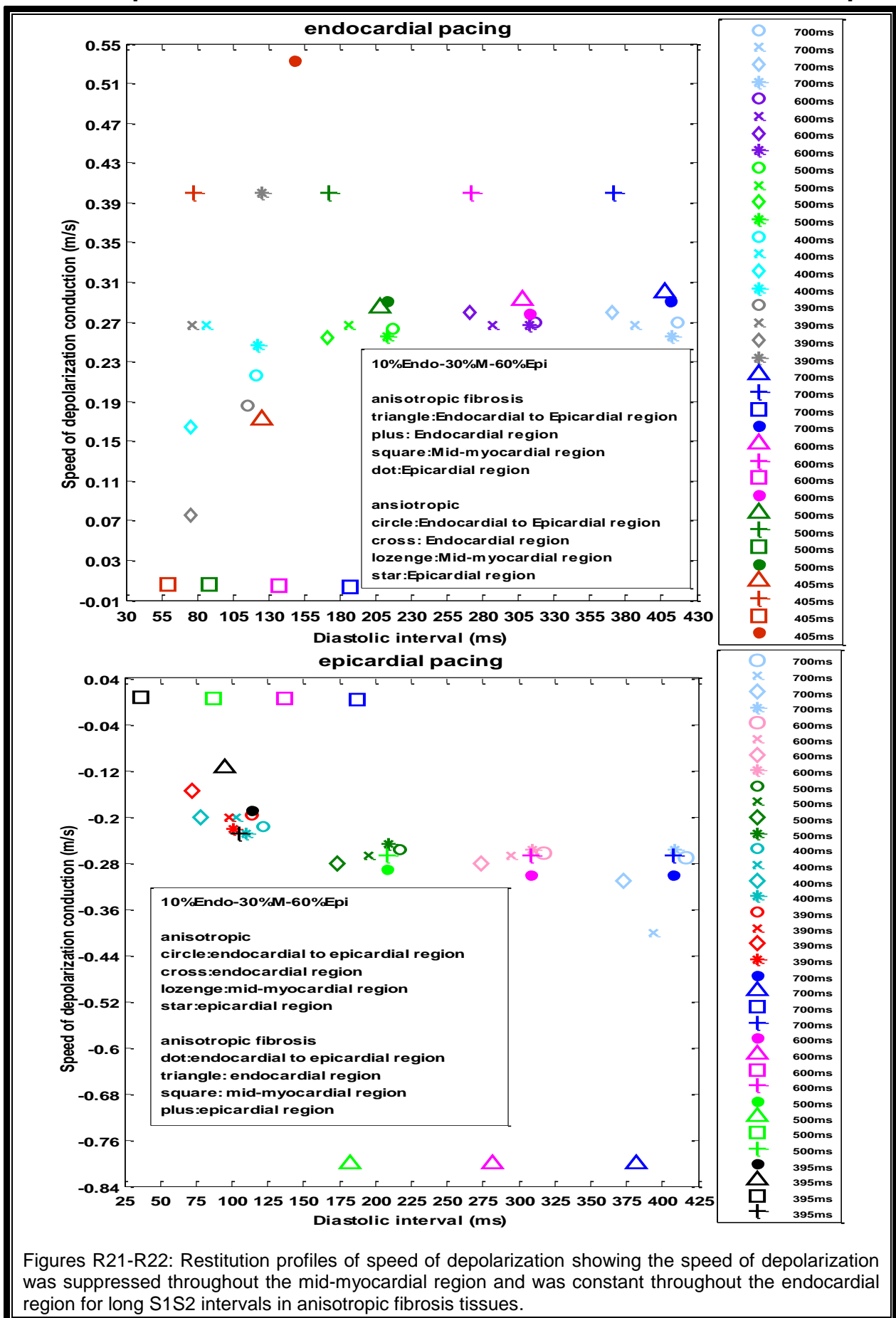
Figures Q37-Q38: Restitution profiles of speed of depolarization conduction and spatial profiles of activation time

In both isotropic and anisotropic tissues, the speed of depolarization conduction in the endocardial region was faster than other regions.

Group R: Profiles of speed of depolarization conduction 2

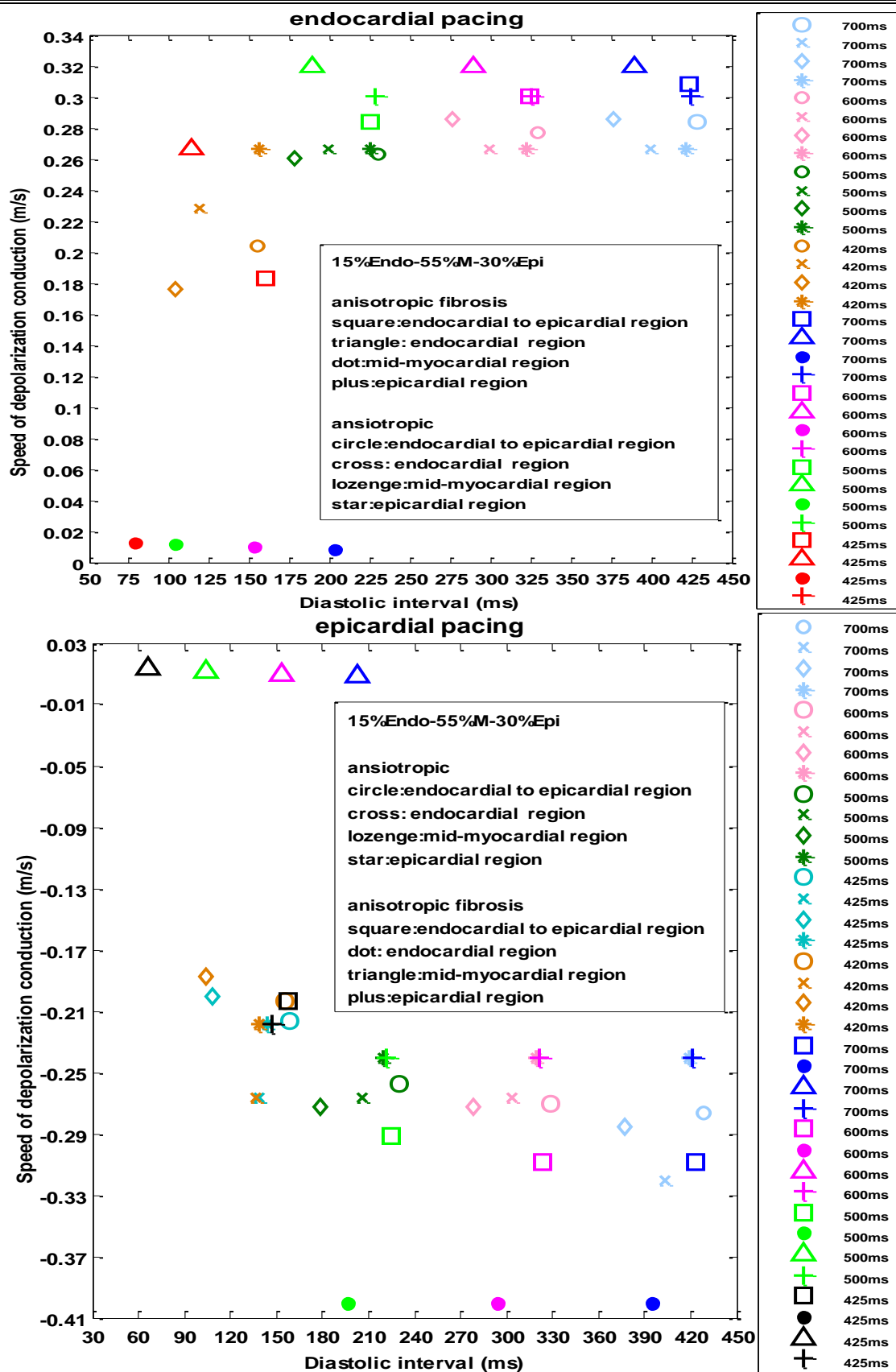
Figure R21 to R26 show restitution profiles of speed of depolarization conduction in anisotropic heterogeneous tissue with and without fibrosis with the FK4V model. The speed of depolarization conduction was suppressed throughout the mid-myocardial region in anisotropic fibrosis heterogeneous tissue composed of 10%Endo-30%M-60%Epi, 60%Endo-30%M-10%Epi, and 15%Endo-55%M-30%Epi with both endocardial and epicardial pacing.

Anisotropic tissue with & without fibrosis: 10%Endo-30%M-60%Epi



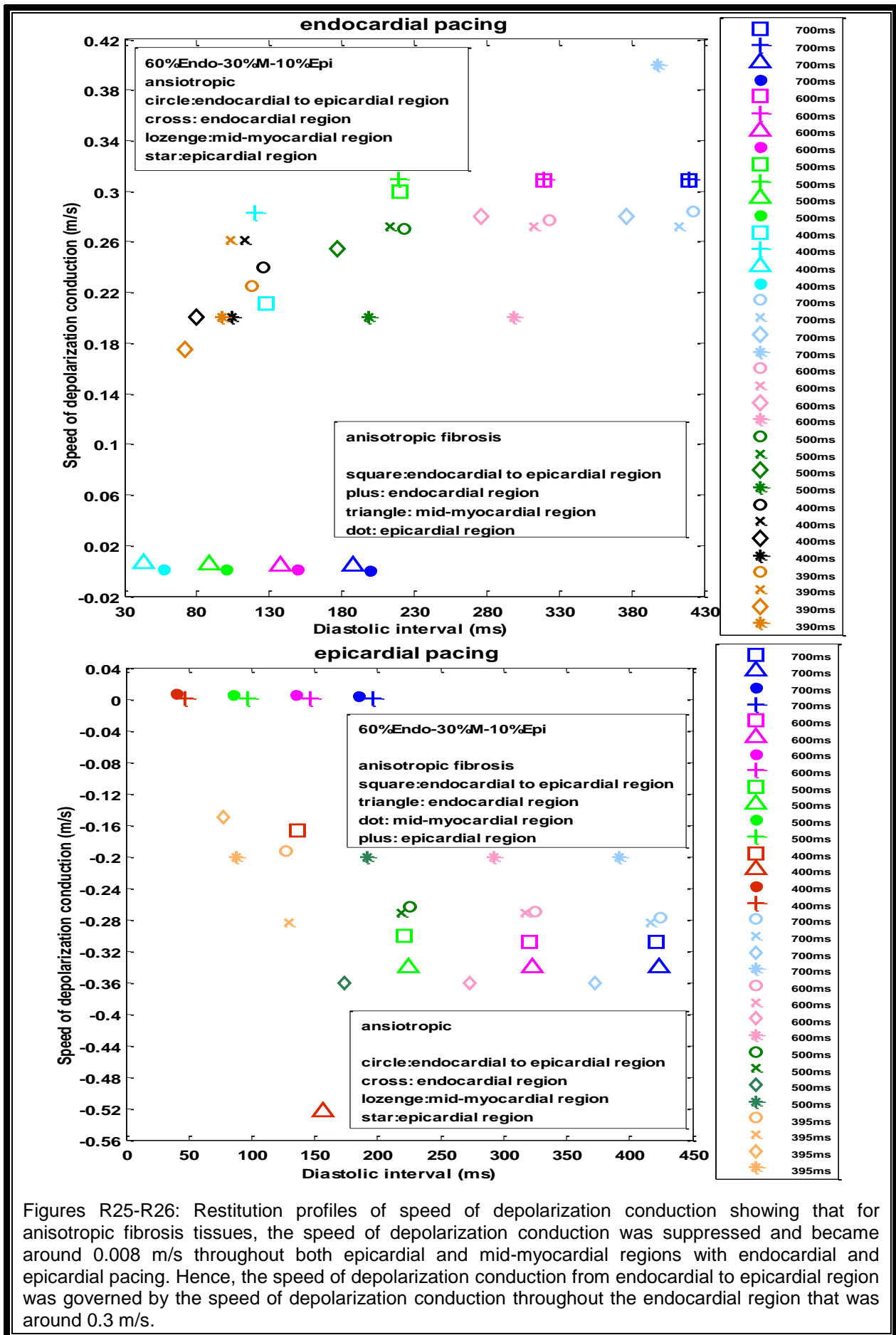
Figures R21-R22: Restitution profiles of speed of depolarization showing the speed of depolarization was suppressed throughout the mid-myocardial region and was constant throughout the endocardial region for long S1S2 intervals in anisotropic fibrosis tissues.

Anisotropic tissue with & without fibrosis: 15%Endo-55%M-30%Epi



Figures R23-R24: Restitution profiles of speed of depolarization showing for anisotropic fibrosis tissue the speed of depolarization decreased to around 0.01 m/s during decreasing S1S2 intervals throughout the mid-myocardial region with both epicardial and endocardial pacing

Anisotropic tissue with & without fibrosis: 60%Endo-30%M-10%Epi



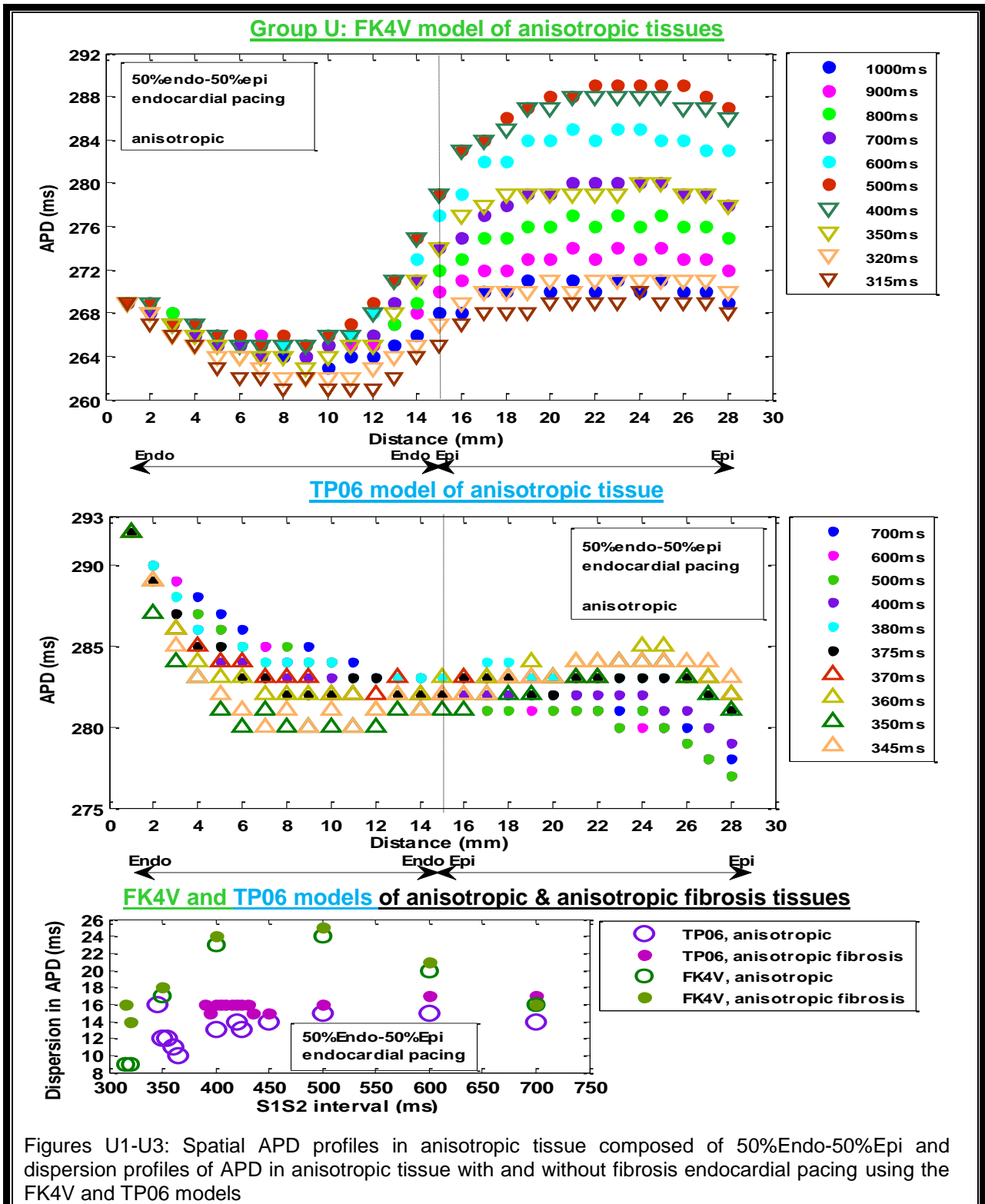
Figures R25-R26: Restitution profiles of speed of depolarization conduction showing that for anisotropic fibrosis tissues, the speed of depolarization conduction was suppressed and became around 0.008 m/s throughout both epicardial and mid-myocardial regions with endocardial and epicardial pacing. Hence, the speed of depolarization conduction from endocardial to epicardial region was governed by the speed of depolarization conduction throughout the endocardial region that was around 0.3 m/s.

Group U: Spatial profiles of APD and APD dispersion

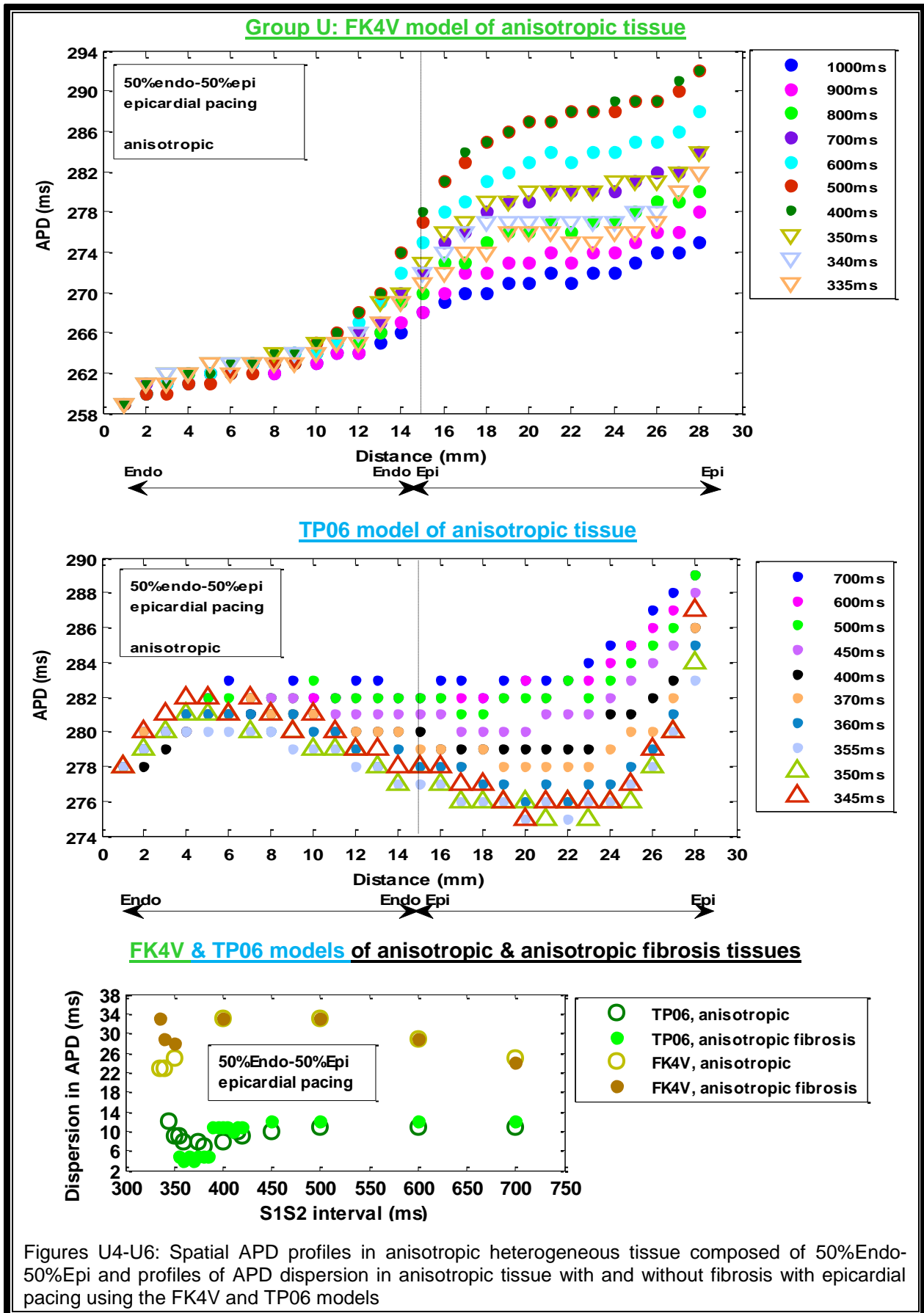
Figure U1 to Figure U24 show (1) spatial profiles of APD in anisotropic heterogeneous tissues; and (2) dispersion profiles of APD in anisotropic heterogeneous tissues with and without fibrosis with the FK4V and the TP06 models.

2 cell type

Heterogeneous tissue composed of 50%Endo-50%Epi with endocardial pacing



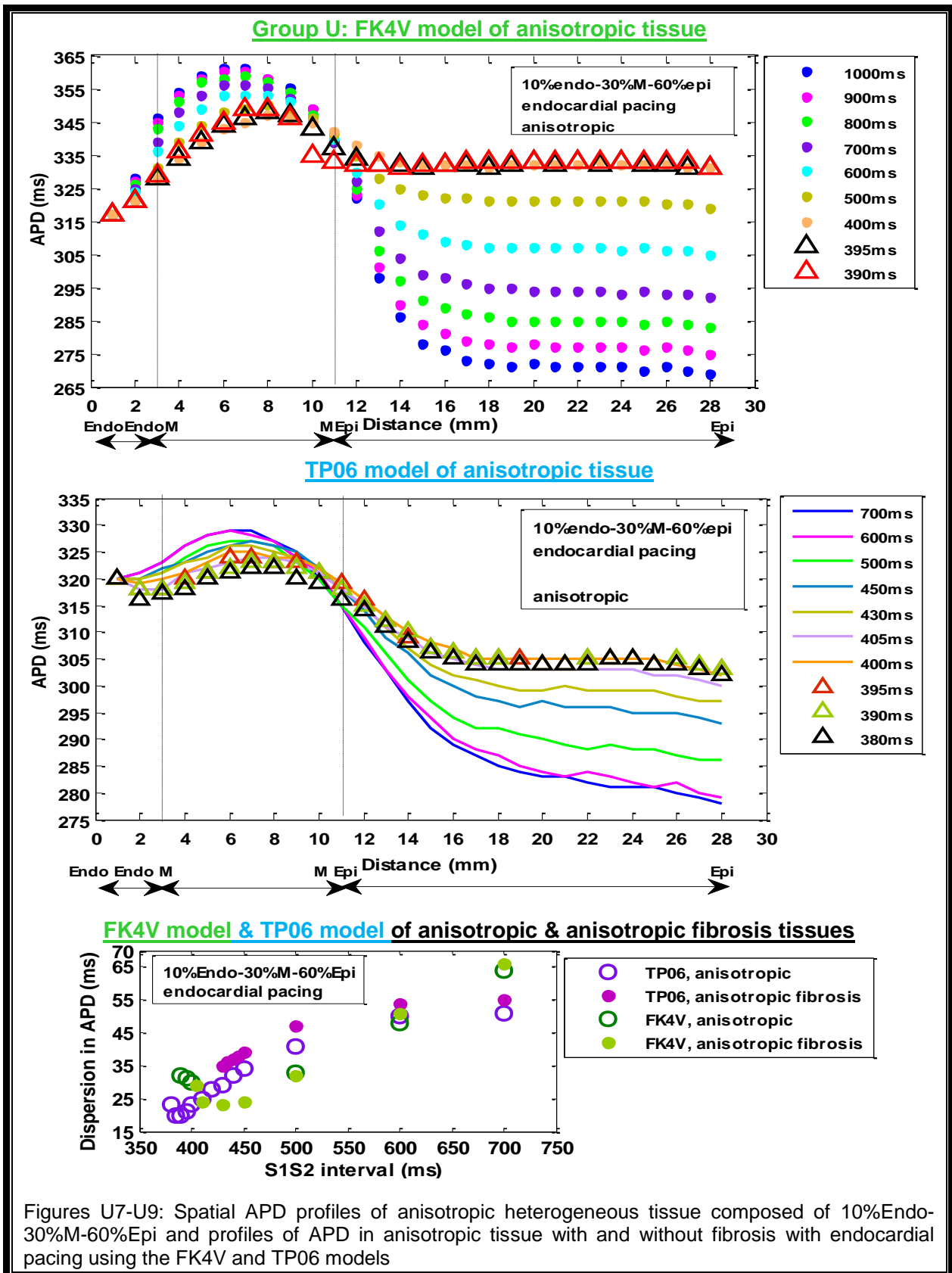
Heterogeneous tissue composed of 50%Endo-50%Epi with epicardial pacing



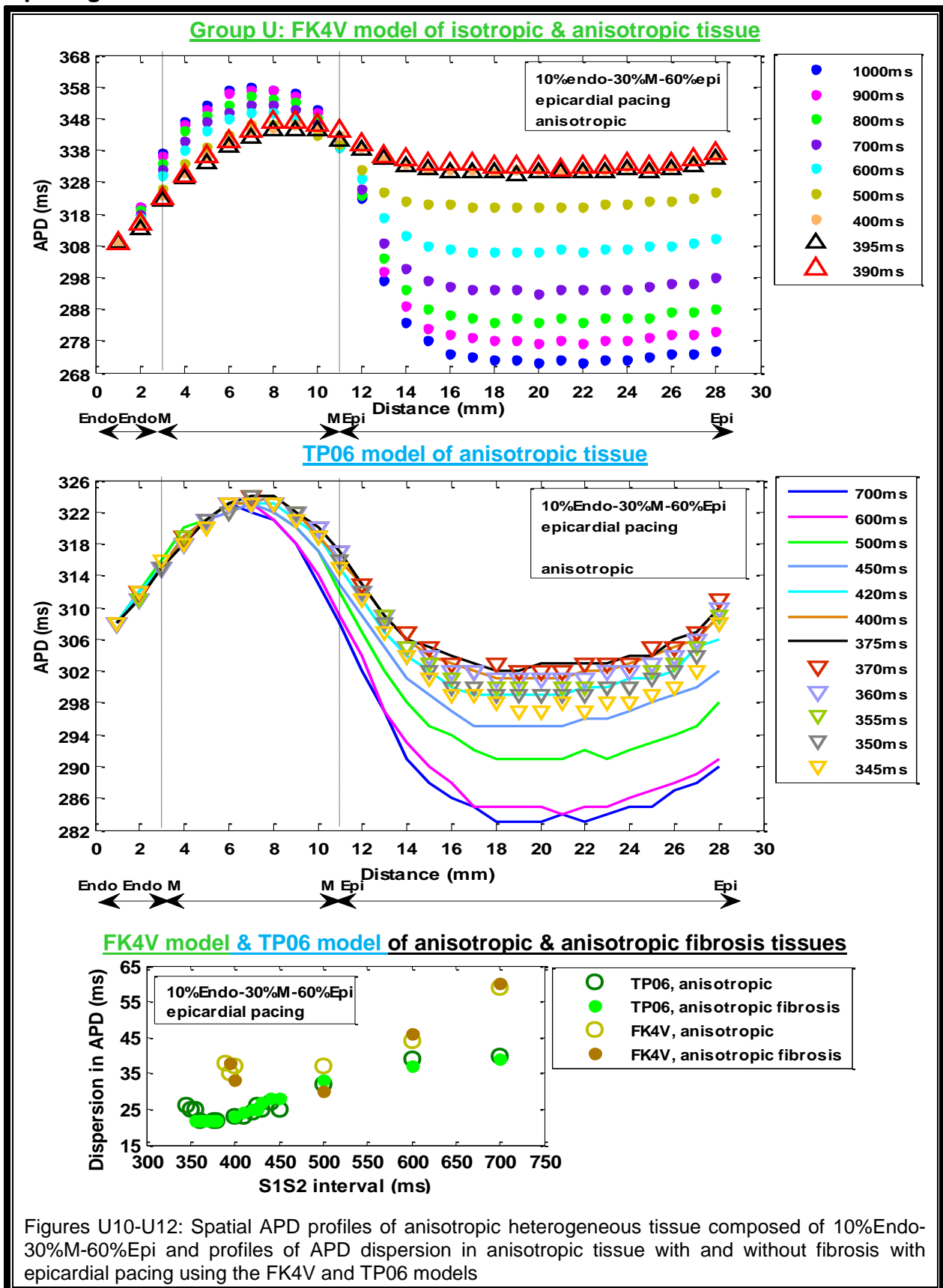
Figures U4-U6: Spatial APD profiles in anisotropic heterogeneous tissue composed of 50%Endo-50%Epi and profiles of APD dispersion in anisotropic tissue with and without fibrosis with epicardial pacing using the FK4V and TP06 models

3 cell type (30%M)

Heterogeneous tissue composed of 10%Endo-30%M-60%Epi with endocardial pacing

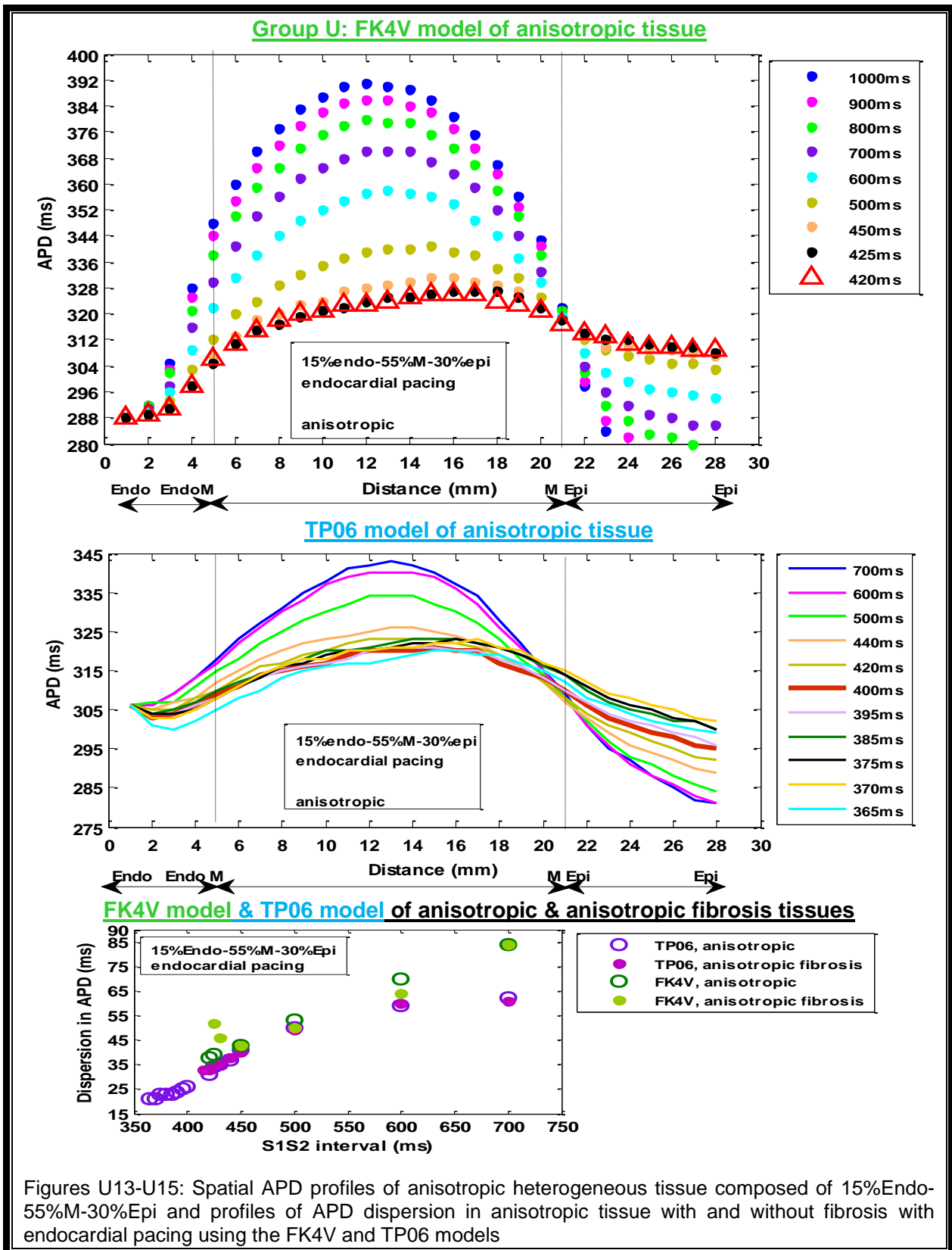


Heterogeneous tissue composed of 10%Endo-30%M-60%Epi with epicardial pacing

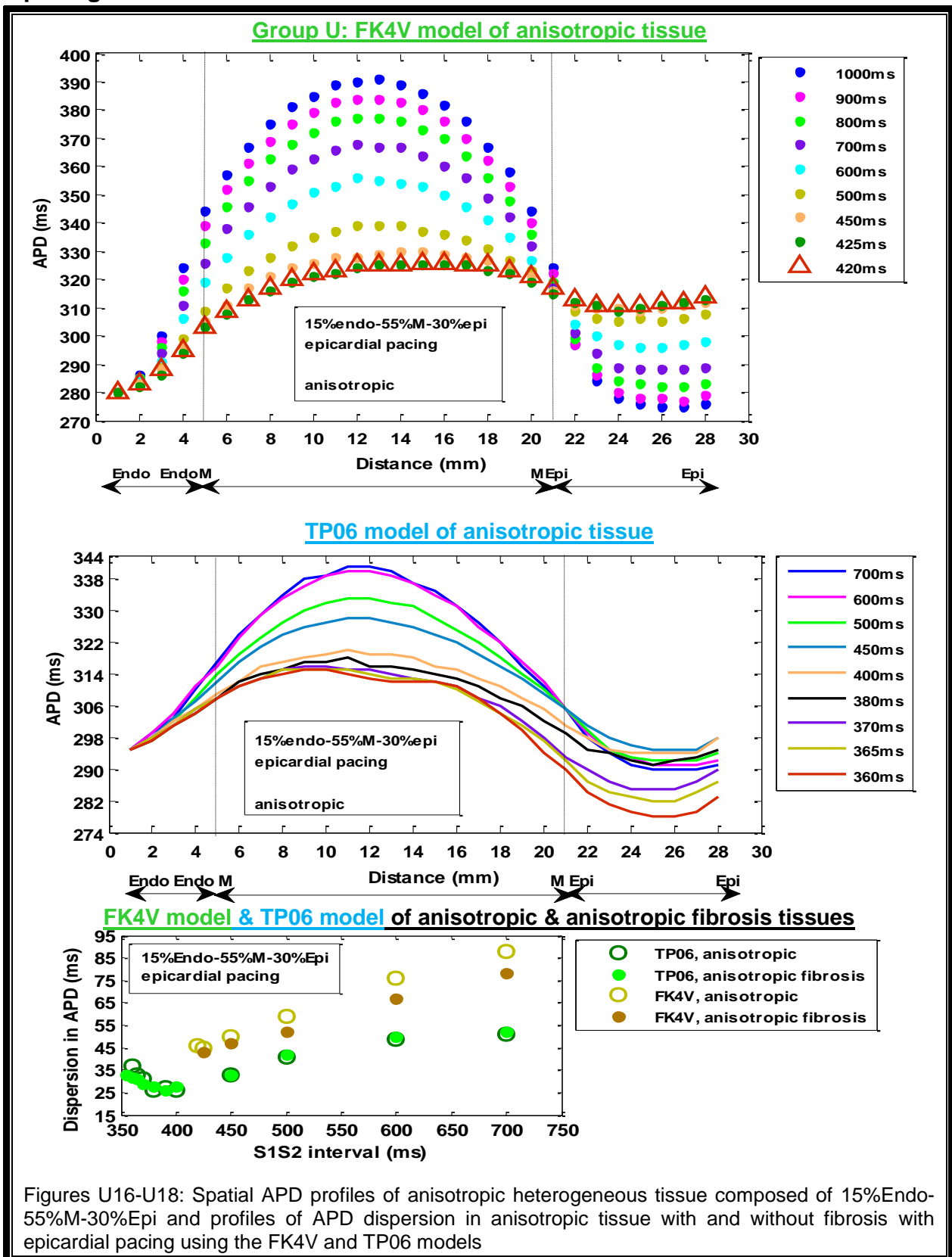


3 cell type (55%M)

Heterogeneous tissue composed of 15%Endo-55%M-30%Epi with endocardial pacing

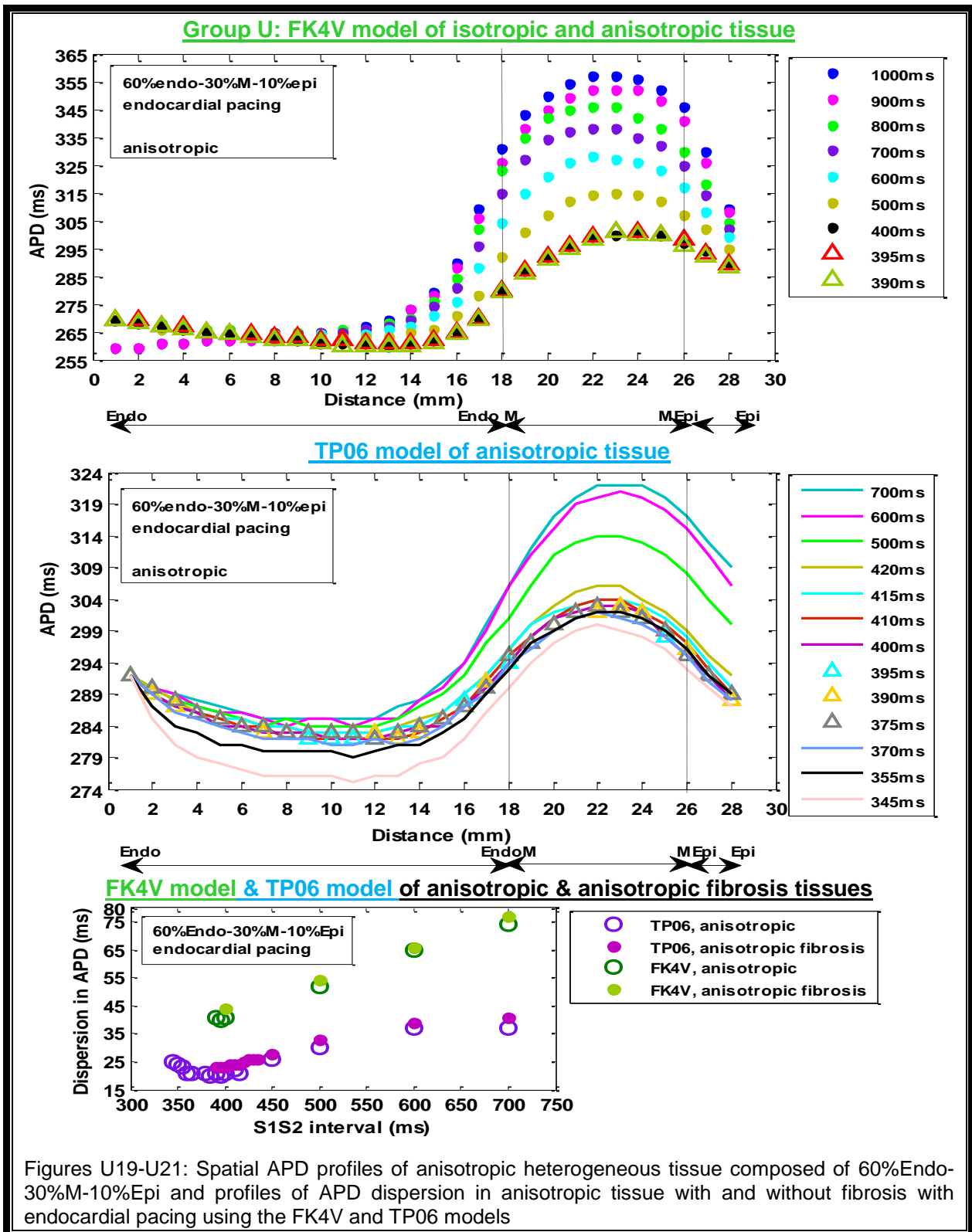


Heterogeneous tissue composed of 15%Endo-55%M-30%Epi with epicardial pacing



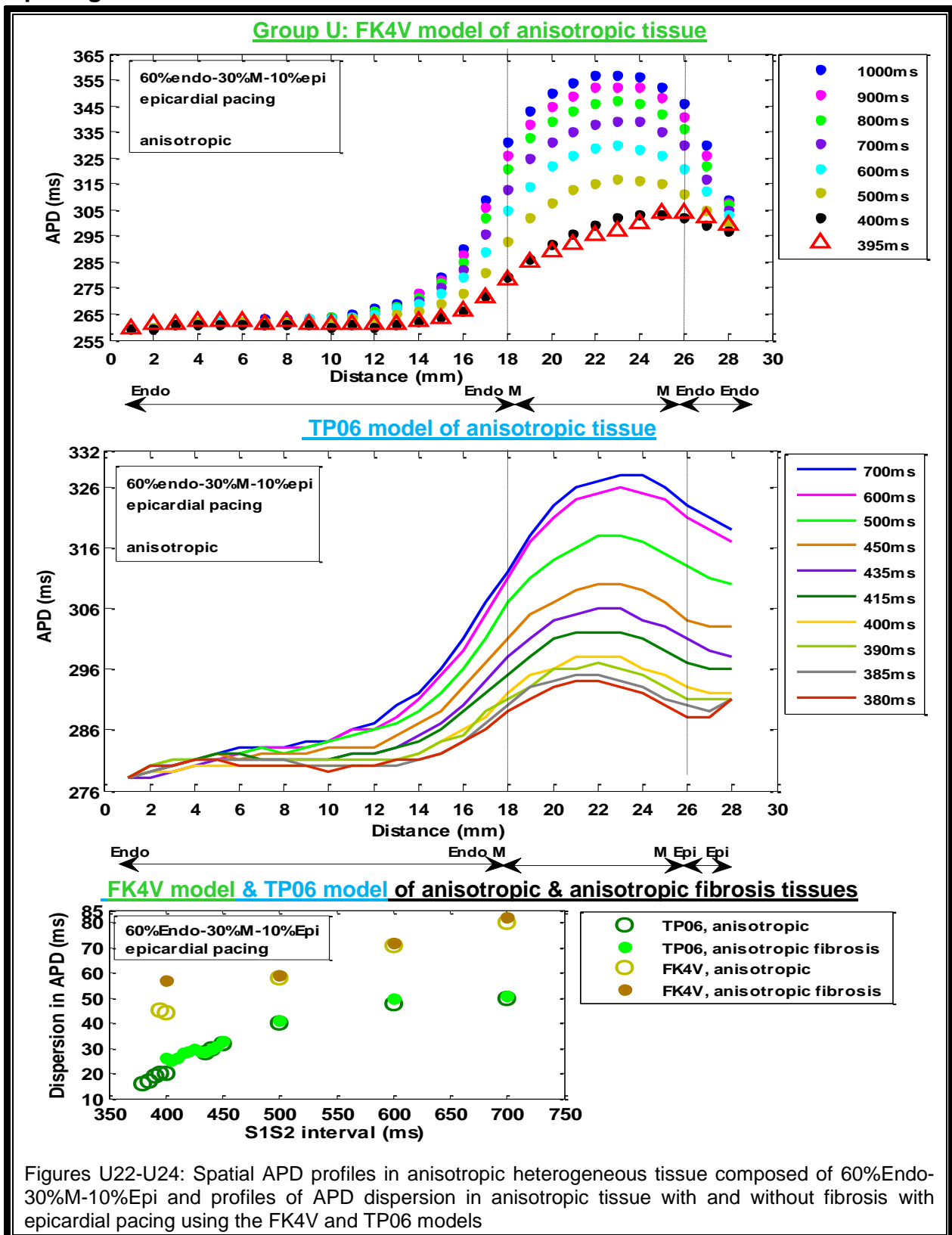
3 cell type (30%M-10%Epi)

Heterogeneous tissue composed of 60%Endo-30%M-10%Epi with endocardial pacing



Figures U19-U21: Spatial APD profiles of anisotropic heterogeneous tissue composed of 60%Endo-30%M-10%Epi and profiles of APD dispersion in anisotropic tissue with and without fibrosis with endocardial pacing using the FK4V and TP06 models

Heterogeneous tissue composed of 60%Endo-30%M-10%Epi with epicardial pacing



Appendix 2

Group X: AP propagation for premature S2 beats in isotropic, anisotropic, and anisotropic fibrosis tissues with a linear and a non-linear fibre orientation using the FK4V and the TP06 models

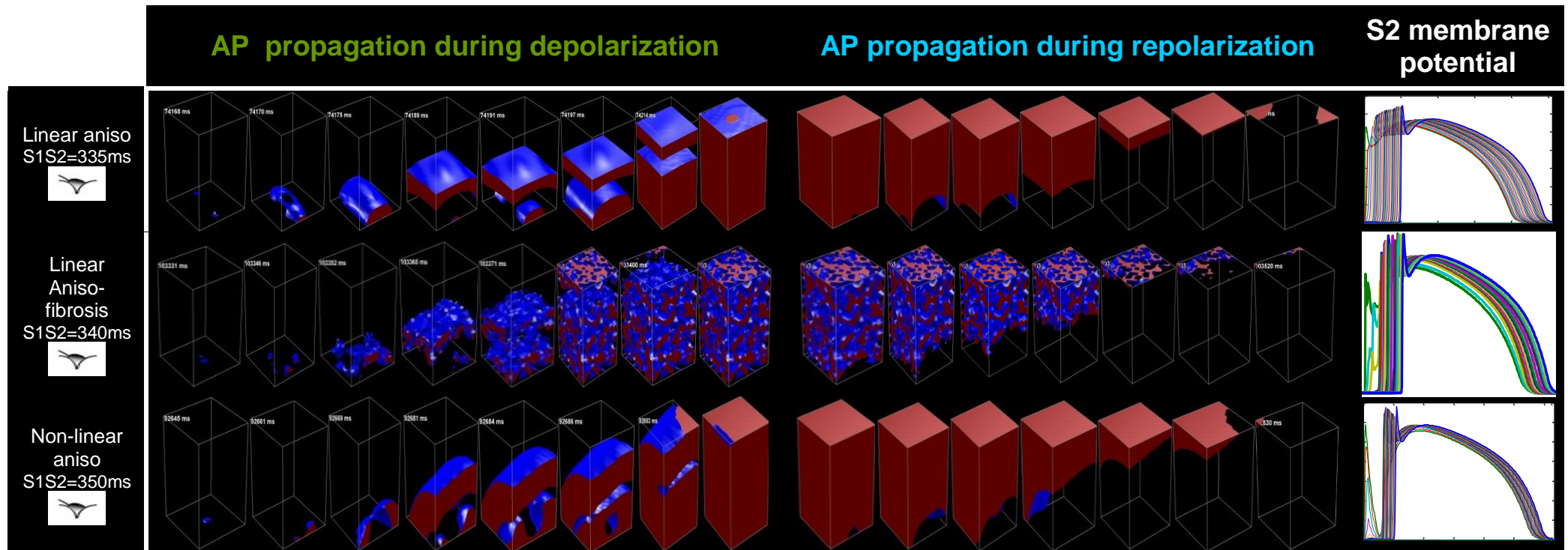


Figure X9: Examples of AP propagation from depolarization to rest in anisotropic **homogenous epicardial tissue** with linear fibre orientation with and without fibrosis as well as non-linear fibre orientation without fibrosis using the FK4V model

During AP depolarization, two waves formed besides tissue, waves joined together in the central region of tissue, another two waves formed besides tissue, waves joined together in the central region of tissue, dimension of the second group of waves was greater than the first one. During AP repolarization, the observable change was on the corner and besides tissues.

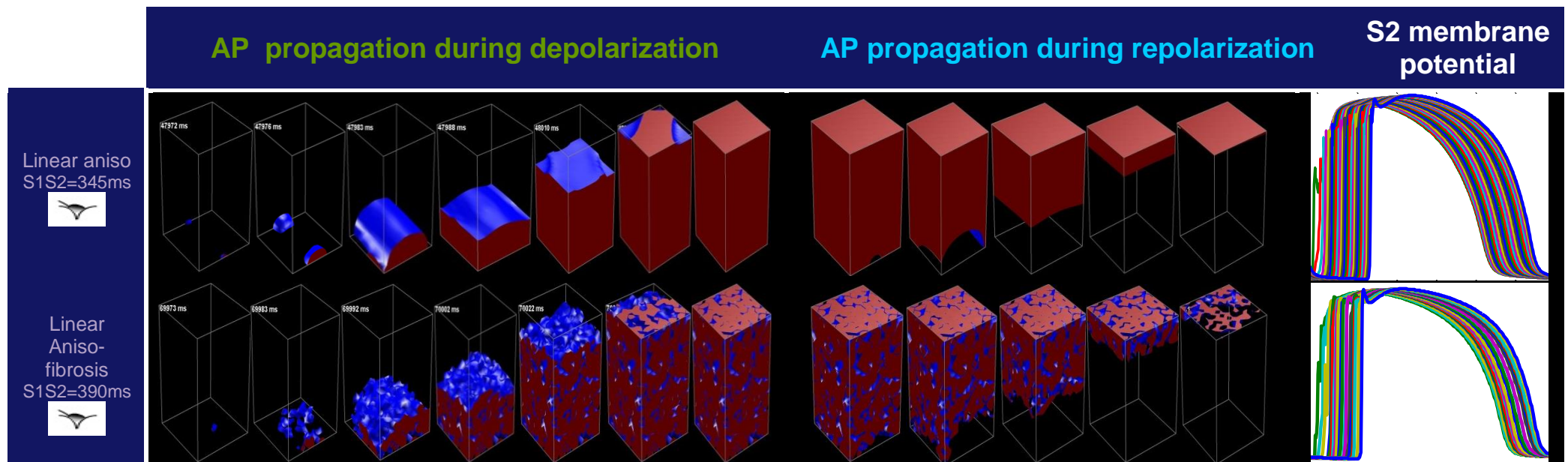


Figure X10: Examples of AP propagation from depolarization to rest in anisotropic **homogenous epicardial tissue** with linear fibre orientation with and without fibrosis using the **TP06 model**

During AP depolarization:

- 1- two waves formed besides tissue
- 2- waves joined together in the central region of tissue
- 3- the shape of wave changed in corners and besides tissue

During AP repolarization, the observable change was besides tissues.

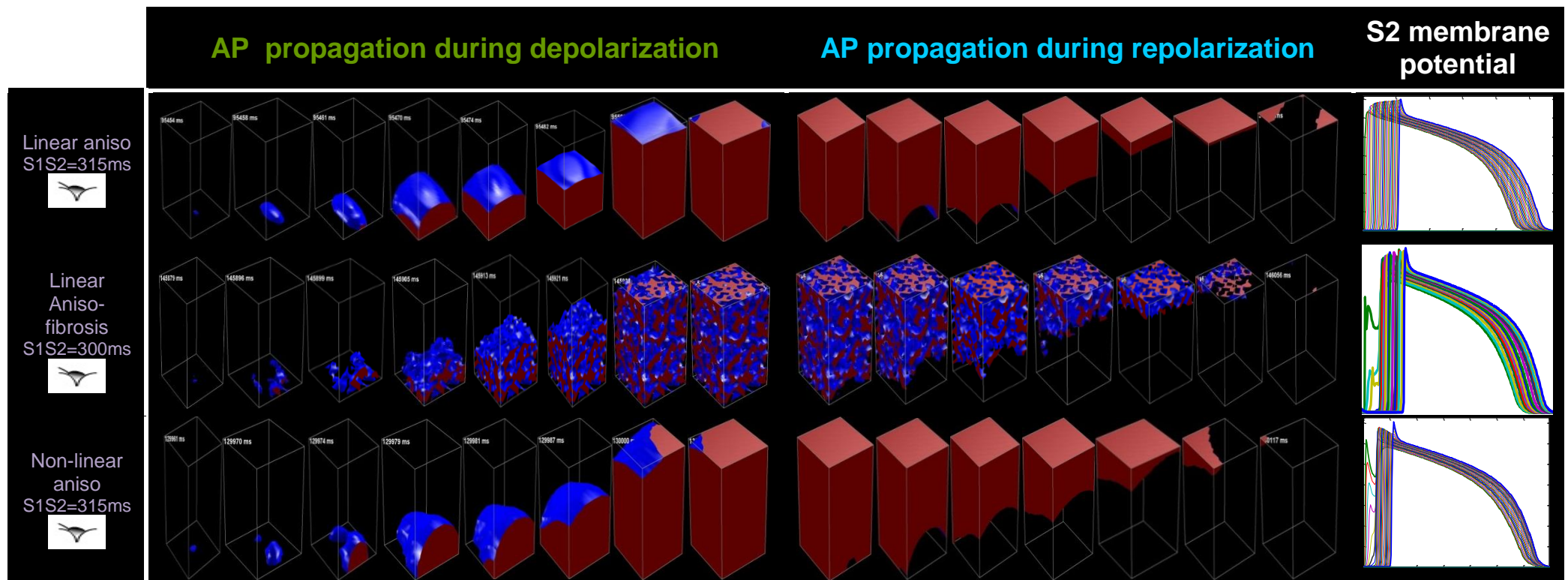


Figure X11: Examples of AP propagation from depolarization to rest in anisotropic **homogenous endocardial tissue** with linear fibre orientation with and without fibrosis as well as non-linear fibre orientation without fibrosis using the FK4V model

During AP depolarization:

- 1- one wave formed in the bottom surface of tissue
- 2- waves propagated besides tissues and upward till AP plateau
- 3- the shape of waves changed in the central region of 3D cube of tissue and top corners of tissue

During AP repolarization, the observable change was besides tissues.

AP propagation during depolarization

AP propagation during repolarization

S2 membrane potential

Linear aniso
S1S2=345ms



Linear
Aniso-
fibrosis
S1S2=390ms

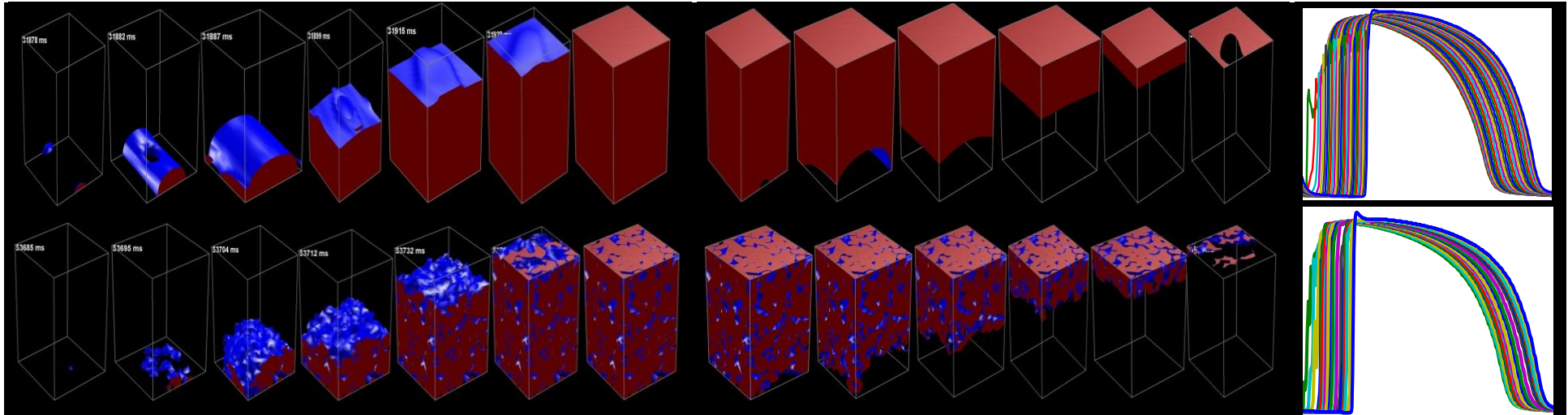


Figure X12: Examples of AP propagation from depolarization to rest in anisotropic **homogenous endocardial tissue** with linear fibre orientation with and without fibrosis using the [TP06 model](#)

During AP depolarization:

- 1- two waves formed besides tissue
- 2- waves joined together in the central region of tissue
- 3- the shape of waves changed in the central region of 3D cube of tissue

During AP repolarization, the observable change was besides tissues.

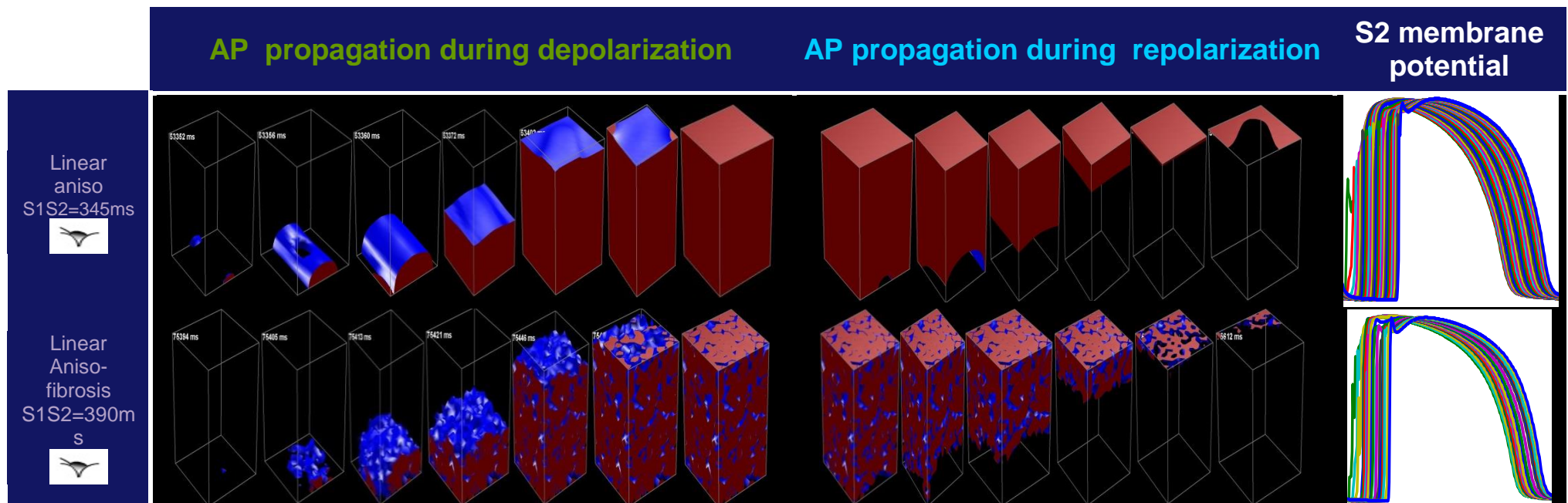


Figure X13: Examples of AP propagation from depolarization to rest in anisotropic **heterogeneous 50%Endo-50%Epi tissue with endocardial pacing** with linear fibre orientation with and without fibrosis using the [TP06 model](#)

During AP depolarization:

- 1- two waves formed besides tissue
- 2- waves joined together in the central region of tissue
- 3- the shape of waves changed in the central region of 3D cube of tissue and corners on the top surface of tissue

During AP repolarization, the observable change was besides tissues.

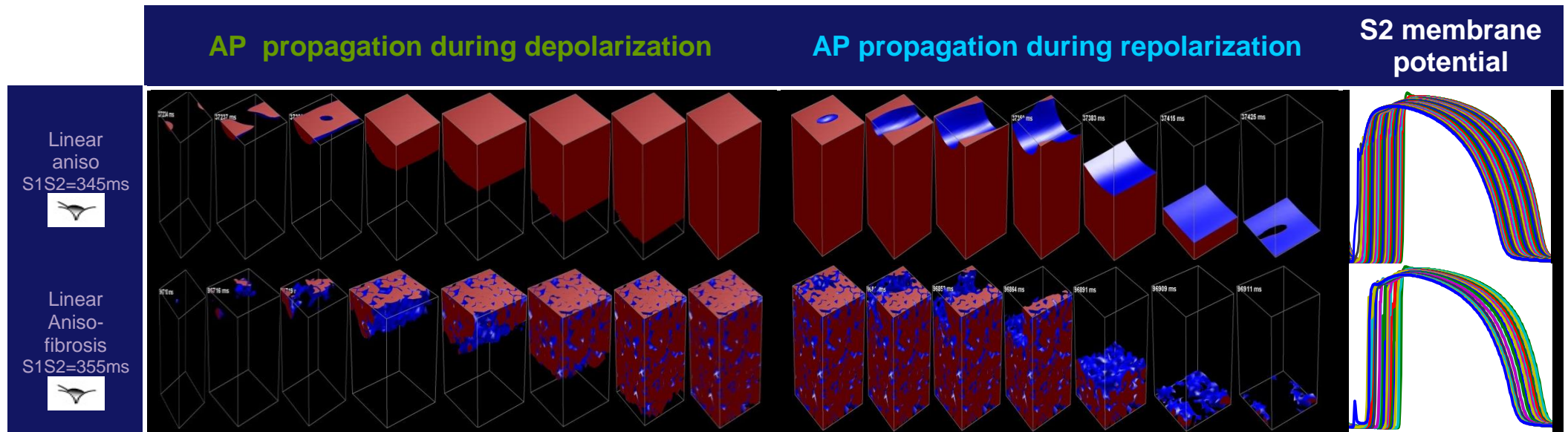


Figure X14: Examples of AP propagation from depolarization to rest in anisotropic **heterogeneous 50%Endo-50%Epi tissue with epicardial pacing** with linear fibre orientation with and without fibrosis using the [TP06 model](#)

During AP depolarization:

- 1- two waves formed besides tissue on the top surface of tissue in the epicardial region
- 2- waves joined together in the central region of epicardial tissue
- 3- waves propagated toward endocardial region before AP plateau

During AP repolarization:

- 1- the wave initially spread besides tissue in the epicardial region
- 2- the wave propagated toward endocardial region till AP rest

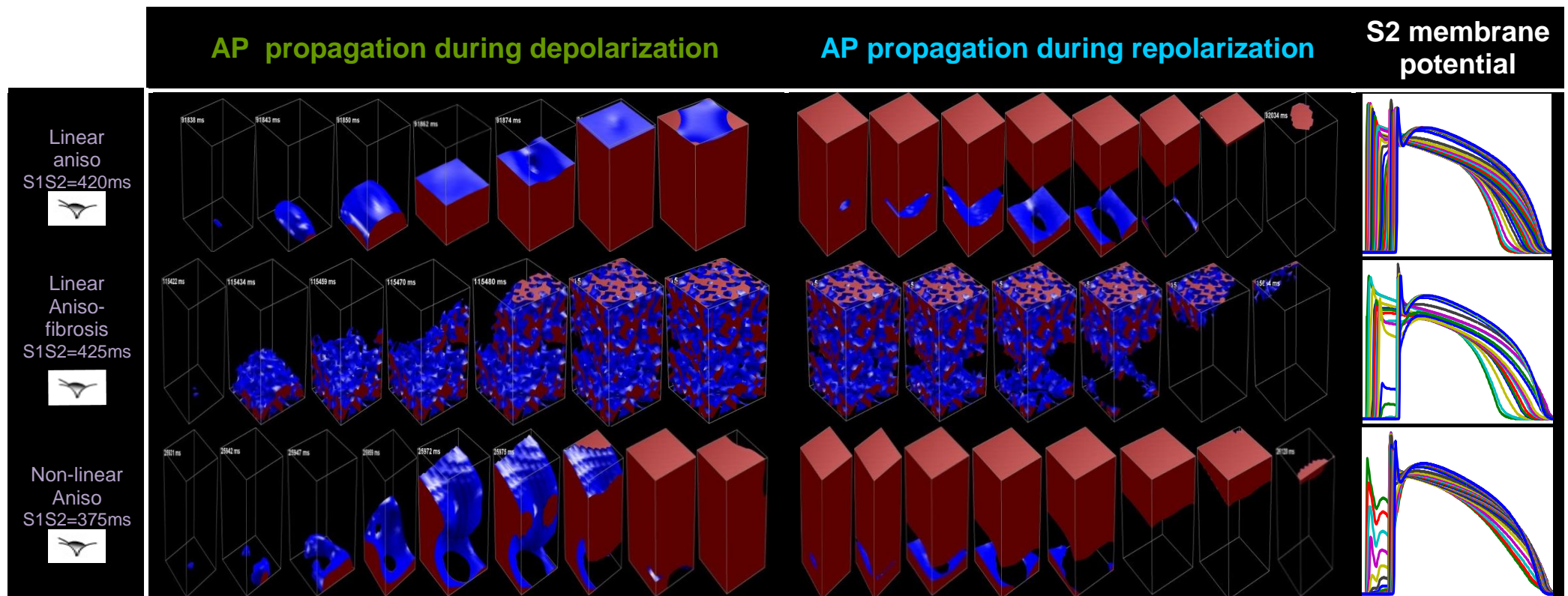


Figure X15: Examples of AP propagation from depolarization to rest in anisotropic **heterogeneous 15%Endo-55%M-30%Epi** tissue with endocardial pacing with linear fibre orientation with and without fibrosis as well as non-linear fibre orientation without fibrosis using the FK4V model

During AP depolarization:

- 1- one wave formed in the bottom surface of tissue in the endocardial region
- 2- waves propagated besides tissues and upward
- 3- the shape of the waves changed in the mid-myocardial region and corners in epicardial region

During AP repolarization:

- the wave broke approximately in the endocardial region in two parts: the bottom waves broke into two parts and vanished besides tissues while top waves continued propagation till AP rest in the epicardial region

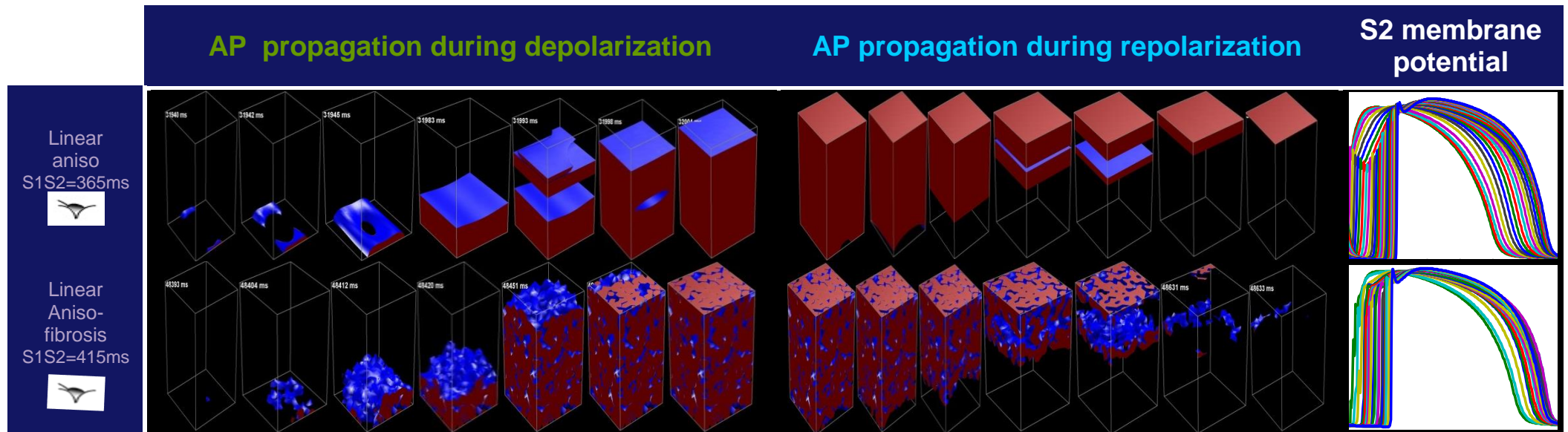


Figure X16: Examples of AP propagation from depolarization to rest in anisotropic **heterogeneous 15%Endo-55%M-30%Epi tissue with endocardial pacing** with linear fibre orientation with and without fibrosis using the [TP06 model](#)

During AP depolarization:

- 1- two waves formed besides tissue on the bottom surface of tissue in the endocardial region and then joined together
- 2- another wave formed close to region between mid-myocardial and epicardial regions
- 3- waves joined together close to region between endocardial and mid-myocardial regions and propagated toward epicardial region before AP plateau

During AP repolarization:

- 1- the wave broke into two parts close to the region between mid-myocardial and epicardial regions
- 2- the wave propagated toward epicardial region till AP rest

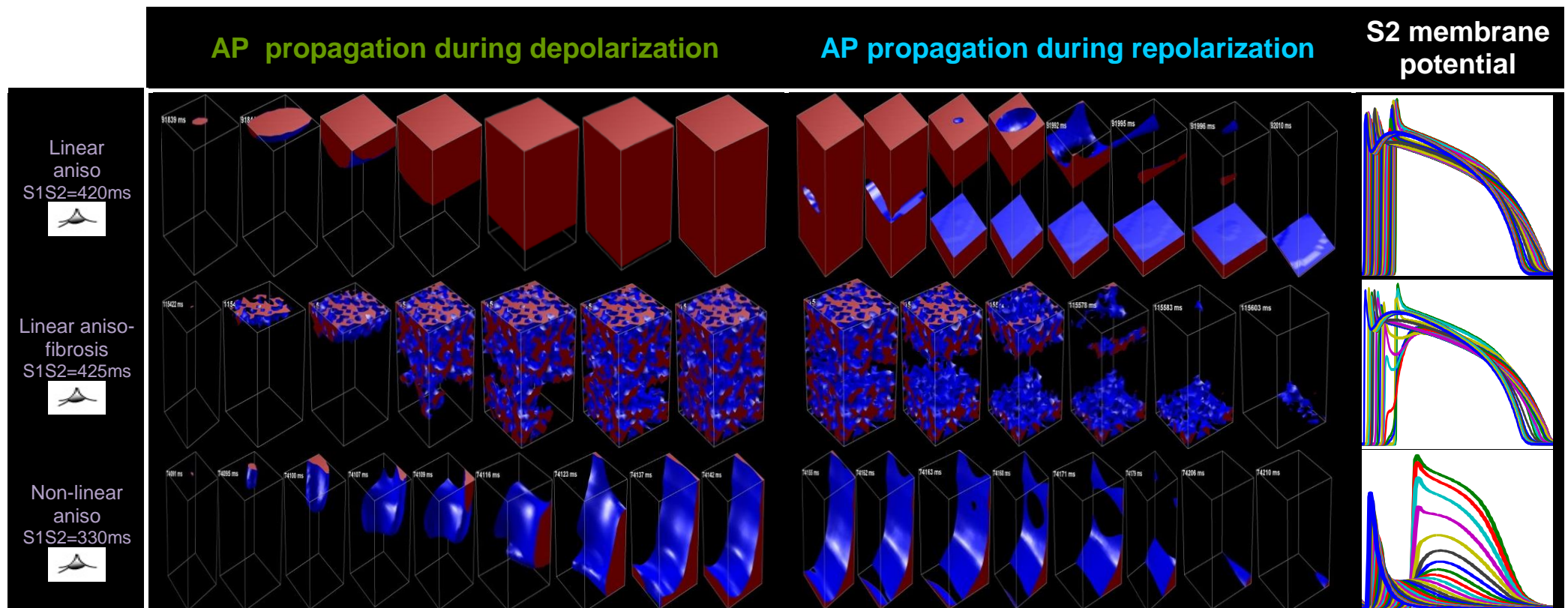


Figure X17: Examples of AP propagation from depolarization to rest in anisotropic **heterogeneous 15%Endo-55%M-30%Epi** tissue with **epicardial pacing** with linear fibre orientation with and without fibrosis as well as non-linear fibre orientation without fibrosis using the FK4V model

During AP depolarization:

- 1- one wave formed on the top surface of tissue in the epicardial region and propagated besides tissues
- 2- the wave propagated gradually toward epicardial region before AP plateau

During AP repolarization, the wave broke into two parts approximately in the region close to the endocardial and mid-myocardial regions: the top wave broke into two parts and vanished besides tissues while the bottom wave continued propagation till AP rest in the endocardial region.

AP propagation during depolarization

AP propagation during repolarization

S2 membrane potential

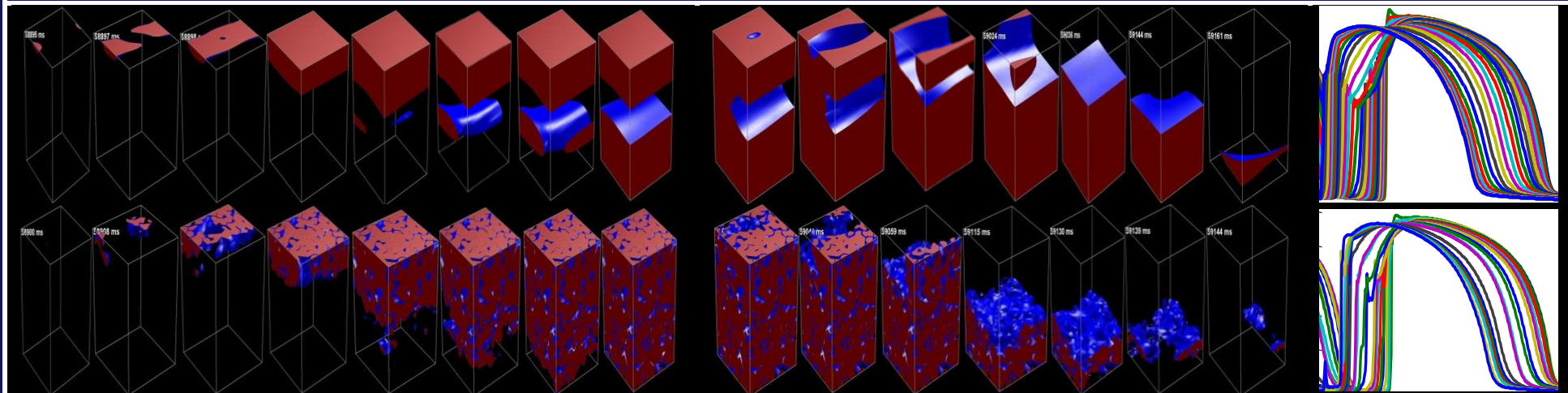


Figure X18: Examples of AP propagation from depolarization to rest in anisotropic **heterogeneous 15%Endo-55%M-30%Epi** tissue with epicardial pacing with linear fibre orientation with and without fibrosis using the [TP06 model](#)

During AP depolarization:

- 1- two waves formed besides tissue on the top surface of tissue in the epicardial region and then joined together and propagated for seconds and then stopped propagation
- 2- another wave formed besides tissue close to region between mid-myocardial and epicardial regions and propagated toward endocardial region
- 3- no complete AP plateau

During AP repolarization:

- 1- the wave broke into two parts close to the region between mid-myocardial and epicardial regions
- 2- the top wave vanished in corner and the bottom wave propagated toward endocardial region

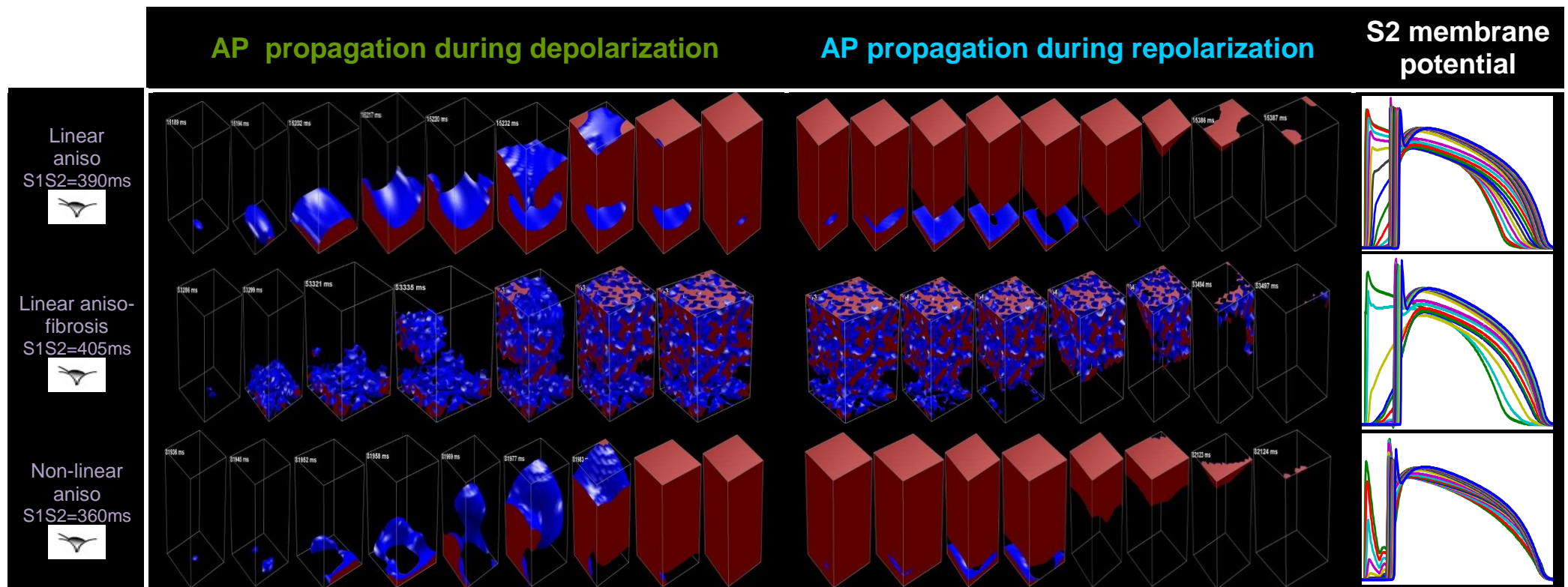


Figure X19: Examples of AP propagation from depolarization to rest in anisotropic **heterogeneous 10%Endo-30%M-60%Epi tissue with endocardial pacing** with linear fibre orientation with and without fibrosis as well as non-linear fibre orientation without fibrosis using the FK4V model

During AP depolarization:

- 1- one wave formed on the bottom surface of tissue in the endocardial region and propagated besides tissue
- 2- the shape of the wave changed significantly in the mid-myocardial region
- 3- the wave propagated upward and joined together in the region between mid-myocardial and epicardial regions
- 4- no complete AP plateau

During AP repolarization, the wave broke into two parts in the region close to the mid-myocardial and endocardial regions: the bottom wave broke into two parts and vanished besides tissues while top wave continued propagation and vanish in top corner till AP rest in epicardial region

AP propagation during depolarization

AP propagation during repolarization

S2 membrane potential

Linear
aniso
S1S2=380ms



Linear
Aniso-
fibrosis
S1S2=430ms

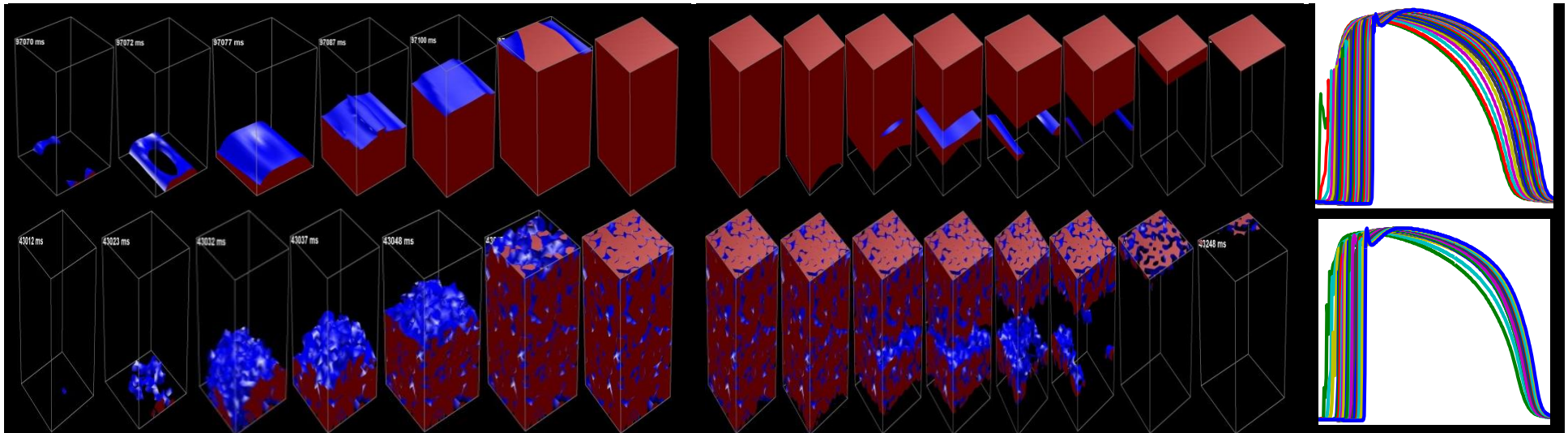


Figure X20: Examples of AP propagation from depolarization to rest in anisotropic **heterogeneous 10%Endo-30%M-60%Epi** tissue with endocardial pacing with linear fibre orientation with and without fibrosis using the [TP06 model](#)

During AP depolarization:

- 1- two waves formed on the bottom surface of tissue in the endocardial region and then joined together
- 2- the shape of the wave changed in central the region of tissue during propagation upward
- 3- the shape of the wave changed significantly in the mid-myocardial region
- 4- the shape of the wave change besides tissue on top surface of tissue in the epicardial region

During AP repolarization, the wave broke into two parts in the region close to the mid-myocardial and epicardial regions: the bottom wave broke into two parts and vanished besides tissues while the top wave continued propagation and vanished in top surface of tissue in epicardial region

AP propagation during depolarization

AP propagation during repolarization

S2 membrane potential

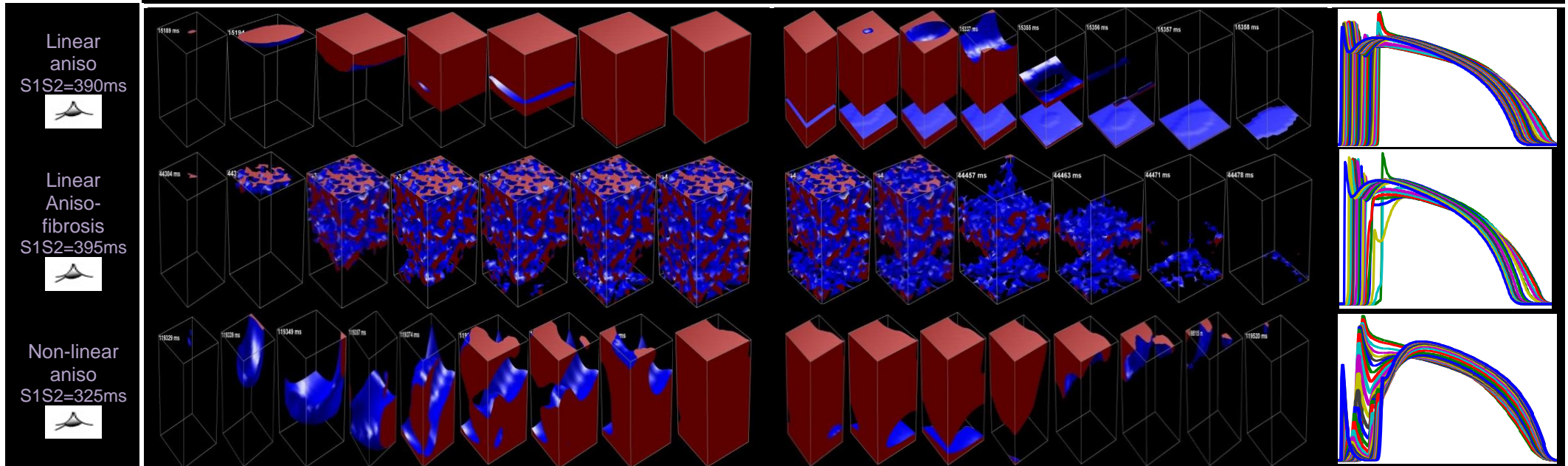


Figure X21: Examples of AP propagation from depolarization to rest in anisotropic **heterogeneous 10%Endo-30%M-60%Epi** tissue with epicardial pacing with linear fibre orientation with and without fibrosis as well as non-linear fibre orientation without fibrosis using the FK4V model

During AP depolarization:

- 1- one wave formed on the top surface of tissue in the epicardial region
- 2- the wave broke into two parts in the region between mid-myocardial and epicardial regions but joined again approximately in this region
- 3- the wave propagated toward endocardial region till AP plateau

During AP repolarization:

- the wave broke into two parts in the region close to the endocardial and mid-myocardial regions
- the top wave broke into two parts on the top surface of tissue in the epicardial region and vanished besides tissues while the bottom wave continued propagation and vanished on the bottom surface of tissue in the endocardial region

Note: All anisotropic heterogeneous tissues with fibrosis suppressed the speed of depolarization in the mid-myocardial region in this tissue with linear fibre orientation that may explain the difference in the pattern of depolarization in anisotropic and anisotropic fibrosis tissues.

AP propagation during depolarization

AP propagation during repolarization

S2 membrane potential

Linear
aniso
S1S2=345ms



Linear aniso-
fibrosis
S1S2=355ms

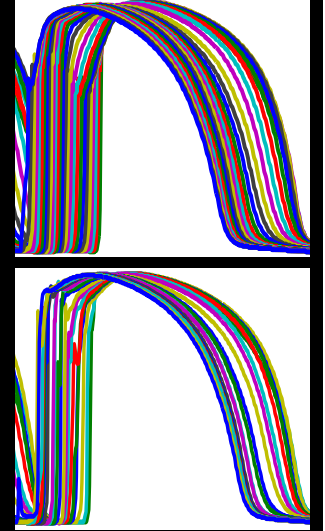
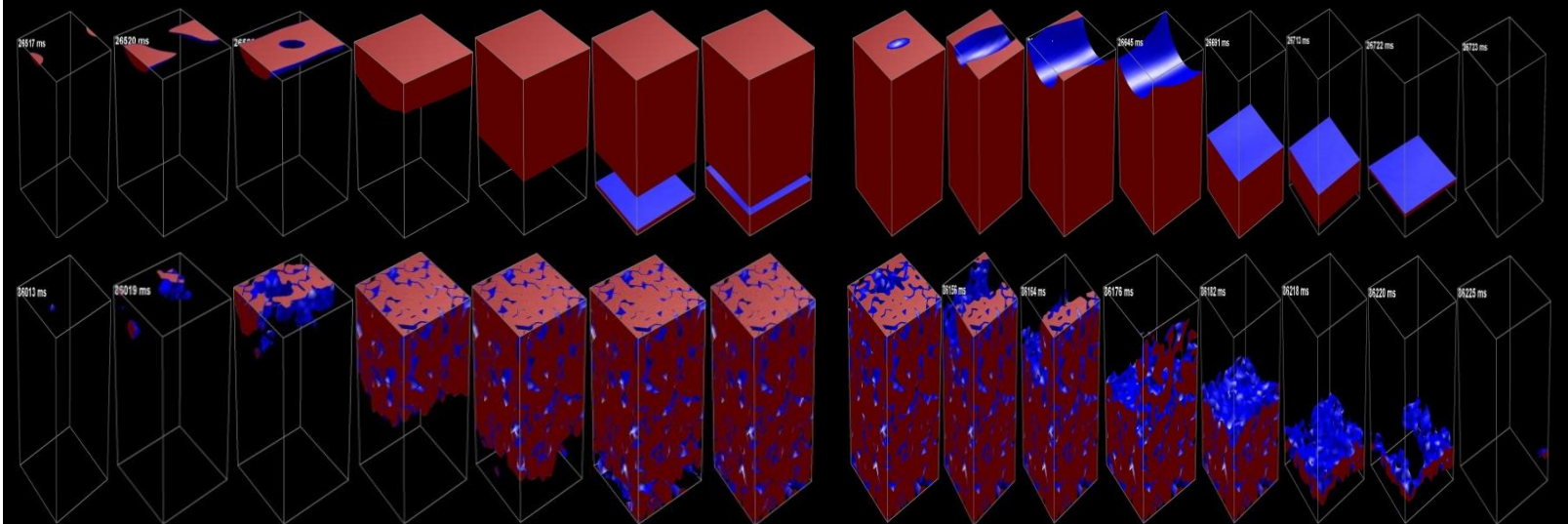


Figure X22: Examples of AP propagation from depolarization to rest in anisotropic **heterogeneous 10%Endo-30%M-60%Epi** tissue with epicardial pacing with linear fibre orientation with and without fibrosis using the [TP06 model](#)

During AP depolarization:

- 1- two waves formed besides tissue on the top surface of tissue in the epicardial region and then joined together and propagated toward mid-myocardial region
- 2- another wave formed on the bottom of tissue in the endocardial region and joined with the top wave before AP plateau

During AP repolarization:

- 1- the wave propagated downward, and then
- 2- the wave propagated upward in the endocardial region and vanished in the region between endocardial and mid-myocardial regions